



**UNIL** | Université de Lausanne

Unicentre

CH-1015 Lausanne

<http://serval.unil.ch>

---

*Year : 2018*

## Developmental cell biology of the SRXpathway in hormonal régulation and root stem cell régénération

Cattaneo Pietro Cattaneo

Cattaneo Pietro Cattaneo, 2018, Developmental cell biology of the SRXpathway in hormonal régulation and root stem cell régénération

Originally published at : Thesis, University of Lausanne

Posted at the University of Lausanne Open Archive <http://serval.unil.ch>

Document URN : urn:nbn:ch:serval-BIB\_4E395C9171DE3

### **Droits d'auteur**

L'Université de Lausanne attire expressément l'attention des utilisateurs sur le fait que tous les documents publiés dans l'Archive SERVAL sont protégés par le droit d'auteur, conformément à la loi fédérale sur le droit d'auteur et les droits voisins (LDA). A ce titre, il est indispensable d'obtenir le consentement préalable de l'auteur et/ou de l'éditeur avant toute utilisation d'une oeuvre ou d'une partie d'une oeuvre ne relevant pas d'une utilisation à des fins personnelles au sens de la LDA (art. 19, al. 1 lettre a). A défaut, tout contrevenant s'expose aux sanctions prévues par cette loi. Nous déclinons toute responsabilité en la matière.

### **Copyright**

The University of Lausanne expressly draws the attention of users to the fact that all documents published in the SERVAL Archive are protected by copyright in accordance with federal law on copyright and similar rights (LDA). Accordingly it is indispensable to obtain prior consent from the author and/or publisher before any use of a work or part of a work for purposes other than personal use within the meaning of LDA (art. 19, para. 1 letter a). Failure to do so will expose offenders to the sanctions laid down by this law. We accept no liability in this respect.



UNIL | Université de Lausanne

Faculté de biologie  
et de médecine

Département de biologie moléculaire végétale

**Developmental cell biology of the *BRX* pathway in  
hormonal regulation and root stem cell regeneration**

**Thèse de doctorat ès sciences de la vie (PhD)**

Présentée à la

Faculté de biologie et médecine  
de l'Université de Lausanne

par

**Pietro Cattaneo**

Biologiste Master de l'Università degli Studi di Milano

**Jury**

Prof. Winship HERR, Président  
Prof. Christian HARDTKE, Directeur de thèse  
Prof. Christian FANKHAUSER, expert  
Prof. Dolf WEIJERS, expert

Lausanne, 2017



UNIL | Université de Lausanne

Faculté de biologie  
et de médecine

Ecole Doctorale

Doctorat ès sciences de la vie

# Imprimatur

Vu le rapport présenté par le jury d'examen, composé de

<i>Président·e</i>	Monsieur	Prof. Winship <b>Herr</b>
<i>Directeur·rice de thèse</i>	Monsieur	Prof. Christian <b>Hardtke</b>
<i>Experts·es</i>	Monsieur	Prof. Christian <b>Fankhauser</b>
	Monsieur	Prof. Dolf <b>Weijers</b>

le Conseil de Faculté autorise l'impression de la thèse de

**Monsieur Pietro Cattaneo**

Dottore Magistrale in Molecular cell Biology Milan

intitulée

**Developmental cell biology of the *BRX* pathway in  
hormonal regulation and root stem cell regeneration**

Lausanne, le 15 décembre 2017

pour le Doyen  
de la Faculté de biologie et de médecine

Prof. Winship Herr





**UNIL** | Université de Lausanne

Faculté de biologie  
et de médecine

**Département de biologie moléculaire végétale**

**Developmental cell biology of the *BRX* pathway in  
hormonal regulation and root stem cell regeneration**

**Thèse de doctorat ès sciences de la vie (PhD)**

Présentée à la

Faculté de biologie et médecine  
de l'Université de Lausanne

par

**Pietro Cattaneo**

Biologiste Master de l'Università degli Studi di Milano

**Jury**

Prof. Winship HERR, Président  
Prof. Christian HARDTKE, Directeur de thèse  
Prof. Christian FANKHAUSER, expert  
Prof. Dolf WEIJERS, expert

Lausanne, 2017

## Index

<b>Acknowledgements</b>	<b>1</b>
<b>Abstract</b>	<b>2</b>
<b>Résumé</b>	<b>4</b>
<b>Résumé public</b>	<b>6</b>
<b>Introduction</b>	<b>7</b>
<ul style="list-style-type: none"><li>• Plant innovations in evolution</li><li>• A matter of growth</li><li>• A model to study growth and size mechanisms: the <i>Arabidopsis</i> leaf</li><li>• Plant root development</li><li>• Mechanisms controlling and maintaining root growth</li><li>• Long-distance transport in plants: xylem versus phloem</li><li>• Origin of protophloem</li><li>• <i>BREVIS RADIX (BRX)</i>: a positive regulator of protophloem development</li><li>• Screening of <i>brx-2</i> genetic suppressors: what's new?</li><li>• Research outline</li></ul>	
<b>Chapter 1</b>	<b>27</b>
Antagonistic peptide technology for functional dissection of CLE peptides revisited	
<b>Chapter 2</b>	<b>38</b>
Molecular genetic framework for protophloem formation	
<b>Chapter 3</b>	<b>47</b>
Perception of root-active CLE peptides requires CORYNE function in the phloem vasculature	
<b>Chapter 4</b>	<b>74</b>
BIG BROTHER uncouples cell proliferation from elongation in the <i>Arabidopsis</i> primary root	
<b>Chapter 5</b>	<b>86</b>
Functional FYRC domain of the <i>Arabidopsis</i> JUMONJI14 protein is crucial for root growth restoration in impaired genetic backgrounds	
<b>Conclusion and outlook</b>	<b>109</b>

## ACKNOWLEDGEMENTS

Foremost, I would like to express my deep gratitude to Prof. Christian Hardtke, my research supervisor, for his guidance and useful critiques of this research work.

Joining his lab has been an amazing, stimulating and challenging work experience.

I would like to particularly thank Alice, with whom I have shared not only my lab bench, but also exciting and frustrating moments during these four years.

I am grateful for the assistance given by Amelia for running the lab and for technical advices. I would like also to thank Yeon and Antia for their help and scientific experience at the beginning of my work.

I also fully enjoyed working in the department of plant molecular biology. In particular, Peter, Rodrigo, Lothar, Kian, Raphaël, Elia and Jules have helped me with their valuable technical support and scientific opinions. Discussing with them definitely enhanced the value of my work.

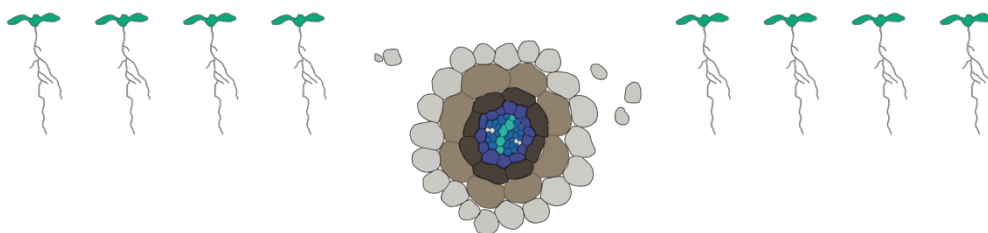
I am extremely thankful to my lab colleagues Bernard, Amandine, Alja, Pauline, Irina, Petra, Moritz and Takayuki for the healthy scientific and competitive environment, as well as the cheerful atmosphere we have achieved all together. I wish they had realized my dedication to work made me moody.

Beyond science, Christelle coached me while I was learning French, a language I have never thought to speak in my life. Debora and Laurence simplified my paperwork and with all of them I shared my weekly cardio sport activities.

Then, I wish to profoundly thank my father Serafino who transmitted me the perseverance, humbleness and the sense of responsibility, while I inherited from my mother Francesca manual skills and the love and respect for plants. Likewise, my aunt Maria Nicoletta, who passed down to me the pleasure of discovery, was essential.

Finally, I was incredibly lucky to meet Paul, Elisa and Leo among my flat mates. I found them authentic friends with whom I enjoyed my stay in Lausanne.

Pietro



## ABSTRACT

Plants evolved innovative solutions to survive and disseminate during land colonization. The key to success was the development of several systems driven by the new needs in the terrestrial environment. The root architecture system functions to mechanically support the plant and anchor it in the soil, as well as to acquire water and minerals.

Concomitantly, plants evolved a long distance transport system composed of xylem, which distributes water and minerals, and phloem (proto- and meta-phloem), which transports so-called sap. Phloem sap, charged in carbohydrates and signalling molecules, is transported from the above-ground source organs to sink organs, such as the root. The protophloem functions as the final conduit into the root apical meristem (RAM), unloading the sap into the developing root apex.

The RAM exhibits specific domains in which each cell undergoes specific sequence of division and differentiation. Intersected gene networks, phytohormones and epigenetic markers allow the maintenance of this pattern and maintain the division/differentiation rate to ensure the optimal root growth.

In *Arabidopsis thaliana*, *BREVIS RADIX (BRX)* counteracts the *CLAVATA3/EMBRYO SURROUNDING REGION 45 – BARELY ANY MERISTEM 3 (BAM3)* module that inhibits protophloem development. The local hyperactivity of this module in *brx* loss-of-function mutants generates undifferentiated cells (so-called gaps) which interrupt protophloem differentiation and thereby transport, and lead to a pleiotropic root phenotype (i.e. a shorter primary root and a more branched root system).

Here I show the effects of a weakened variant of the CLE45 ligand, in which the crucial glycine at position six is replaced by a threonine. CLE45G6T roots are morphologically similar to *brx* and display a stochastic occurrence of gaps.

In order to dissect the protophloem development genetically, I screened for *brx* suppressors uncovering several unknown *bam3* alleles. Likewise, among *brx*

suppressors, deleterious mutations either in *BIG BROTHER* (*BB*) or in *JUMONJI 14* (*JMJ14*) can partially rescue the impaired root growth. Both genes are expressed in the primary root, but their biological function in root development is largely unknown. Here I show that *BB* limits cell proliferation but not elongation. *bb* loss-of-function mutants exhibit enhanced meristematic cell number, but *bb* surprisingly has no longer root compared to wild type. Dissection of the root meristem revealed as well a considerable enhancement of cell density within the root stele. I deduce that *bb* radial cell proliferation might slow down the overall root growth. However, in sensitized genetic backgrounds, such as *brx*, the supernumerary cells counterbalance the reduced root length. My findings therefore reveal a general role for *BB* in limiting cell proliferation in *Arabidopsis* roots. Contrary to *bb*, *jmj14* mutants display neither differences in cell number, nor in cell elongation. *JMJ14*, an H3K4 demethylase, might modulate gene expression and thus indirectly influence root growth in *brx*.

In summary, I identified several second site suppressors of the *brx*, which enhance our understanding of protophloem development and of root development in general.

## RÉSUMÉ

Les plantes ont sélectionné des solutions innovantes pour survivre et se disséminer en milieu aérien. L'un des éléments-clés de ce succès est l'acquisition d'un système racinaire servant à la fois de support mécanique, pour ancrer la plante dans le sol, et aussi d'atout physiologique, permettant à la plante de puiser l'eau et les minéraux présents dans le sol. De manière concomitante, la plante a développé un système de transport longue distance composé du xylème, conduisant la sève brute, et du phloème (composé de proto et méta-phloème), conduisant la sève élaborée. Cette dernière, chargée en photoassimilats et autres molécules signal indispensables à la croissance, est transportée depuis les organes sources photosynthétiques vers les organes puits en cours de développement tel que la racine. Ainsi, le proto-phloème assure le transport ultime de sève élaborée où elle est déchargée au niveau du Méristème Apical Racinaire (MAR) en cours de développement.

Chez *Arabidopsis thaliana*, *BREVIS RADIX (BRX)* inhibe *CLAVATA3/EMBRYO SURROUNDING REGION 45 (CLE45) - BARELY ANY MERISTEM 3 (BAM3)*, module qui inhibe la différenciation du proto-phloème. L'hyperactivité locale de ce module dans les mutants *brx*, chez lesquels BRX n'est pas fonctionnel, génère des cellules indifférenciées (appelées gaps) qui interrompent la différenciation du protophloème et produisent ainsi un phénotype pléiotropique (c'est-à-dire une racine primaire plus courte et un système racinaire plus ramifié).

Dans ce travail, je montre l'effet d'une version atténuée du peptide CLE45: le peptide CLE45G6T présentant la substitution d'une glycine par une thréonine en position six du peptide. Les plantes exprimant CLE45G6T présentent les mêmes défauts de développement que le mutant *brx*, à savoir une différenciation stochastique du phloème.

Un «screen» supresseur mené sur le mutant *brx* a permis l'identification de nombreux acteurs impliqués dans la différenciation du proto-phloème y compris des

allèles inconnus de *bam3*. Ainsi, *big brother (bb)* et *jumonji 14 (jmj14)* permettent de rétablir partiellement la croissance racinaire chez *brx*. Ces deux gènes sont exprimés dans la racine mais leurs fonctions biologiques dans la racine sont peu décrites. Chez le mutant *bb* le nombre de cellules méristématiques est augmentée alors que la longueur de la racine ne l'est pas comparée à la forme sauvage. La prolifération cellulaire radiale chez *bb* pourrait ralentir la croissance racinaire globale. Cependant, chez des mutants affectés dans le développement tel que *brx*, ces cellules surnuméraires pourraient contrebalancer les défauts de croissance. Mes travaux montrent que *BB* limite la prolifération cellulaire dans la racine d'*Arabidopsis* mais n'affecte pas l'élongation cellulaire. Contrairement à *bb*, *jmj14* ne présente pas de différence dans le nombre de cellules, ni dans l'élongation cellulaire. De par son activité de H3K4 demethylase, *JMJ14* pourrait moduler l'expression de certains gènes et ainsi promouvoir indirectement la croissance racinaire chez *brx*.

En résumé, j'ai identifié plusieurs mutations suppressives du mutant *brx*, nous permettant ainsi d'approfondir notre compréhension du phloème et du développement de la racine en général.

Traduit par Bernard Moret

## RÉSUMÉ PUBLIC

Pietro Cattaneo

Département de Biologie Moléculaire Végétale

Les plantes ont sélectionné des solutions innovantes pour survivre et se disséminer en milieu aérien. L'un des éléments clef de ce succès est l'acquisition d'un système racinaire servant à la fois de support mécanique pour ancrer la plante dans le sol mais c'est également un atout physiologique permettant à la plante de puiser l'eau et les minéraux présents dans le sol.

De manière concomitante, la plante a évolué un système de transport longue distance composé du xylème conduisant la sève brute et du phloème (composé de proto et méta-phloème) conduisant la sève élaborée. Cette sève élaborée, chargée en sucres et autres molécules de signalisation indispensables à la croissance, est transportée depuis les parties aériennes vers les organes puits en cours de développement tel que la racine. Ainsi, le proto-phloème assure le transport ultime de sève élaborée où elle est déchargée au niveau de la pointe racinaire en cours de développement. Une mise en place impropre du proto-phloème endommage la continuité du tissu phloémien altérant ainsi sur la distribution de la sève. Ce phénotype microscopique se répercute à l'échelle de la plante entière par une racine courte et une augmentation du nombre de racines latérales (comme chez le mutant *brevis radix (brx)*). Chez *Arabidopsis thaliana*, le gène *BRX* est un régulateur positif clef de la mise en place du proto-phloème dans la racine. Cependant sa fonction biologique est inconnue. Afin d'étudier la fonction génétique et les événements moléculaires contrôlant un processus biologique, le criblage génétique est une approche de choix. Les défauts de différenciation du proto-phloème et ses répercussions sur la croissance racinaire ont été utilisés pour identifier les seconds sites de mutation dans les mutants *brx* restaurant alors une croissance comparable aux plantes sauvages. J'ai ainsi identifié différents allèles du gène *BARELY ANY MERISTEM 3 (BAM3)* permettant à la fois de rétablir la continuité du phloème chez le mutant *brx* mais également sa croissance racinaire.

Par ailleurs, j'ai identifié deux autres gènes permettant de rétablir la longueur de la racine chez *brx* mais n'agissant pas sur la mise en place du proto-phloème. Ainsi *BIG BROTHER (BB)* limite la prolifération cellulaire à la fois de manière radiale et longitudinale sans pour autant agir sur l'élongation cellulaire. De même *jumonji 14 (jmj14)* restaure partiellement la croissance racinaire du mutant *brx*. De par son activité moléculaire, *JMJ14* pourrait moduler l'expression de certains gènes et ainsi promouvoir indirectement la croissance racinaire chez le mutant *brx*.

En résumé, j'ai identifié plusieurs gènes, nous permettant ainsi d'approfondir notre compréhension du développement de la racine en général.

Traduit par Pauline Anne

# INTRODUCTION

- **Plant innovations in evolution**

The plant kingdom shaping the terrestrial biosphere is the result of a long and fascinating evolutionary process that started around 470 million years ago (Harrison, 2017). New needs caused by the shift from aquatic to terrestrial environment favoured novel developmental solutions in plants. In particular, they evolved innovative mechanisms to implement CO<sub>2</sub> exchange, water and nutrient transport, but also structural support (Harrison, 2017; Lucas et al., 2013). One of the factors that undoubtedly contributed to land colonization was the development of the root system. The earliest and simplest root systems conferred mechanical support, anchoring the plant in the soil and mediating mineral uptake. Because plants are physically anchored to the place where they germinate and grow, in natural conditions they cannot escape exposure to local abiotic and biotic environmental factors (among them UV radiation, drought, salinity, extreme temperature and herbivores) (Harrison, 2017). As sessile organisms they thus developed different mechanisms to not only compensate, but also adapt to environmental changes (Osmont et al., 2007). Therefore, genetic adaptation and developmental plasticity contributed to the complex variations in anatomy, appearance and architecture of the plant kingdom. The ability to adapt their growth has been one of the keys to success that permitted plants to survive and propagate in any environment (Bauby et al, 2007; Gujas et al., 2012; Osmont et al., 2007).

Contrary to animals, plants begin developing true, adult organs only after germination. The post-germination organogenesis and development is supported by indeterminate meristems, specialized regions that keep the balance between cell proliferation and the incorporation of newly produced cells into organs through cellular differentiation (Heidstra et al., 2014). A meristem is composed of three distinct domains: a confined pool of slowly dividing, self-renewing stem cells; a region where the derived undifferentiated daughter cells divide rapidly; and a third domain in which the cells undergo differentiation. The identity and the partitioning of each domain is maintained

by a unique hormonal profile, as well as a specific gene expression program that is also subject to epigenetic regulation (Heidstra et al., 2014; Pikaard et al., 2014).

Shoot and root apical meristems are the two primary meristems that guarantee consecutive and indefinite growth above-ground and below-ground, respectively. They are established already during embryo development, each at the opposite end of the apical-basal axis. Plants also have secondary meristems that emerge only later during development and contribute to size increase and plastic growth response, which can constitute a fitness advantage. Overall, the three-dimensional growth in multiple axes is the result of the combination of primary and secondary meristems (Harrison et al., 2017; Heidstra et al., 2014; Niklas, 1997;).

Biologists have always been attracted by the complex and dynamic process of plant development. Beyond human curiosity, elucidating the mechanisms that modulate plant growth could be of high interest in view of the increasing need for plant-derived products. Due to its developmental simplicity, its small size, its short life cycle, its high seed production and its sequenced genome, the dicotyledonous plant *Arabidopsis thaliana* (*Arabidopsis*) has been used extensively as a model organism to study anatomy, genetics, metabolism and development.

- **A matter of growth**

Among plant species, organ size displays remarkable differences. Even individuals of the same species can modulate organ growth in response to environmental inputs. Nevertheless, comparatively low intraspecific variation was observed in the final size of *Arabidopsis* organs. This might be explained by developmental constraints imposed by tight genetic controls during plant organ growth (Krizek, 2009). In general, plant growth rate can be regulated by cell proliferation, cell expansion, dispersed cell divisions and energy balance. Each of these factors is controlled by a specific genetic regulatory network, although altogether they contribute to the final size (Vanhaeren et al., 2016). Mechanisms of cross-talk contribute to link the different pathways, thereby allowing a dynamic and accurate level of control. Many genes have been reported to

enhance or limit plant organ size. Some of them act downstream of plant hormones, while others appear to act independently (Busov et al., 2007). Because the description of the growth machinery is still very incomplete, the discovery of new key regulators of organ growth is necessary to advance our current understanding of these networks. Moreover, it remains unclear whether gene functions are strictly conserved across different organs.

- **A model to study growth and size mechanisms: the *Arabidopsis* leaf**

Over the past years *Arabidopsis* leaves have been used to identify growth regulators and gene networks that control final organ size. Unlike most plant organs, leaves display a determinate growth pattern. They originate at the flanks of the shoot apical meristem and grow mainly through cell proliferation in the early stages. Later, cells at the tip of the leaf stop dividing, a cell cycle arrest front moves basipetally (i.e. towards the stem the leaf originates from) and gradually leads cells to switch from division to expansion. During this transition, chloroplasts start differentiating, while cells in the epidermis called meristemoids give rise to stomatal lineages. A further increase in cell expansion leads to the final organ size. These observations highlight the cooperation between cell proliferation and expansion to accomplish final organ size and shape. The two processes are synchronized spatially and temporally by a set of networks that interact and also respond to environmental inputs (González et al., 2015; Tsukaya, 2013).

Many genes have been reported to control the duration of the cell proliferation phase: *AINTEGUMENTA (ANT)*, *GROWTH REGULATOR FACTOR 3 (GFR3)* and *GRF5* are mainly positive regulators of cell proliferation (González et al., 2012). When overexpressed, they induce larger leaves. By contrast, other genes limit cell proliferation: *DA1* encodes an ubiquitin receptor that restricts cell proliferation. *da1-1* dominant-negative mutants produce larger organs by prolonging the cell division phase (Li et al., 2008). Also *BIG BROTHER (BB)*, an E3 ubiquitin ligase, is known to

be involved in limiting organ size (Dish et al., 2006). *BB* is also known as *ENHANCER OF DA1 (EOD1)*, because the mutant amplifies the growth effects of *da1-1* (Li et al., 2008). As recently reported (Vanhaeren et al., 2017), the *bb* mutants display a delay in cell differentiation as a consequence of a prolonged cell division phase. In the early growth phase, young leaves are smaller than wild type because of prolonged cell division activity. The *bb* phenotype emerges later during leaf growth when the expansion activity is also completed. *da1-1 bb* double mutants display even bigger leaves as a result of the synergism between the two genes. Among regulators that influence various cellular processes *ANGUSTIFOLIA 3 (AN3)* seems to control both the rate and the length of the cell division phase (Tsukaya et al., 2006).

Overall it becomes evident that organ morphogenesis is a complex mechanism controlled by the precise regulation of cell size and number. These two events likely contribute equally, although how these two processes are buffered still remains subject of continuing investigation. The compensatory effect that emerged from the analysis of some mutants and overexpression lines introduces a further level of complexity. For instance, loss-of-function *ant* mutants display small leaves compared to wild type. Despite a reduced cell number, further observations revealed a greater cell volume compared to wild type. Likewise, the *an3* mutant displays a decrease in cell number that is accompanied by an increase in cell size, however overexpression of both *ANT* and *AN3* increases cell number in leaves without any reduction in cell volume (Tsukaya, 2013). Those findings suggest a crosstalk between cell division and expansion that in particular conditions, such as a reduction in cell proliferation, may reinforce cell expansion activity. This presumably may be a strategy to assure a certain organ size threshold and avoid growth defects that negatively affect the plant's fitness. Remarkably, experimental observations indicate that cell proliferation or cell expansion alone are not sufficient to control final organ size (Anastasiou et al., 2007). Up to now several players of the complex leaf growth machinery have been identified. Among them many have been functionally characterized; however, the genetic basis is still not completely uncovered. Apart from genetic constraints, various environmental factors influence final size. The multilevel networks and the broad connections make the final pattern even more complex to decipher.

- **Plant root development**

The development of the root system strongly contributed to the land colonization by plants. The root system functions primarily to provide mechanical support by anchoring the plant in the soil, and to mediate water and nutrient uptake. Roots also can contribute to photoassimilate storage and phytohormone synthesis (Osmont et al., 2007).

Plant growth and reproductive capacity strongly depend on the availability of water and nutrients. Therefore, the high variability of the root system morphology is a direct consequence of adaptation to variable environmental conditions (Lucas et al., 2013).

The primary root of *Arabidopsis* originates during embryogenesis. It is only after germination that its allorhizic root system starts developing: the primary root breaks into the soil and grows deep along the gravity vector. Lateral roots, which grow at more horizontal angles, derive from the primary root later on during root system development (Osmont et al., 2007).

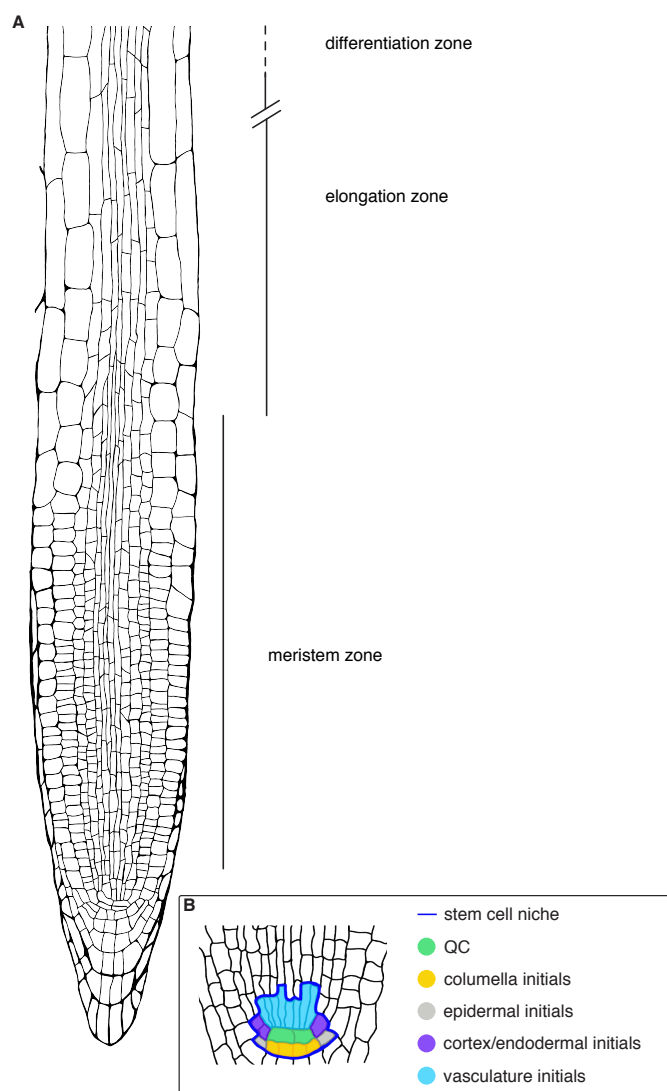


**Figure 1 | *Arabidopsis* root tip.**

A | The scheme shows the longitudinal root organization and B | the stem cell niche cell types within the meristem.

can be divided into four regions: columella, meristematic zone, elongation zone and differentiation zone. The columella allows the root to grow through the soil and protects the above tissues. The meristematic zone provides new cells for root growth, while in the elongation zone, cells rapidly elongate through cell wall expansion. Cell identity is acquired in the differentiation zone (Gujas et al., 2011; Taiz and Zeiger, Plant Physiology second edition) (Figure 1a). While its differentiation starts earlier in the root, the radial tissue pattern is complete and visible only in the differentiation zone (Bauby et al., 2007).

Contrary to leaves, roots display a continuous growth. Consequently, cell proliferation, elongation and differentiation occur simultaneously within the root tip. The spatio-temporal synchronization and orchestration of those different phases is modulated by a class of signalling molecules called phytohormones, specific gene networks and epigenetic markers. In addition, checkpoints are established to determine whether a cell could switch from one phase to another (Osmont et al., 2007; Takatsuka et al., 2015; Ubeda-Tomás et al., 2012). During the past years, new discoveries contributed to the elucidation of the mechanisms that maintain the root stem cell niche and orchestrate the spatial subdivision in specialized domains within the root apex.

- **Mechanisms controlling and maintaining root growth**

Root meristem growth is meticulously controlled by a small pool of slowly dividing cells, the quiescent centre (QC), in the stem cell niche. These cells provide the molecular signals that control stem cell division rate and maintain stem cell identity (Figure 1B) (Tian et al., 2014). Stem cell divisions generate pluripotent daughter cells that acquire identity throughout positional molecular signals that lead to anticlinal and periclinal divisions, which establish the cell lineages for the developing radial tissue pattern (Helariutta, 2007). The maintenance of the QC thus is crucial during the entire plant life cycle.

The transcription factor *WUSCHEL-RELATED HOMEODOMAIN 5* (*WOX5*) is expressed in the quiescent centre from inception onwards. Loss-of-function *wox5* mutants display

QC misspecification, indicating essential *WOX5* functions in stem cell maintenance. The *WOX5* function is counteracted by *CLAVATA3/EMBRYO SURROUNDING REGION-RELATED 40 (CLE40)*. *CLE40* encodes a peptide that is secreted from differentiated columella cells and is perceived by receptors that are expressed below the QC. *CLE40-WOX5* balance therefore contributes to keeping the QC spatially intact over time (Heidstra et al., 2014).

The two *PLETHORA (PLT1 and 2)* transcription factors also participate in stem cell niche maintenance and root meristem zonation: loss-of-function *plt1* and *plt2* mutants display an early meristem arrest as a consequence of stem cell differentiation, whereas in a gradient-dependent manner *PLT2* gain-of-function leads to an enlarged meristem and shoot-ward shift of the high division rate domain. Moreover, induction of *PLT2* inhibits cell expansion, suggesting that the decline in *PLT* levels along the gradient contributes to the transition to cell differentiation. The *PLT* gradient shape defines the spatial location of two boundaries: the boundary between slowly and rapidly cycling cells and the shoot-ward boundary of the meristem (Mähönen et al., 2014).

As mentioned above, phytohormones can also influence root growth. The *AUXIN RESPONSE FACTORS 10 (ARF10)* and *ARF16* genes have been found to restrict distal stem cell daughter fate and promote columella cell differentiation in response to auxin. *arf10 arf16* double mutant roots display an enlarged undifferentiated cell domain. In contrast, higher auxin levels reduce *WOX5* expression thereby increasing stem cell differentiation (Heidstra et al., 2014).

Furthermore, an interplay between the auxin gradient and *PLTs* has been shown to be relevant in defining zonation within the developing root. Auxin influences cell division, expansion and differentiation rate, but also promotes *PLT* transcription. The cooperation between auxin and *PLT* occurs on different timescales, allowing roots to better adapt to environmental conditions. Whereas auxin mediates rapid response during root growth, the stable *PLT* levels prevent loss of coordination in zonation (Mähönen et al., 2014; Takatsuka et al., 2015).

Another mechanism orchestrating stem cell niche and meristem control is epigenetic: i.e. concerns heritable changes in gene expression in a cell lineage. In the nucleus,

the genetic material is arranged as chromatin. DNA is wrapped around histone core protein complexes and package into structural units called nucleosomes. Amino acids at the N-terminal tails of H3 and H4 histones protrude from nucleosomes and thus are easy to modify. Among histone covalent modifications, acetylation and methylation are the best characterized in plants. Both influence the density of the chromatin, its consequent accessibility for the transcriptional machinery, and thus overall gene expression level (Takatsuka et al., 2015).

Histone H3 lysine 4 (H3K4) di- and tri-methylation (me<sub>2</sub> and me<sub>3</sub>) are normally associated with transcriptional activation in eukaryotes. The *Arabidopsis SET DOMAIN GROUP 2 (SDG2)* gene encodes a H3K4 methyltransferase enzyme: *sdg2* mutants have an abnormal stem cell niche and reduced cell division activity further up in the meristem. Moreover, in *sdg2* mutants, *PLT1* expression is inhibited, suggesting that SDG2 may regulate *PLT1* expression through H3K4 methylation (Takatsuka et al., 2015; Yao et al., 2013).

*WOX5* promoter H3K4me<sub>3</sub> levels can also influence expression of *WOX5* in the QC. The gene *REPRESSOR OF WUSCHEL 1 (ROW1)* is expressed in the root meristem, but not in the QC. ROW1 binding to H3K4me<sub>3</sub> on the *WOX5* promoter might inhibit the positive function that the tri-methylation has on the *WOX5* expression in the proximal meristem (Zhang et al., 2015).

- **Long-distance transport in plants: xylem versus phloem**

To support the three-dimensional growth during land colonization, plants evolved different adaptive strategies. In particular, embryophytes exhibit a recurring organization pattern composed of three mayor types of tissues: a centrally localized vascular cylinder, which is delimited by a ground tissue, which are finally protected by an outermost layer, the epidermis.

The vasculature provides mechanical support to the developing organs and the whole body as well as long distance transport of water, nutrients, photosynthates, hormones and other signalling molecules throughout the plant. Because of the evolutionary

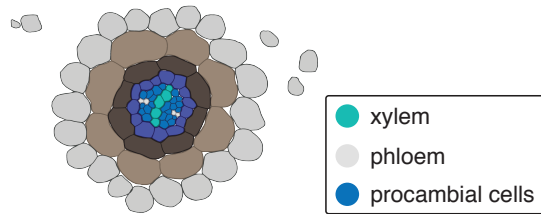


**Figure 2 | Root diarch tissue pattern within the root.**

Schematic representation of the tissue within the *Arabidopsis* root.

advantages, this organization pattern has quickly radiated and been widely adapted in embryophyte organs (Harrison, 2015; Lucas et al., 2013).

Young *Arabidopsis* roots display a simple diarch pattern: a central axis across the stele is formed by the neighbouring protoxylem and metaxylem, while two phloem poles located opposite of each

other and separated by procambial cells flank the xylem tissue (Figure 2) (Lucas et al., 2013).

Xylem cells transport water and minerals from the root to the above-ground organs throughout tracheids or vessels, which are formed from the interconnected cell walls of dead cells without living cellular content (Taiz and Zeiger, Plant Physiology second edition).

The phloem transports photosynthetic assimilates and molecular signals from source organs to sink organs across the plant (Lucas et al., 2013). This tissue was first observed and described in 1837 by Theodor Hartig (Heo et al., 2014). Since then, the progress in microscopy in particular have expanded our knowledge of phloem structure and function. Functional phloem consists of sieve elements (SEs; protophloem and metaphloem) and companion cells (CCs) (Van Bel, 2003). Differentiated sieve elements are slender, elongated and enucleated cells which run along the longitudinal root axis to establish the sieve tube network (Mullendore et al., 2010). In their differentiation, sieve elements undergo cell wall thickening and elongation. Later on, they develop perforated cell walls at the cell junctions (the sieve plates) with the adjacent differentiating sieve element cells. Whereas the reinforced cell walls assure mechanical support against the high turgor pressure derived from the elevated sugar concentration of phloem sap, the sieve plates establish symplastic continuity throughout the sieve tube. Moreover, sieve element tubes undergo drastic changes in cellular organization. To maximize the symplastic transport activity, mature sieve elements have lost many of their organelles: vacuoles, the rough endoplasmic

reticulum and the Golgi apparatus. However, plasma membrane, smooth ER and proteinaceous material are retained as a stock for certain enzymes, and as a track for protein transport. Sieve element differentiation culminates with the enucleation process. The final and differentiated sieve element cells thus look deeply different from their precursors (Lucas et al., 2013; Rodriguez-Villalon et al., 2014). Despite the majority of the cellular components being degenerated, they are still living cells. In addition, sieve elements are abundant in plasmodesmata, microscopic channels that traverse the cell wall, thereby allowing symplastic connection with the neighbouring companion cells. Contrary to sieve elements, companion cells appear densely packed with a large nucleus, small vacuole, numerous mitochondria and abundant ER. Companion cells therefore support the sieve elements with their metabolic functions and keep them alive (Heo et al., 2014).

For several years, microscopy observations were limited to histological descriptions of fixed specimens to describe phloem tissue anatomy. Analysis of mutants, phloem

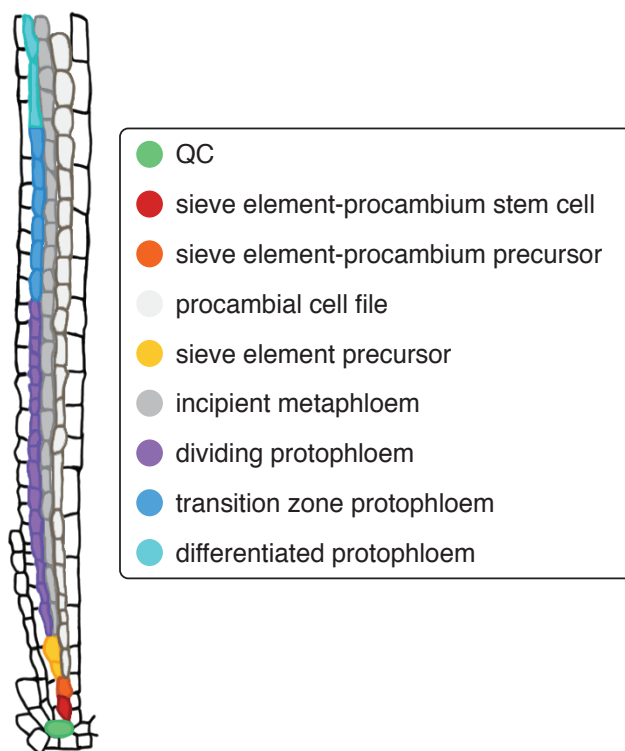


**Figure 3 | Overview on protophloem development in *Arabidopsis*.**

Schematic representation showing the longitudinal ontogeny and cells organization.

markers and new staining protocols have recently uncovered parts of the mechanism controlling phloem ontogeny.

### • Origin of protophloem

One of the most obvious differences that distinguish plants from animals is the presence of the cell wall. It confers structural advantages during organ formation, even if plant cells are thus more rigid and unable to move. Therefore, the position of

the division plane influences the cell lineage fate and tissue growth during organ development (Taiz and Zeiger, Plant Physiology second edition). Periclinal divisions that occur parallel to the surface of the plant body result in radial growth, while anticlinal divisions that occur perpendicular contribute to longitudinal growth (De Rybel et al., 2015). Concomitant with spatial position, the adoption of a specific genetic program concurs with the achievement of cell differentiation. The description of the chronological anticlinal and periclinal divisions that occur early in the root meristem and lead to different cell lineages has been one of the key steps. Each phloem pole derives from a single stem cell that firstly divides anticlinally to generate the stem cell daughter cells. A daughter cell will eventually switch to perform one periclinal division to produce two cells: while the inner cell will give rise to the procambial cell file by extended anticlinal divisions, the outer cell (the sieve element precursor) divides once more periclinally. The inner daughter cell then will give rise to the incipient metaphloem, which will differentiate later to replace the protophloem. The protophloem is generated from the outer daughter cell and becomes the first differentiated root tissue (Figure 3) (Lucas et al., 2013; Rodriguez-Villalon et al., 2014). In 1994, Oparka et al. identified and classified protophloem as a transient tissue that connects the conducting phloem with the receiver cells in sink tissues. In Arabidopsis roots, the unloading of the phloem sap occurs exclusively from protophloem in the zone of root elongation. Recently, Ross-Elliott et al., 2017 provided experimental data with fluorescent probes such as CFDA to support this hypothesis. Protophloem therefore functions as a bridge between the differentiated metaphloem and the actively developing and growing tissues in the root apex. It supplies assimilates to the apical region of the root, where the neighbouring tissues are still differentiating.

The protophloem differentiation process follows different steps, where cells gradually acquire specific features such as thicker cell wall and nucleus degeneration (Rodriguez-Villalon et al., 2014). Based on the particular stage of differentiation, protophloem cells have different competences, which allow the transport and the unloading in the root meristem. Ross-Elliott and co-workers, 2017 identified four different and specialized domains: the protophloem development zone, in correspondence to the QC, is the region where the precursors of the phloem originate

through a sequence of periclinal divisions as previously described. Here cells do not display any transport or unloading activity, probably because of the early stage of development. The following protophloem unloading domain allows the transfer of the sap to the neighbouring pericycle cells across plasmodesmata. Further up, cells in the protophloem translocation domain simply function as a conductive tube. The intense callose deposition leads to the closure of lateral symplastic connections, preventing sap diffusion. The following protophloem transfer zone mediates the switch of the sap flow between the metaphloem and protophloem. Later, the protophloem gradually degenerates and its transport function is replaced by the differentiated metaphloem (Figure 4).

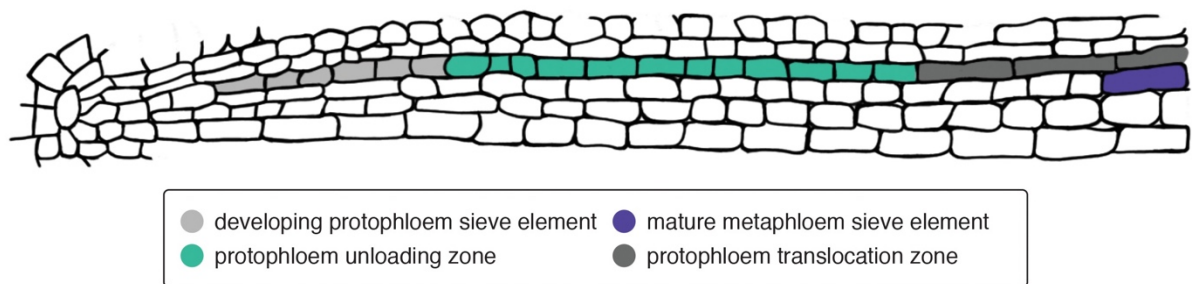


**Figure 4 | Protophloem domains subdivision.**

Schematic representation of the different domains of protophloem sieve element development in the *Arabidopsis* root meristem.

Fully continuous and differentiated protophloem is necessary for sap supply and thus proper root growth. Thus, events disrupting the protophloem continuity or the temporal and spatial domain establishment might severely compromise final root growth (Ross-Elliott et al., 2017). As mentioned before, cell lineage establishment and development has to be supported by genetic programs. Mutant analysis identified several key factors involved in sieve element differentiation, such as the MYB transcription factor ALTERED PHLOEM DEVELOPMENT (*APL*) and the plasma membrane-associated protein of unknown function OCTOPUS (*OPS*) (Bonke et al., 2003; Truernit et al., 2012). The fact that *apl* loss-of-function mutants develop xylem-like cells at the phloem position defines *APL* as a positive regulator of protophloem identity (Bonke et al., 2003). Recently Furuta et al., 2014 partially elucidated the molecular mechanisms that

drive protophloem differentiation. APL controls the expression of the NAC45 and NAC86 transcription factors, which modulate NAC45/86 DEPENDENT EXONUCLEASE DOMAIN PROTEIN1 (NEN1) and NEN4 activity, both nucleases that are involved in the last stage of sieve element differentiation, i.e. enucleation.

Undifferentiated cells that fail to thicken their cell wall and do not undergo enucleation interrupt protophloem continuity in *ops* loss-of-function mutants. Characterization of wild type and *ops* mutants has shown that gap cells appear in the protophloem transition zone, the region where key events of protophloem sieve element differentiation take place. The protophloem disconnections might influence the distribution of metabolites and hormones in the root meristem, leading to the consequent impaired root growth (Truernit et al., 2012; Rodriguez-Villalon et al., 2014, 2015).

The examples mentioned highlight the relevance of the phloem in root growth and the existence of several counteracting pathways that are required for the development of functional phloem, however numerous aspects remain unclear to date.

- ***BREVIS RADIX (BRX)*: a positive regulator of protophloem development**

*BREVIS RADIX (BRX)* was identified from a natural genetic variation screen in *Arabidopsis* root growth and encodes a polarly localized plasma membrane-associated protein (Mouchel et al., 2004; Scacchi et al., 2010). *brx* loss-of-function mutants as well as *ops* loss-of-function mutants display gaps along the protophloem files (Scacchi et al., 2010; Truernit et al., 2012). Comparative analysis of the nuclear marker mDII::VENUS in *brx* and *ops* revealed that in both mutants, the nucleus fails to degenerate in gap cells (Rodriguez-Villalon et al., 2014).

Moreover, analysis of gap cells revealed the absence of the typically strong propidium iodide cell wall staining of protophloem cells. The failure to develop a continuous protophloem strand also negatively affects the differentiation of neighbouring companion cells. Precisely, the expression pattern of the companion cell-specific

marker (*SUCROSE TRANSPORTER 2*) is patchy or absent (Rodriguez-Villalon et al., 2014). The importance of BRX in sieve element development is also suggested by its expression pattern from the sieve element precursor cell throughout the protophloem (Depuydt et al., 2013).

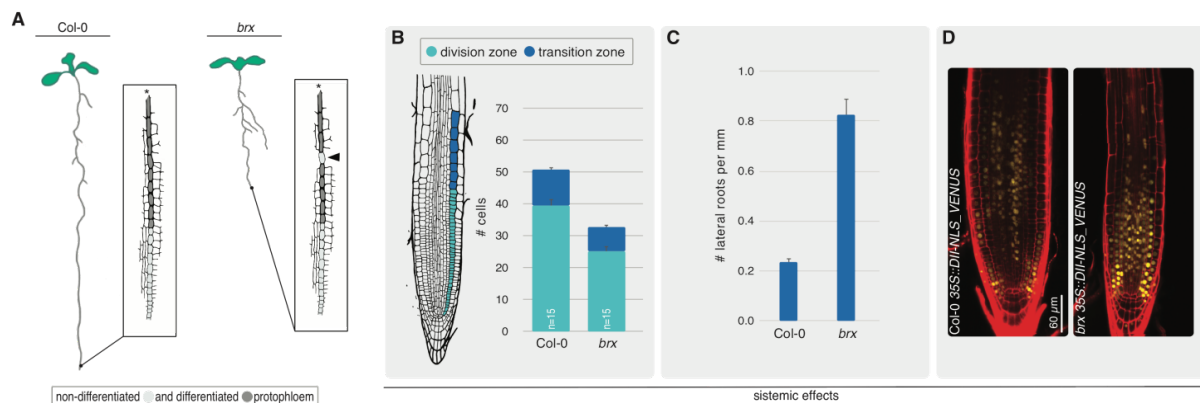


### Figure 5 | *brx* mutant.

A | The schematic representation shows the short root phenotype of *brx* as a consequence of the interrupted protophloem; B | overview of the systemic effects in *brx*: impaired meristematic activity, C | lateral root density compared to wild type and D | auxin distribution in the root tip.

*brx-2* (a *brx* null allele in the *Col-0* reference background) displays a reduced primary root growth (Figure 5A). It displays a small meristem size compared to that of wild type, while the density of the lateral roots is increased (Figure 5B and C) (Mouchel et al., 2004). The inverse auxin activity DII::VENUS revealed in addition reduced levels of the phytohormone auxin in the growing root meristem (Figure 5D).

In our research group, the *barely any meristem 3* (*bam3*) loss-of-function mutant was identified as a *brx-2* second-site suppressor mutant (Depuydt et al., 2013). *BAM3* encodes a receptor-like kinase that perceives CLAVATA 3/EMBRYO SURROUNDING REGION 45 (CLE45) peptide and inhibits protophloem differentiation (Depuydt et al., 2013). Both *BAM3* and *CLE45* are expressed from the precursor of the sieve element cells onwards. BRX negatively regulates *BAM3* expression, thereby possibly controlling the timing of the sieve element differentiation and maintaining the cell identity. The inability to counteract the CLE45/*BAM3* pathway in *brx-2* likely

determines the stochastic gaps along the protophloem (Rodriguez-Villalon et al., 2014, 2015).

Functional protophloem is important to transport metabolites and signalling molecules into the meristem region. Therefore, the impaired unloading of metabolites such as photosynthetic assimilates in the *brx-2* meristem region might lead to a reduced cell division and consequently to a smaller meristem size. Similarly, an impaired auxin flow might elucidate the absence of the incipient metaphloem cell file in *brx-2*, due to the hormone's role in the timing of periclinal divisions in sieve element precursors. To support this hypothesis, wild type seedlings treated with mild concentration of auxinole, a specific inhibitor of the nuclear auxin receptor, show abolished periclinal sieve element precursor divisions (Rodriguez-Villalon et al., 2014, 2015).

Altogether the data suggest that BRX plays a key role in the control of protophloem development. However, because *brx bam3* double mutants develop fully continued protophloem strands it might be possible that the two genes are not directly required for protophloem formation. Rather, they might be part of a regulatory layer that determines the timing of differentiation, and which could also switch in particular environmental conditions. Indeed, the systemic effects caused by the protophloem discontinuity, such as short root growth and higher lateral root density, might lead to a better fitness in extreme environments (Gujas et al., 2012; Rodriguez-Villalon et al., 2014). Nevertheless, the molecular mechanisms of the BRX pathway that lead to sieve element differentiation remain unknown. In order to find additional components of the BRX-dependent pathway, an EMS genetic screen has been performed based on *brx-2* short root recovery (Figure 6) (Depuydt et al., 2013).

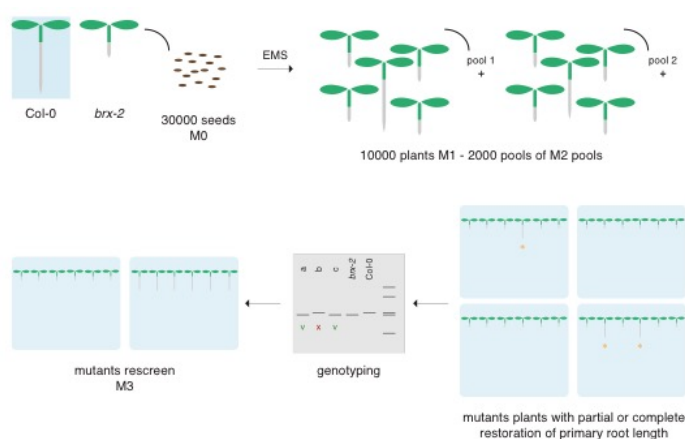


**Figure 6 | EMS screening of *brx-2* genetic suppressors.**

The scheme shows the isolation of *brx-2* suppressors based on the recovery of the primary root growth.

- **Screening of *brx-2* genetic suppressors: what's new?**

The initial M2 generation seedlings screen identified 33 suppressors based on the primary root growth recovery. A few of those candidates were identified (*BAM3*, *CVP2* and *MAKR5*) (Depuydt et al., 2013; Kang et al., 2016; Rodriguez-Villalon et al., 2014, 2015), however other suppressors still remain to be investigated.

- **Research outline**

Initially, *brx* suppressors were identified based on the recovery of the primary root length, because the gap cell phenomenon at the origin of the systemic effects was poorly investigated at the time. Among the different suppressors, *bam3* loss-of-function induced the highest degree of primary root length restoration. Because exogenous application of CLE45 inhibits totally protophloem development already at nM concentrations, to generate knock out mutants of CLE45 peptide became desirable (Rodriguez-Villalon et al., 2014). In the first two chapters I describe the strategy we adopted to generate a CLE45 dominant negative version, and the consequences it has during root development.

Because the role of BRX as a regulator of protophloem differentiation became clearer, we aimed to identify new *brx-2* suppressors. The screen of the *brx-2* mutagenized M2 population continued, but we adopted a multi-faceted strategy rather than consider merely primary root length. In particular, I considered the recovery of the protophloem continuity as a main parameter to classify the *brx* suppressors. The results are presented in chapter 3.

Among the first 33 suppressors, analysis by whole genome sequencing led to the identification of a non-synonymous substitution in the conserved RING-finger domain of the protein BIG BROTHER. The corresponding gene was previously identified as a regulator of floral organ size in 2006 by Dish et al.. Vanharen et al., in 2017 also described the importance of *BB* during leaf growth, highlighting the prolonged proliferation phase in *bb* loss-of-function mutants. Up to date nobody has investigated

whether *BB* might function also during root growth. In chapter 4 I investigate how *bb* partially restores the primary root length of *brx-2* and how it acts during root growth. In the last chapter (5), I present the preliminary results of a new *brx-2* suppressor. *JUMONJI 14* (*JMJ14*) loss-of-function has been recently proven to restore defective *brx* primary root length with the same degree as *bb*. *JMJ14* belongs to a large family of H3K4 demethylases. While *JMJ14* functions regulating the transition from vegetative to floral phase have been described (Ning et al., 2015), we aim to elucidate its role in root development.

## References

- Anastasiou E, Lenhard M (2007) **Growing up to one's standard**. *Current Opinion in Plant Biology* 10: 63-69.
- Bauby H, Divol F, Truernit E, Grandjean O, Palauqui JC (2007) **Protophloem differentiation in early Arabidopsis thaliana development**. *Plant Cell Physiol.* 48: 97-109.
- Bonke M, Thitamadee S, Mähönen AP, Hauser MT, Helariutta Y (2003) **APL regulates vascular tissue identity in Arabidopsis**. *Nature* 426: 181-6.
- Briggs GC, Mouchel CF, Hardtke CS (2006) **Characterization of the plant-specific BREVIS RADIX gene family reveals limited genetic redundancy despite high sequence conservation**. *Plant Physiol.* 140: 1306-16.
- Busov VB, Brunner AM, Strauss SH (2008) **Genes for control of plant stature and form**. *New Phytol.* 177: 589-607.
- Depuydt S, Hardtke CS (2011) **Hormone signalling crosstalk in plant growth regulation**. *Curr Biol.* 21: R365-73.
- Depuydt S, Rodriguez-Villalon A, Santuari L, Wyser-Rmili C, Ragni L, Hardtke CS (2013) **Suppression of Arabidopsis protophloem differentiation and root meristem growth by CLE45 requires the receptor-like kinase BAM3**. *Proc Natl Acad Sci U S A* 110: 7074-9.
- De Rybel B, Mähönen A, Helariutta Y, Weijers D (2015) **Plant vascular development: from early specification to differentiation**. *Nature reviews molecular cell biology* 17: 30-40.
- Disch S, Anastasiou E, Sharma VK, Laux T, Fletcher JC, Lenhard M (2006) **The E3 ubiquitin ligase BIG BROTHER controls arabidopsis organ size in a dosage-dependent manner**. *Curr Biol.* 16: 272-9.
- Furuta KM, Yadav SR, Lehesranta S, Belevich I, Miyashima S, Heo JO, Vatén A, Lindgren O, De Rybel B, Van Isterdael G, Somervuo P, Lichtenberger R, Rocha R, Thitamadee S, Tähtiharju S, Auvinen P, Beeckman T, Jokitalo E, Helariutta Y (2014) **Plant development. Arabidopsis NAC45/86 direct sieve element morphogenesis culminating in enucleation**. *Science* 345: 933-7.
- González N, Vanhaeren H, Inzé D (2012) **Leaf size control: complex coordination of cell division and expansion**. *Trends Plant Sci.* 17: 332-40.
- González N, Inzé D (2015) **Molecular systems governing leaf growth: from genes to networks**. *Journal of Experimental Botany* 66: 1045-1054.
- Gujas B, Alonso-Blanco C, Hardtke CS (2012) **Natural Arabidopsis brx loss-of-function alleles confer root adaptation to acidic soil**. *Curr Biol.* 22: 1962-8.
- Harrison J (2017) **Developmental and genetic innovations in the evolution of plant body plans**. *Proceedings of the Royal Society B: Biological Sciences* 372: 20150490.
- Heidstra R, Sabatini S (2014) **Plant and animal stem cells: similar yet different**. *Nat Rev Mol Cell*

Biol. 15: 301-12.

Helariutta Y (2007) **Cell signalling during vascular morphogenesis**. *Biochem Soc Trans.* 35: 152-5.

Heo JO, Roszak P, Furuta KM, Helariutta Y (2014) **Phloem development: current knowledge and future perspectives**. *Am J Bot.* 101: 1393-402.

Kang YH, Hardtke CS (2016) **Arabidopsis MAKR5 is a positive effector of BAM3-dependent CLE45 signaling**. *EMBO Rep.* 17:1145-54.

Krizek BA (2009) **Making bigger plants: key regulators of final organ size**. *Curr Opin Plant Biol.* 12: 17-22.

Li Y, Zheng L, Corke F, Smith C, Bevan MW (2008) **Control of final seed and organ size by the DA1 gene family in Arabidopsis thaliana**. *Genes Dev.* 22: 1331-1336.

Lucas WJ, Groover A, Lichtenberger R, Furuta K, Yadav SR, Helariutta Y, He XQ, Fukuda H, Kang J, Brady SM, Patrick JW, Sperry J, Yoshida A, López-Millán AF, Grusak MA, Kachroo P (2013) **The plant vascular system: evolution, development and functions**. *J Integr Plant Biol.* 55: 294-388.

Mähönen AP, Ten Tusscher K, Siligato R, Smetana O, Díaz-Triviño S, Salojärvi J, Wachsman G, Prasad K, Heidstra R, Scheres B (2014) **PLETHORA gradient formation mechanism separates auxin responses**. *Nature* 515: 125-129.

Mouchel CF, Briggs GC, Hardtke CS (2004) **Natural genetic variation in Arabidopsis identifies BREVIS RADIX, a novel regulator of cell proliferation and elongation in the root**. *Genes Dev.* 18: 700-714.

Mouchel CF, Osmont KS, Hardtke CS (2006) **BRX mediates feedback between brassinosteroid levels and auxin signalling in root growth**. *Nature* 443: 458-61.

Mullendore DL, Windt CW, Van As H, Knoblauch M (2010) **Sieve tube geometry in relation to phloem flow**. *Plant Cell* 22: 579-93.

Ning YQ, Ma ZY, Huang HW, Mo H, Zhao TT, Li L, Cai T, Chen S, Ma L, He XJ (2015) **Two novel NAC transcription factors regulate gene expression and flowering time by associating with the histone demethylase JMJ14**. *Nucleic Acids Res.* 43: 1469-84.

Oparka KJ, Duckett CM, Priori OAM, Fisher DB (1994) **Real-time imaging of phloem unloading in the root tip of Arabidopsis**. *The Plant Journal* 6: 759-766.

Osmont KS, Sibout R, Hardtke CS (2007) **Hidden Branches: developments in root system architecture**. *Annu Rev. Plant Biol.* 58: 93-113.

Pikaard CS, Mittelsten Scheid O (2014) **Epigenetic regulation in plants**. *Cold Spring Harb Perspect Biol.* 6: a019315.

Rodriguez-Villalon A, Gujas B, Kang YH, Breda AS, Cattaneo P, Depuydt S, Hardtke CS (2014) **Molecular genetic framework for protophloem formation**. *Proc Natl Acad Sci U S A* 111: 11551-6.

Rodriguez-Villalon A, Gujas B, van Wijk R, Munnik T, Hardtke CS (2015) **Primary root protophloem**

**differentiation requires balanced phosphatidylinositol-4,5-biphosphate levels and systemically affects root branching.** *Development* 142: 1437-46.

Ross-Elliott TJ, Jensen KH, Haaning KS, Wager BM, Knoblauch J, Howell AH, Mullendore DL, Monteith AG, Paultre D, Yan D, Otero S, Bourdon M, Sager R, Lee JY, Helariutta Y, Knoblauch M, Oparka KJ (2017) **Phloem unloading in Arabidopsis roots is convective and regulated by the phloem-pole pericycle.** *eLife* 6: 24125.

Scacchi E, Salinas P, Gujas B, Santuari L, Krogan N, Ragni L, Berleth T, Hardtke CS (2010) **Spatio-temporal sequence of cross-regulatory events in root meristem growth.** *Proc Natl Acad Sci U S A* 107: 22734-9.

Taiz and Zeiger, *Plant Physiology* second edition.

Takatsuka H and Umeda M (2015) **Epigenetic Control of Cell Division and Cell Differentiation in the Root Apex.** *Front Plant Sci.* 6: 1178.

Tian H, Jia Y, Niu T, Yu Q, Ding Z (2014) **The key players of the primary root growth and development also function in lateral roots in Arabidopsis.** *Plant Cell Rep.* 33: 745-53.

Truernit E, Bauby H, Belcram K, Barthélémy J, Palauqui JC (2012) **OCTOPUS, a polarly localised membrane-associated protein, regulates phloem differentiation entry in Arabidopsis thaliana.** *Development* 139: 1306-15.

Tsukaya H, Beemster GT (2006) **Genetics, cell cycle and cell expansion in organogenesis in plants.** *J Plant Res.* 119: 1-4.

Tsukaya H (2013) **Leaf Development.** *Arabidopsis Book* 11: e0163.

Ubeda-Tomás S, Beemster GT, Bennett MJ (2012) **Hormonal regulation of root growth: integrating local activities into global behaviour.** *Trends in Plant Science* 17: 326-331.

Van Bel A JE (2003) **Transport Phloem: Low Profile, High Impact.** *Plant Physiol.* 131: 1509-1510.

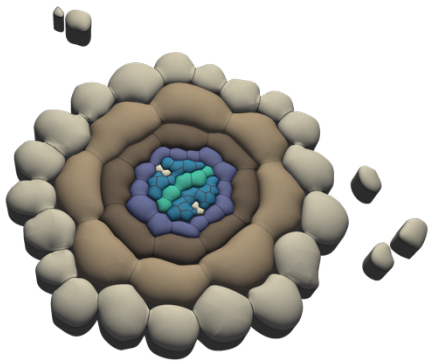
Vanhaeren H, Inzé D, González N (2016) **Plant Growth Beyond Limits.** *Trends Plant Sci.* 21: 102-9.

Vanhaeren H, Nam YJ, De Milde L, Chae E, Storme V, Weigel D, González N, Inzé D (2017) **Forever Young: The Role of Ubiquitin Receptor DA1 and E3 Ligase BIG BROTHER in Controlling Leaf Growth and Development.** *Plant Physiol.* 173: 1269–1282.

Yao X, Feng H, Yu Y, Dong A, Shen WH (2013) **SDG2-mediated H3K4 methylation is required for proper Arabidopsis root growth and development.** *PLoS One* 8: 56537.

Zhang Y, Jiao Y, Liu Z, Zhu YX (2015) **ROW1 maintains quiescent centre identity by confining WOX5 expression to specific cells.** *Nat Commun.* 6: 6003.

# Chapter 1



## **Antagonistic peptide technology for functional dissection of CLE peptides revisited**

Czyzewicz N, Wildhagen M, Cattaneo P, Stahl Y, Pinto KG, Aalen RB, Butenko MA, Simon R, Hardtke CS, De Smet I

Journal of Experimental Botany, 2015 Aug; 66 (17): 5367-74

### **Highlights**

- Application of the potentially dominant-negative antagonistic peptide approach to different CLE peptides has been proposed to be a useful tool to study the function of some peptides.
- Both physiological assays and *in planta* observations demonstrated that mCLE45pG6T is a weaker variant rather than antagonist version of the correspondence peptide.
- In general, whether the amino acidic substitution has an effect or not may depend on the conformational context.

### **My contribution**

I applied the antagonistic peptide approach to CLE45p. Through physiological assays and *in planta* analysis, I investigated the morphological consequences in the root caused by such a modification. Simultaneously I evaluated the differences between mCLE45pG6T and CLE45p activities on root development. I provided data presented in Fig. 2B, C and D.



RESEARCH PAPER

## Antagonistic peptide technology for functional dissection of CLE peptides revisited

Nathan Czyzewicz<sup>1</sup>, Mari Wildhagen<sup>2</sup>, Pietro Cattaneo<sup>3</sup>, Yvonne Stahl<sup>4</sup>, Karine Gustavo Pinto<sup>4</sup>, Reidunn B. Aalen<sup>2</sup>, Melinka A. Butenko<sup>2</sup>, Rüdiger Simon<sup>4</sup>, Christian S. Hardtke<sup>3</sup>, Ive De Smet<sup>1,5,6,7,\*</sup>

<sup>1</sup> Division of Plant and Crop Sciences, School of Biosciences, University of Nottingham, Loughborough LE12 5RD, UK

<sup>2</sup> Department of Biosciences, Section for Genetics and Evolutionary Biology, University of Oslo, N-0316 Oslo, Norway

<sup>3</sup> Department of Plant Molecular Biology, University of Lausanne, CH-1015, Lausanne, Switzerland

<sup>4</sup> Institute for Developmental Genetics, Heinrich-Heine University, D-40225 Düsseldorf, Germany

<sup>5</sup> Centre for Plant Integrative Biology, University of Nottingham, Loughborough LE12 5RD, UK

<sup>6</sup> Department of Plant Systems Biology, VIB, B-9052 Ghent, Belgium

<sup>7</sup> Department of Plant Biotechnology and Genetics, Ghent University, B-9052 Ghent, Belgium

\* To whom correspondence should be addressed. E-mail: [ive.desmet@psb.vib-ugent.be](mailto:ive.desmet@psb.vib-ugent.be)

Received 23 February 2015; Revised 10 April 2015; Accepted 20 April 2015

Editor: Thomas Dresselhaus

### Abstract

In the *Arabidopsis thaliana* genome, over 1000 putative genes encoding small, presumably secreted, signalling peptides can be recognized. However, a major obstacle in identifying the function of genes encoding small signalling peptides is the limited number of available loss-of-function mutants. To overcome this, a promising new tool, antagonistic peptide technology, was recently developed. Here, this antagonistic peptide technology was tested on selected CLE peptides and the related IDA peptide and its usefulness in the context of studies of peptide function discussed. Based on the analyses, it was concluded that the antagonistic peptide approach is not the ultimate means to overcome redundancy or lack of loss-of-function lines. However, information collected using antagonistic peptide approaches (in the broad sense) can be very useful, but these approaches do not work in all cases and require a deep insight on the interaction between the ligand and its receptor to be successful. This, as well as peptide ligand structure considerations, should be taken into account before ordering a wide range of synthetic peptide variants and/or generating transgenic plants.

**Key words:** CLE, IDA, peptide structure, peptide variants, root, small signalling peptides.

### Introduction

Small signalling peptides are able to elicit a vast array of biological and physiological responses, allowing the plant to develop and adapt to changes in the surrounding environment (Czyzewicz *et al.*, 2013; Murphy *et al.*, 2012). In the *Arabidopsis thaliana* genome, over 1000 putative genes encoding small, presumably secreted, signalling peptides can be recognized (Lease and Walker, 2006). These small signalling peptides are mainly perceived

by receptors, such as receptor kinases, and in the *A. thaliana* genome, over 600 genes encoding putative receptor-like kinase (RLK) proteins have been detected (Shiu and Bleeker, 2001a, b). However, to date, only a small portion of these putative small signalling peptides have been functionally characterized and few have been linked to a receptor (Butenko *et al.*, 2009; Czyzewicz *et al.*, 2013; Lee and Torii, 2012; Murphy *et al.*, 2012).

© The Author 2015. Published by Oxford University Press on behalf of the Society for Experimental Biology.

This is an Open Access article distributed under the terms of the Creative Commons Attribution License (<http://creativecommons.org/licenses/by/3.0/>), which permits unrestricted reuse, distribution, and reproduction in any medium, provided the original work is properly cited.

Small signalling peptides consist of usually <20 amino acids in their mature form and rarely >120 amino acids as a full-length precursor. Although there are hardly any data for most small signalling peptides, they are likely often present at very low (nanomolar range) physiological concentrations. Forward and reverse genetic approaches have been employed to study the biological function of genes encoding small signalling peptides. For example, CLAVATA3 (CLV3), a peptide regulating maintenance of plant stem cells, was identified in a forward genetic screen (Clark *et al.*, 1995; Fletcher *et al.*, 1999). The *clv3* mutants have an enlarged shoot apical meristem (SAM) and floral meristems, which generate supernumerary floral organs, suggesting a general role in regulating above-ground meristematic growth (Clark *et al.*, 1996). CLV3 belongs to the family of CLV3/EMBRYO SURROUNDING REGION-related (CLE) peptides, which consists of 31 members in *A. thaliana*. These peptides share a conserved 12–14 amino acid C-terminal domain that is proteolytically released and has been shown to function in various contexts, including shoot and root meristem development, nodulation, embryo and endosperm development, regulation of root architecture in response to nutrients, and vascular development (Araya *et al.*, 2014; Cock and McCormick, 2001; Fiers *et al.*, 2005; Fiume and Fletcher, 2012; Hirakawa *et al.*, 2008; Hobe *et al.*, 2003; Jun *et al.*, 2010; Lim *et al.*, 2011; Mortier *et al.*, 2010; Okamoto *et al.*, 2013; Reid *et al.*, 2011; Stahl *et al.*, 2009). Genetic interaction studies suggested CLV3 to act as a small signalling peptide since mutations in the RLK encoding gene, *CLV1*, had a similar phenotype to *clv3* mutants and the overexpression phenotype of *CLV3* was lost in the *clv1* mutant background (Brand *et al.*, 2000). Indeed, the identification of the mature active CLV3 peptide and biochemical evidence for its interaction with CLV1 was confirmed almost a decade later (Ogawa *et al.*, 2008; Ohyama *et al.*, 2009). This example illustrates some of the difficulties in identifying the mature active form of small signalling peptides in plants and thereafter finding their receptors and/or interacting signalling partners.

One major obstacle in identifying the function of genes encoding small signalling peptides is the limited number of available loss-of-function mutants, since most have no useful T-DNA insertions, partly because small genes are less likely to be targeted by a T-DNA insertion. To complicate matters further, the functional redundancy of some small signalling peptides and RLKs can mask phenotypes when only one family member is successfully disrupted. Although some small signalling peptides have been discovered through screening of T-DNA or transposon insertion mutants—such as INFLORESCENCE DEFICIENT IN ABSCISSION (IDA), TAPETUM DETERMINANT1 (TPD1), CLV3, and CLE40 (Butenko *et al.*, 2003; Fletcher *et al.*, 1999; Hobe *et al.*, 2003; Yang *et al.*, 2003), new approaches and technologies are required to facilitate the functional analyses of genes encoding small signalling peptides and their putative corresponding receptor partners (Butenko *et al.*, 2014; Stes *et al.*, 2015).

To interfere with and unravel endogenous peptide function, antagonistic peptides—such as mutant peptide variants,

chemically modified peptides or peptide-like molecules that can affect peptide ligand–receptor (kinase) pathways are an important tool. In this context, structure-function/activity analyses can provide useful information on peptide residues critical for function. With respect to CLE peptides, such analyses were used to test, for example, suppression of nodulation capability in soybean (*Glycine max*) roots of the nodulation-controlling RHIZOBIA-INDUCED CLE1 (GmRIC1) (Reid *et al.*, 2013) or regulation of primary and lateral root growth of various CLE peptides (Czyzewicz *et al.*, 2015; Kondo *et al.*, 2008). Recently, this approach was used to develop a promising new tool, referred to as antagonistic peptide technology, for functional dissection of CLE peptides (Song *et al.*, 2013). Based on transgenic plants carrying CLV3 variants where each of the 12 residues in the core CLE motif were one by one replaced by alanine (Ala), it was shown that the glycine (Gly) to Ala substitution at position six gave a weak *clv3* phenotype. Subsequently, replacing this highly conserved Gly residue with other amino acids revealed that a Gly to threonine (Thr) produced a phenotype most similar to *clv3* mutants. This was further tested using synthetic CLV3 peptide with the Gly to Thr substitution (CLV3p<sup>6Thr</sup>), which was also able to produce—although less effective—the *clv3* mutant phenotype, and which could compete with wild-type synthetic CLV3 peptide (CLV3p). These exciting observations suggested that the CLV3p<sup>6Thr</sup> variant could act as an antagonistic peptide. Specifically, a loss-of-function phenotype is suggested to be obtained through competitive inhibition, namely the peptide is proposed to be able to bind to the native receptor, but unable to activate it, since a functionally critical amino acid is mutated. Probably the CLV3p<sup>6Thr</sup> variant has compromised peptide flexibility leading to stronger interaction with corresponding receptors and to disrupted downstream signal transduction. Taken together, such antagonistic peptides would provide a powerful tool for the functional dissection of CLEs in plants, and might also have the potential to be used for other plant peptides. Based on this assumption and the conserved nature of the Gly at position six (Fig. 1), this technology was applied to CLE8 (giving rise to embryo-lethal phenotype) and CLE22 (giving rise to short root phenotype) (Song *et al.*, 2013).

Here, this antagonistic peptide technology was tested, specifically Gly<sup>6</sup>-to-Ala or Gly<sup>6</sup>-to-Thr, as used by Song *et al.* (2013), on selected CLE peptides and the related IDA peptide, and its usefulness discussed in the context of studies of peptide function.

## Materials and methods

### Plant growth conditions

For the work on CLE40 and CLV3, seeds were surface sterilized with chlorine gas and imbibed in 0.1% (w/v) agarose for 2 d at 4 °C before being plated onto 0.5× Murashige and Skoog (MS) medium with Gamborgs No. 5 vitamins (Duchefa), 0.5 g/l 2-(*N*-morpholino) ethanesulfonic acid (MES), 1% (w/v) sucrose, and 1.2% (w/v) plant agar. Plates were incubated vertically in a growth chamber with constant light at 21 °C for 5 d. For peptide-containing plates, synthetic dodecapeptides were added to a final concentration of 1 μM. For the work on CLE1/4, CLE7, CLE26, and CLE27, seeds were surface sterilized by immersion in 70% ethanol for 30 s, and incubated

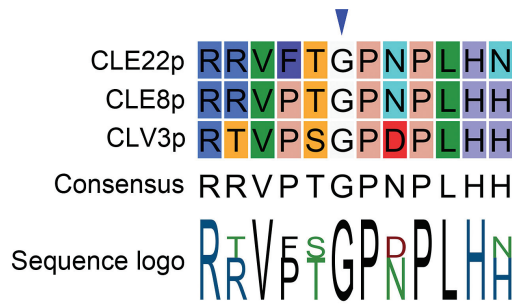


**Fig. 1.** Alignment of CLE peptides used in Song *et al.* (2013). Conserved glycine (G) at position six is indicated with a blue arrowhead. (This figure is available in colour at JXB online.)

in 20% bleach at room temperature for 20 min. Sterile seeds were vernalized in water at 4 °C for 2 d, before being plated onto 0.5× MS medium supplemented with 0.1 g/l Myo-inositol (Sigma Aldrich), 0.5 g/l MES (Sigma Aldrich), and 1% (w/v) bacteriological agar. Plants were incubated vertically under constant light at 21 °C until 12 d after germination. Synthetic CLE was added to a final concentration of 10 μM or 10 nM. The work on CLE45 was essentially performed as previously described (Rodríguez-Villalón *et al.*, 2014).

#### Starch staining

Starch granules and cell walls in root tips were stained with the mPSP1 method and imaged with a confocal microscope as previously described (Truernit *et al.*, 2008).

#### Oxidative burst experiments

For transient expression, *Agrobacterium tumefaciens* carrying HAESA-LIKE 2 (HSL2) in frame with eGFP in an estradiol-inducible expression vector described previously (Bleckmann *et al.*, 2010), was infiltrated into *Nicotiana benthamiana* leaves according to (Mueller *et al.*, 2012). The oxidative burst experiment was performed as previously described by (Butenko *et al.*, 2014), with the exception that 3 d after infiltration with *A. tumefaciens*, leaf pieces of *N. benthamiana* were induced with 20 μM estradiol before cut. Light emission was measured in a Wallac 1420 VICTOR<sup>2</sup> microplate luminometer (PerkinElmer).

#### Peptide structure predictions

The recently published solution structure of CLE10p, solved using nuclear magnetic resonance (NMR) (MMDB ID: 125940; PMBID: 2MD), depicts the backbone of the PXGP core (position 4–7) as a smooth curve protruding from the rest of the peptide. To investigate the effect of mutations in this core of the peptides investigated, amino acid sequences with the structure AAA[core]AAA with the core PGGP, PGAP, PGTP, PRGP, PRTP, PSAp, or PSTP were submitted for analysis in PEP-FOLD (<http://mobylerpbs.univ-paris-diderot.fr/cgi-bin/portal.py?form=PEP-FOLD#forms::PEP-FOLD>) using standard settings.

## Results and discussion

### 'Antagonistic' CLE peptides

Among many processes (Cock and McCormick, 2001; Fiume and Fletcher, 2012; Hirakawa *et al.*, 2008; Okamoto *et al.*, 2013), various CLE peptides affect primary and lateral root

growth and development (Czyzewicz *et al.*, 2015; Depuydt *et al.*, 2013; Fiers *et al.*, 2005; Hobe *et al.*, 2003; Jun *et al.*, 2010; Rodríguez-Villalón *et al.*, 2014; Rodríguez-Villalón *et al.*, 2015; Stahl *et al.*, 2009). To build on previous work investigating CLE peptides in the context of lateral root development, primary root growth, root apical stem cell maintenance, and vascular development, putative antagonistic versions of CLV3, CLE1/4, CLE7, CLE26, CLE27, CLE40, and CLE45 peptides were designed—based on the findings by Song *et al.* (2013)—to further unravel CLE peptide function (Figs 2A, 3A, 4A). To assess the function of these mutated chemically synthesized CLE peptides with Gly/cysteine (Cys) to Ala or Gly/Cys to Thr substitutions (referred to as mCLEp<sup>Ala6</sup> or mCLEp<sup>6Thr</sup>, respectively), a number of biological assays were used.

The antagonistic peptide technology was first applied to CLE45 peptide (CLE45p), which, when applied exogenously, leads to shorter primary roots because it suppresses protophloem differentiation (Depuydt *et al.*, 2013; Rodríguez-Villalón *et al.*, 2014). To explore a potential loss-of-function phenotype, synthetic mCLE45p<sup>6Thr</sup> peptide was applied and its effect on primary root development upon external application evaluated (Fig. 2A, B). This revealed that at the low nanomolar range mCLE45p<sup>6Thr</sup> does not have an effect on primary root length as compared with the wild-type CLE45p (Fig. 2B), again confirming that position six is important for peptide activity. However, a higher concentration of 1 μM mCLE45p<sup>6Thr</sup> had the same effect as the unmodified wild-type CLE45p (Fig. 2B). In addition, this peptide was not able to out-compete the effects of simultaneous CLE45p application (Fig. 2B). Thus, while the mCLE45p<sup>6Thr</sup> peptide does not act as an antagonistic peptide, a CLE45p variant was obtained, which has identical effects as the wild-type version but required application of higher peptide concentrations. The notion that mCLE45p<sup>6Thr</sup> is a weak CLE45p, rather than an antagonistic version, was confirmed *in planta* (Rodríguez-Villalón *et al.*, 2014). Plants that express a wild-type *pCLE45::CLE45* transgene are notoriously difficult to create, presumably because of the detrimental effects of increased CLE45 dosage. However, the few lines that were eventually obtained recapitulated the root phenotype observed upon external CLE45p application (Fig. 2C). Specifically, in *pCLE45::CLE45* lines, root growth was impaired, the periclinal division of the sieve element precursor cell was frequently abolished, and protophloem differentiation was often suppressed (Fig. 2D). This phenotype is similar to plants that express a corresponding *pCLE45::CLE45<sup>6Thr</sup>* transgene, which are much easier to obtain (Rodríguez-Villalón *et al.*, 2014). Thus, the data for both tissue culture assay and *in planta* are consistent with the interpretation that mCLE45p<sup>6Thr</sup> is a weak rather than an antagonistic version of the CLE45 peptide.

Next, the antagonistic peptide approach for CLE40 was explored (Fig. 3A). It was previously shown that an increasing concentration of synthetic CLE40 peptide reduces stemness and causes differentiation of columella stem cells (CSCs), quiescent centre (QC) cells, and proximal initial (P1) cells in wild-type roots (Fig. 3B, D, H, Supplementary Table S1 available at JXB online) (Stahl *et al.*, 2013). Also

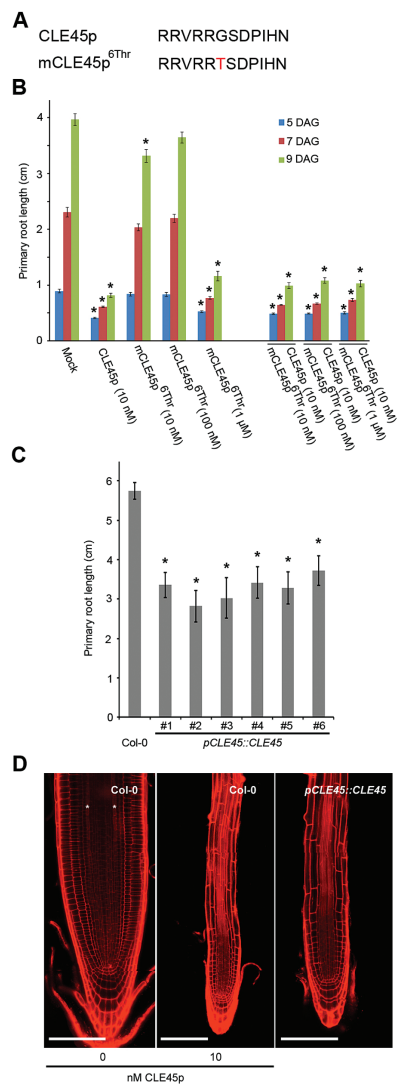


**Fig. 2.** CLE45 peptide treatment and *pCLE45::CLE45* transgenic lines. (A) Sequence of synthetic CLE45p and mCLE45p<sup>6Thr</sup>. (B) Primary root length following treatment of wild-type seedlings with indicated concentrations of CLE45p or mCLE45p<sup>6Thr</sup>. The bar graph indicates the mean  $\pm$  standard error. Statistical significance (Student's *t*-test) compared with mock is indicated for each time point (DAG, days after germination): \*  $P < 0.01$ . (C) Primary root length of *pCLE45::CLE45* lines. The bar graph indicates the mean  $\pm$  standard error. Statistical significance (Student's *t*-test) compared with Col-0 is indicated: \*  $P < 0.01$ . (D) Confocal images of primary root meristems of 7-d-old seedlings (propidium iodide-stained; composite images). The asterisks highlight the two protophloem strands that can be distinguished in wild-type (Col-0) grown on mock (left), but that do not develop when grown on 10 nM CLE45p (middle). Protophloem strands also do not develop in wild-type seedlings that express a *pCLE45::CLE45* transgene (right). Scale bar, 100  $\mu$ m.

synthetic CLV3 peptide acts similarly on the stemness in the root tip (Fig. 3E, G, Supplementary Table S1 available at *JXB* online). In contrast, in the shorter *cle40* mutant roots, differentiation of CSC daughters into CCs was significantly delayed (Fig. 3B, F, H, Supplementary Table S1 available at *JXB* online) (Hobe et al., 2003; Stahl et al., 2009). Wild-type roots carry mostly one (at D1 position) or, after a recent cell division, two layers of CSCs distal to the QC (at D1 and D2 positions), which lack stainable starch granules (Fig. 3B, H, Supplementary Table S1). In *cle40* root tips, additional CSCs in more distal positions (D2) were found (Fig. 3B, C, H, Supplementary Table S1). To assess if synthetic mCLE40p<sup>6Thr</sup> and mCLV3p<sup>6Thr</sup> variants could be used as antagonistic peptides to obtain a loss-of-function phenotype, their impact on the distal root stemness was evaluated (Fig. 3A). This revealed a response comparable with the wild-type CLE40p or CLV3p treatments (Fig. 3E, G, H, Supplementary Table S1 available at *JXB* online). Taken together, this suggests that the Gly to Thr substitution in CLE40 and CLV3 does not give rise to an antagonistic peptide.

Finally, while treatment of *A. thaliana* seedlings with 10  $\mu$ M wild-type CLE1/4p, CLE7p, CLE26p, and CLE27p resulted in a short primary root and more lateral roots (Fig. 4B, C) (Czyzewicz et al., 2015; Depuydt et al., 2013; Kinoshita et al., 2007; Rodriguez-Villalon et al., 2014), this does not necessarily reflect their natural function. However, based on the *CLE1/4*, *CLE7*, *CLE26*, and *CLE27* expression patterns, a role in lateral root development might be expected (Czyzewicz et al., 2015; Jun et al., 2010). In this context, only CLE26p gave rise to a short primary root and increased lateral root density at a concentration of 10 nM (Fig. 4B) (Czyzewicz et al., 2015; Rodriguez-Villalon et al., 2015), further supporting caution when interpreting exogenous peptide application results, especially at higher concentrations. To assess if the above-mentioned CLE peptides have a role in primary and lateral root development, the antagonistic peptide technology was attempted (Fig. 4A). However, analysis of mutated chemically synthesized CLE peptides (mCLEp) at 10  $\mu$ M revealed that, although mCLE1/4p<sup>6Ala/Thr</sup> and mCLE7p<sup>6Ala/Thr</sup> did not induce a primary root shortening or a lateral root density increase—unlike the non-mutated forms of these peptides, mCLE1/4p<sup>6Thr</sup> and mCLE7p<sup>6Ala/Thr</sup> were also unable to produce an obvious dominant negative root phenotype, namely an expected longer primary root and/or decrease in lateral root density (Fig. 4B, C). However, for mCLE1/4p<sup>6Ala</sup>, a subtle increase in primary root length, but no effect on lateral root density was observed (Fig. 1C). It should be pointed out that since the receptor, and the associated loss-of-function phenotype, for these peptides is not known, the expected dominant negative root phenotype remains speculative. Nevertheless, this outcome suggested that for CLE1p, CLE4p, and CLE7p activity, the Gly at position six is essential, but that this mutant form did not appear to act as an antagonistic peptide. In contrast, mCLE26p<sup>6Ala/Thr</sup> and mCLE27p<sup>6Ala/Thr</sup> displayed a similar phenotype to the non-mutated forms, namely a significant reduction in primary root length (92–95%) and increased lateral root density (110–151%) (Fig. 4B, C), suggesting that the sixth amino acid in their respective sequences is not critical

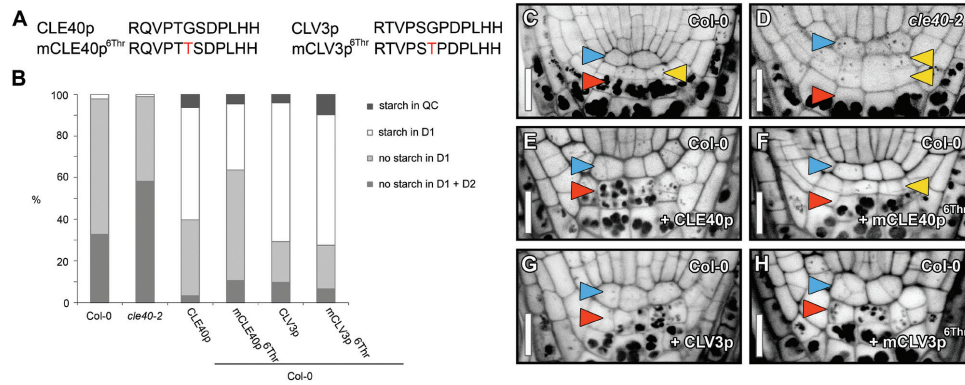


**Fig. 3.** Distal root phenotypes after antagonistic peptide treatments. (A) Sequence of synthetic CLE and mCLE peptides used. (B–H) Distal root cell fates were analysed by mPSP1 staining 5 d after germination in wild-type (Col-0) and *cle40-2* mutant roots (C, D). Representative examples of Col-0 roots grown on media with 1  $\mu$ M CLE40p (E), mCLE40p<sup>6Thr</sup> (F), CLV3p (G), and mCLV3p<sup>6Thr</sup> (H) are shown. Frequency of roots carrying starch granules in the designated domains is shown in (B). Arrowheads: blue, QC position; yellow, CSC position (D1); red, CC position (D2). Double yellow arrowheads indicate CSC fate in D2, whereas the lack of a yellow arrowhead indicates CC fate in D1 position. QC, quiescent centre position; D1, distal layer position one; D2, distal layer position two; CC, columella cell position. Scale bars represent 15  $\mu$ m.

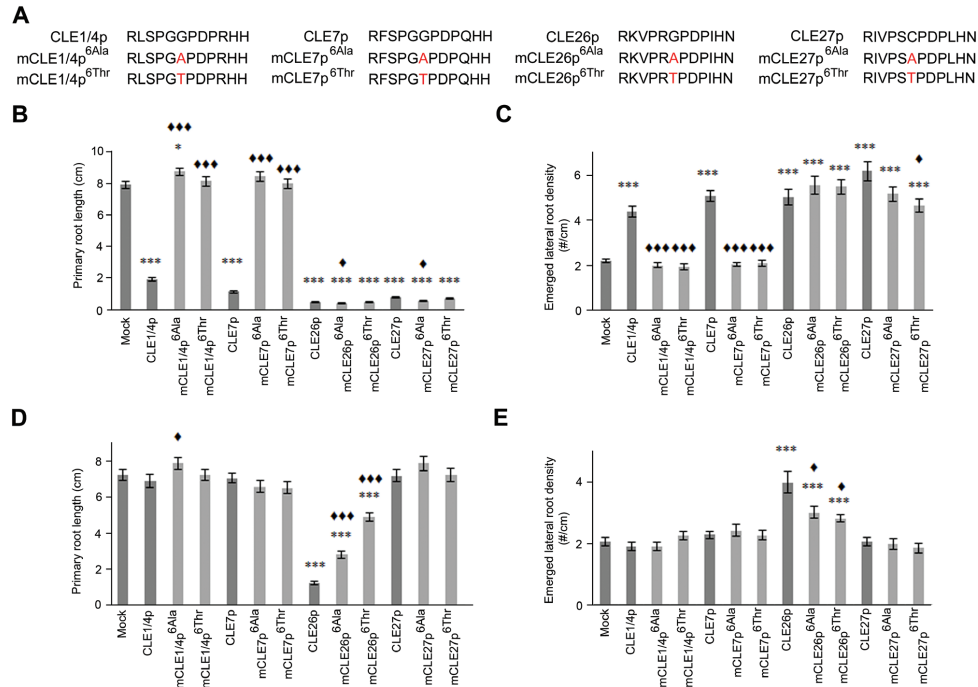


**Fig. 4.** CLE1/4, CLE7, CLE26, and CLE27 peptide treatment. (A) Sequence of synthetic CLE and mCLE peptides used. (B–E) Treatment of wild-type seedlings with 10  $\mu$ M (B, C) or 10 nM (D, E) of CLE or mCLE peptide. Quantification of primary root length (B, D) and emerged lateral root density (C, E) for CLEp and mCLEp-treated wild-type seedlings. The bar graph indicates the mean  $\pm$  standard error. Statistical significance (Student's *t*-test) compared with no peptide (\*) and to CLEp treatment (•) is indicated: \*\*\*/\*\*\*\*,  $P < 0.001$ , \*/\*,  $P < 0.05$ . (This figure is available in colour at JXB online.)

to their function, and also, did not appear to give rise to an antagonistic peptide when mutated. Intriguingly, at 10 nM, mCLE26p<sup>6Ala/6Thr</sup> retained activity, but was less potent than

CLE26p. This suggests that mCLE26p<sup>6Ala/6Thr</sup> is a weak rather than an antagonistic version of the CLE26 peptide, which is in agreement with the results on CLE45. In contrast, most

mCLE1/4p, mCLE7p, and mCLE27p variants had no altered activity compared with the wild-type variant at 10 nM, except mCLE1/4p<sup>6Ala</sup> (Fig. 4D, E). In general, it appears that also for CLE1/4p, CLE7p, CLE26p, and CLE27p, the antagonistic peptide technology is not easily applicable.

In conclusion, other amino acid mutations are likely required to give rise to (strong) antagonistic CLE1p, CLE4p, CLE7p, CLE26p, CLE27p, CLE40p, and CLE45p peptides, or alternatively, this approach cannot be universally applied with respect to synthetic CLE peptides. A poor effect of synthetic antagonistic peptides could be due to delivery to relevant tissues and/or instability. However, synthetic peptide stability issues were not observed in these assays or with respect to synthetic control peptides, nor was a lack of phenotypes observed when synthetic (antagonistic) peptides were exogenously applied to the root. While the latter can be a non-specific effect in some cases, specific and local phenotypes were also observed.

#### 'Antagonistic' IDA peptides

In addition, the extent of the antagonistic peptide technology can be applied to other small signalling peptides was assessed. For this, the IDA and IDA-LIKE (IDL) family were chosen, given their sequence similarity to CLEs (Stenvik et al., 2006). The IDA and IDL1 peptides of 12 amino acids share a common core at positions four to seven [PS(G/A)P] and the C-terminal end [H(N/H)] with CLV3 and some CLE peptides (Figs 5A, 6A). Like CLV3, hydroxylation of the Pro at position seven of the IDA dodecapeptide (IDAp, also referred to as PIPPo) increases the activity of the peptide (Butenko et al., 2014). An oxidative burst response in *Nicotiana benthamiana* can be employed as readout for the RLK HAESA-LIKE2 (HSL2) activation by exogenously applied synthetic IDA peptides (Butenko et al., 2014). Previous results indicated that IDAp binds to HSL2 with a K<sub>d</sub> of 20 nM (Butenko et al., 2014). As the wild-type IDA peptide has an Ala at position six corresponding to the Gly at that position in CLV3, and the *ida* mutant phenotype can be fully rescued by IDL1, which has a Gly at this position (Stenvik et al., 2008) (Fig. 6A); both of these small amino acids are evidently compatible with high signalling activity. It was, however, conceivable that substitution to the larger Thr (mIDAp<sup>6Thr</sup>) (Fig. 5A) could have an effect on receptor binding and/or activation. Therefore, the activity of mIDAp<sup>6Thr</sup> in comparison with the activity of synthetic IDAp was assessed in an oxidative burst assay. For all peptide concentrations tested, mIDAp<sup>6Thr</sup> gave the same response as IDAp in the presence of its receptor HSL2 (Fig. 5B), indicating that the mutated peptide was just as active as its wild-type counterpart. In conclusion, this mutation neither produced a ligand with weaker activity, nor a peptide with antagonistic effect.

#### Conclusion

Information collected using antagonistic peptide approaches (in the broad sense) can be very useful, but these approaches do not work in all cases and require a deep insight on the

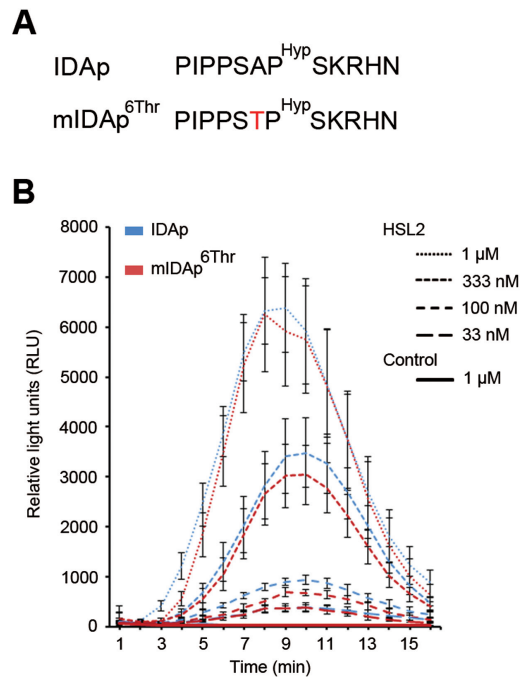


**Fig. 5.** IDA peptide treatment. (A) Sequence of synthetic IDA peptides used. (B) *N. benthamiana* leaf pieces expressing HSL2 were exposed to various concentrations of peptides as indicated. Oxidative burst by the luminol-based assay was monitored over time as relative light units (RLU). Leaf pieces infiltrated with *Agrobacterium* without HSL2 were exposed to 1 μM of both peptides and used as control. Error bars indicate standard error of  $n=3$  or 4 replicates.

interaction between the ligand and its receptor to be successful. While the antagonistic peptide approach might work in a number of cases, as described by Song et al. (2013) and Xu et al. (2015), its universal applicability remains to be determined. Initial data were presented for CLV3, CLE8, and CLE22, and recently for CLE19 but in the absence of the pertinent wild-type control transgenes and genetic knock-out lines, it remains difficult to judge whether the phenotypes triggered by mCLE8<sup>6Thr</sup>, mCLE19<sup>6Thr</sup>, and mCLE22<sup>6Thr</sup> transgenes are antagonistic or not. Importantly, in view of the results presented here, and in agreement with the results of Song et al. (2013), it appears that the antagonistic peptide technology cannot be easily applied to synthetic CLE peptides and—at least—requires expressing mutant variants to deliver dominant peptides to their endogenous locations. However, as was shown with the CLE45<sup>6Thr</sup> transgene, the latter also does not always work. Nevertheless, it can provide novel insight that can lead to other tools to dissect peptide activity, as—for example—the weakened activity of mCLE45<sup>6Thr</sup> could be used to functionally characterize CLE45. In addition, it also does not appear to be straightforward to translate this approach to other peptide families, as exemplified

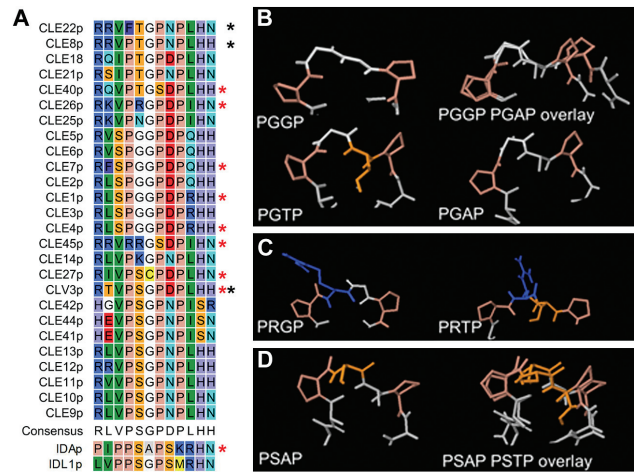


**Fig. 6.** Peptide structure. (A) Manually adjusted alignment of the 12 amino acids of CLE peptides, with IDA and IDL1 for comparison. Red stars mark peptides used in the present study, black stars those tested by Song *et al.* (2013). (B–D) Examples of structures of the PXXP core predicted by PEP-FOLD. (B) PGGP. The larger Thr might interfere with receptor binding, and substitution of Gly6 with Ala6 may change the angles between the Pro residues. (C) PRGP. The side chain of Arg may change direction when the Gly6 is exchanged with a Thr. (D) PSAP. A change from Ala to Thr in position six may not result in major conformational changes when Ser is present in the core. (This figure is available in colour at *JXB* online.)

through analyses on IDA. In general, it was observed that whether the mutations have an effect or not, seems dependent on the context, with differential sensitivity to conformational changes (Fig. 6A and Supplementary Table S2 available at *JXB* online). CLE1/4p and CLE7p are highly similar peptides with the same PGGP core at position four to seven, and both lose activity when the Gly at position six is mutated to Ala or Thr. Structure prediction for the peptides may suggest that a mutation in this context, with the small Gly at position five, easily changes the peptide conformation (Fig. 6B). Alternatively, all size increases in the side chain of the amino acid at position six could interfere with binding of the putative receptor(s) of CLE1, CLE4, and CLE7. CLE26p and CLE45p both have an Arg in the core sequence (PRGP and RRGSP, respectively) and react similarly to the introduced mutations, namely weaker activity when the Gly at position six is mutated. The long side chain of Arg might change direction in the mutant peptides, which might reduce its binding affinity for a receptor (Fig. 6C). In contrast, mutation of Ala at position six to Thr did not reduce the activity of the IDA peptide, which has a PSAP core, suggesting that the serine (Ser) residue might stabilize the peptide structure (Fig. 6D).

In conclusion, the antagonistic peptide approach can be a useful tool to study the function of some CLE genes (Song *et al.*, 2013; Xu *et al.*, 2015), but not the ultimate means to overcome redundancy or lack of loss-of-function lines (Rodríguez-Villalón *et al.*, 2014; this study). However, while the approach described by Song *et al.* (2013), when applied to synthetic CLE peptide variants, did not work—for the peptides selected in this study and with respect to the phenotypes investigated, it does not preclude there being any other substitution, modification, or combination thereof or a transgene that may induce the desired effects. This, as well as structure

considerations, should be taken into account before ordering a wide range of synthetic peptide variants and/or generating transgenic plants.

## Supplementary data

Supplementary data are available at *JXB* online.

Supplementary Table S1. Quantification of distal root phenotypes after antagonistic peptide treatments.

Supplementary Table S2. Summary of mutations and phenotypes.

## Acknowledgements

This work was supported by a BBSRC David Phillips Fellowship (BB\_BB/H022457/1) and a Marie Curie European Reintegration Grant (PERG06-GA-2009-256354) to IDS, a BBSRC CASE Studentship co-funded by Bayer CropScience to NC, and a Swiss National Science Foundation grant (310030B\_147088) to CSH. This work was supported by Grants 13785/F20, 218735, and 204756 to MAB, MW, and RBA, and 230849/F20 and 225299 to MAB from the Research Council of Norway. Work by RS, YS, and KGP was supported by the German excellence initiative (CEPLAS, EXC1028).

## References

- Araya T, Miyamoto M, Wibowo J, *et al.* 2014. CLE-CLAVATA1 peptide-receptor signaling module regulates the expansion of plant root systems in a nitrogen-dependent manner. *Proceedings of the National Academy of Sciences USA* **111**, 2029–2034.
- Bleckmann A, Weidtkamp-Peters S, Seidel CAM, Simon R. 2010. Stem Cell Signaling in *Arabidopsis* Requires CRN to Localize CLV2 to the Plasma Membrane. *Plant Physiology* **152**, 166–176.
- Brand U, Fletcher JC, Hobe M, Meyerowitz EM, Simon R. 2000. Dependence of stem cell fate in *Arabidopsis* on a feedback loop regulated by CLV3 activity. *Science* **289**, 617–619.

- Butenko MA, Patterson SE, Grini PE, Stenvik GE, Amundsen SS, Mandal A, Aalen RB.** 2003. Inflorescence deficient in abscission controls floral organ abscission in *Arabidopsis* and identifies a novel family of putative ligands in plants. *The Plant Cell* **15**, 2296–2307.
- Butenko MA, Vie AK, Brembu T, Aalen RB, Bones AM.** 2009. Plant peptides in signalling: looking for new partners. *Trends in Plant Science* **14**, 255–263.
- Butenko MA, Wildhagen M, Albert M, Jehle A, Kalbacher H, Aalen RB, Felix G.** 2014. Tools and Strategies to Match Peptide-Ligand Receptor Pairs. *The Plant Cell* **26**, 1838–1847.
- Clark SE, Running MP, Meyerowitz EM.** 1995. CLAVATA3 is a specific regulator of shoot and floral meristem development affecting the same processes as CLAVATA1. *Development* **121**, 2057–2067.
- Clark SE, Jacobsen SE, Levin JZ, Meyerowitz EM.** 1996. The CLAVATA and SHOOT MERISTEMLESS loci competitively regulate meristem activity in *Arabidopsis*. *Development* **122**, 1567–1575.
- Cock JM, McCormick S.** 2001. A large family of genes that share homology with CLAVATA3. *Plant Physiology* **126**, 939–942.
- Czyzewicz N, Yue K, Beeckman T, De Smet I.** 2013. Message in a bottle: small signalling peptide outputs during growth and development. *Journal of Experimental Botany* **64**, 5281–5296.
- Czyzewicz N, Shi C, Vu LD, Van De Cotte B, Butenko MA, De Smet I.** 2015. Modulation of *Arabidopsis* and monocot root architecture by CLAVATA3/EMBRYO SURROUNDING REGION 26 peptide. *Journal of Experimental Botany* **66**, 5229–5243.
- Depuydt S, Rodriguez-Villalon A, Santuari L, Wyser-Rmili C, Ragni L, Hardtke CS.** 2013. Suppression of *Arabidopsis* protophloem differentiation and root meristem growth by CLE45 requires the receptor-like kinase BAM3. *Proceedings of the National Academy of Sciences USA* **110**, 7074–7079.
- Fiers M, Golemic E, Xu J, van der Geest L, Heidstra R, Stiekema W, Liu CM.** 2005. The 14-amino acid CLV3, CLE19, and CLE40 peptides trigger consumption of the root meristem in *Arabidopsis* through a CLAVATA2-dependent pathway. *The Plant Cell* **17**, 2542–2553.
- Fiume E, Fletcher JC.** 2012. Regulation of *Arabidopsis* embryo and endosperm development by the polypeptide signaling molecule CLE8. *The Plant Cell* **24**, 1000–1012.
- Fletcher JC, Brand U, Running MP, Simon R, Meyerowitz EM.** 1999. Signaling of cell fate decisions by CLAVATA3 in *Arabidopsis* shoot meristems. *Science* **283**, 1911–1914.
- Hirakawa Y, Shinohara H, Kondo Y, et al.** 2008. Non-cell-autonomous control of vascular stem cell fate by a CLE peptide/receptor system. *Proceedings of the National Academy of Sciences USA* **105**, 15208–15213.
- Hobe M, Muller R, Grunewald M, Brand U, Simon R.** 2003. Loss of CLE40, a protein functionally equivalent to the stem cell restricting signal CLV3, enhances root waving in *Arabidopsis*. *Development Genes and Evolution* **213**, 371–381.
- Jun J, Fiume E, Roeder AH, et al.** 2010. Comprehensive analysis of CLE polypeptide signaling gene expression and overexpression activity in *Arabidopsis*. *Plant Physiology* **154**, 1721–1736.
- Kinoshita A, Nakamura Y, Sasaki E, Kyoizuka J, Fukuda H, Sawa S.** 2007. Gain-of-function phenotypes of chemically synthetic CLAVATA3/ESR-related (CLE) peptides in *Arabidopsis thaliana* and *Oryza sativa*. *Plant and Cell Physiology* **48**, 1821–1825.
- Kondo T, Nakamura T, Yokomine K, Sakagami Y.** 2008. Dual assay for MCLV3 activity reveals structure-activity relationship of CLE peptides. *Biochemical and Biophysical Research Communications* **377**, 312–316.
- Lease KA, Walker JC.** 2006. The *Arabidopsis* unannotated secreted peptide database, a resource for plant peptidomics. *Plant Physiology* **142**, 831–838.
- Lee JS, Torii KU.** 2012. A tale of two systems: peptide ligand-receptor pairs in plant development. *Cold Spring Harbor Symposia on Quantitative Biology* **77**, 83–89.
- Lim CW, Lee YW, Hwang CH.** 2011. Soybean nodule-enhanced CLE peptides in roots act as signals in GmNARK-mediated nodulation suppression. *Plant and Cell Physiology* **52**, 1613–1627.
- Mortier V, Den Herder G, Whitford R, Van de Velde W, Rombauts S, D'Haeseleer K, Holsters M, Goormachtig S.** 2010. CLE peptides control *Medicago truncatula* nodulation locally and systemically. *Plant Physiology* **153**, 222–237.
- Mueller K, Bittel P, Chinchilla D, Jehle AK, Albert M, Boller T, Felix G.** 2012. Chimeric FLS2 receptors reveal the basis for differential flagellin perception in *Arabidopsis* and tomato. *The Plant Cell* **24**, 2213–2224.
- Murphy E, Smith S, De Smet I.** 2012. Small signaling peptides in *Arabidopsis* development: how cells communicate over a short distance. *The Plant Cell* **24**, 3198–3217.
- Ogawa M, Shinohara H, Sakagami Y, Matsubayashi Y.** 2008. *Arabidopsis* CLV3 peptide directly binds CLV1 ectodomain. *Science* **319**, 294.
- Ohya K, Shinohara H, Ogawa-Ohnishi M, Matsubayashi Y.** 2009. A glycopeptide regulating stem cell fate in *Arabidopsis thaliana*. *Nature Chemical Biology* **5**, 578–580.
- Okamoto S, Shinohara H, Mori T, Matsubayashi Y, Kawaguchi M.** 2013. Root-derived CLE glycopeptides control nodulation by direct binding to HAR1 receptor kinase. *Nature Communications* **4**, 2191.
- Reid DE, Ferguson BJ, Gresshoff PM.** 2011. Inoculation- and nitrate-induced CLE peptides of soybean control NARK-dependent nodule formation. *Molecular Plant-Microbe Interactions* **24**, 606–618.
- Reid DE, Li D, Ferguson BJ, Gresshoff PM.** 2013. Structure-function analysis of the GmRIC1 signal peptide and CLE domain required for nodulation control in soybean. *Journal of Experimental Botany* **64**, 1575–1585.
- Rodriguez-Villalon A, Gujas B, Kang YH, Breda AS, Cattaneo P, Depuydt S, Hardtke CS.** 2014. Molecular genetic framework for protophloem formation. *Proceedings of the National Academy of Sciences USA* **111**, 11551–11556.
- Rodriguez-Villalon A, Gujas B, van Wijk R, Munnik T, Hardtke CS.** 2015. Primary root protophloem differentiation requires balanced phosphatidylinositol-4,5-bisphosphate levels and systemically affects root branching. *Development* **142**, 1437–1446.
- Shiu SH, Bleeker AB.** 2001a. Plant receptor-like kinase gene family: diversity, function, and signaling. *Science Signaling* **2001**, re22.
- Shiu SH, Bleeker AB.** 2001b. Receptor-like kinases from *Arabidopsis* form a monophyletic gene family related to animal receptor kinases. *Proceedings of the National Academy of Sciences USA* **98**, 10763–10768.
- Song XF, Guo P, Ren SC, Xu TT, Liu CM.** 2013. Antagonistic peptide technology for functional dissection of CLV3/ESR genes in *Arabidopsis*. *Plant Physiology* **161**, 1076–1085.
- Stahl Y, Wink RH, Ingram GC, Simon R.** 2009. A signaling module controlling the stem cell niche in *Arabidopsis* root meristems. *Current Biology* **19**, 909–914.
- Stahl Y, Grabowski S, Bleckmann A, et al.** 2013. Moderation of *Arabidopsis* root stemness by CLAVATA1 and ARABIDOPSIS CRINKLY4 receptor kinase complexes. *Current Biology* **23**, 362–371.
- Stenvik GE, Butenko MA, Urbanowicz BR, Rose JK, Aalen RB.** 2006. Overexpression of INFLORESCENCE DEFICIENT IN ABCISSION activates cell separation in vestigial abscission zones in *Arabidopsis*. *The Plant Cell* **18**, 1467–1476.
- Stenvik GE, Tandstad NM, Guo Y, Shi CL, Kristiansen W, Holmgren A, Clark SE, Aalen RB, Butenko MA.** 2008. The EPIP peptide of INFLORESCENCE DEFICIENT IN ABCISSION is sufficient to induce abscission in *Arabidopsis* through the receptor-like kinases HAESA and HAESA-LIKE2. *The Plant Cell* **20**, 1805–1817.
- Stes E, Gevaert K, De Smet I.** 2015. Phosphoproteomics-based peptide ligand-receptor kinase pairing. Commentary on: "A peptide hormone and its receptor protein kinase regulate plant cell expansion". *Frontiers in Plant Science* **6**, 224.
- Truernit E, Bauby H, Dubreucq B, Grandjean O, Runions J, Barthelemy J, Palauqui JC.** 2008. High-resolution whole-mount imaging of three-dimensional tissue organization and gene expression enables the study of phloem development and structure in *Arabidopsis*. *The Plant Cell* **20**, 1494–1503.
- Xu T-T, Ren S-C, Song X-F, Liu C-H.** 2015. CLE19 expressed in the embryo regulates both cotyledon establishment and endosperm development in *Arabidopsis*. *Journal of Experimental Botany* **66**, 5217–5227.
- Yang SL, Xie LF, Mao HZ, Puah CS, Yang WC, Jiang L, Sundaresan V, Ye D.** 2003. Tapetum determinant1 is required for cell specialization in the *Arabidopsis* anther. *The Plant Cell* **15**, 2792–2804.

## SUPPLEMENTAL TABLES

	starch in D1	no starch in D1	no starch in D1+D2	starch in QC	starch in P1	n
Col-0	2.20	65.20	32.60	0.00	0.00	89
<i>cle40-2</i>	1.20	40.70	58.10	0.00	0.00	86
Col-0 + CLE40p	53.97	36.51	3.17	6.35	0.00	63
Col-0 + CLE40p <sup>61hr</sup>	31.82	53.03	10.61	4.55	0.00	66
Col-0 + CLV3p	66.67	19.44	9.72	4.17	0.00	72
Col-0 + CLV3p <sup>61hr</sup>	62.90	20.97	6.45	9.68	0.00	62

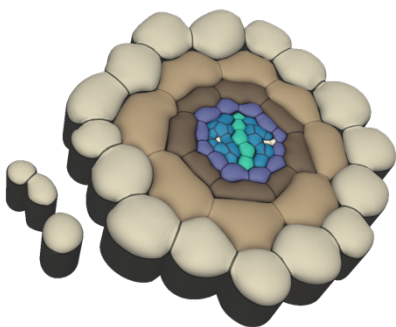
**Table S1. Quantification of distal root phenotypes after antagonistic peptide treatments.**

Frequency in percent of *A. thaliana* roots carrying starch granules in the designated domains with or without peptide treatment. Seedlings were assayed by mPSPI staining 5 days after germination on medium  $\pm$  1  $\mu$ M of peptide. P1 = proximal layer position one; QC = quiescent center position; D1 = distal layer position one; D2 = distal layer position two; n = number of main root tips analysed.

Name	Sequence	6A	6T
CLV3p	RTVPSGPDPLHH	nd	++
IDAp	PIPPSAPGRKHN	++	++
CLE40p	RQVPTGSDPLHH	nd	++
CLE27p	RIVPSCPDLHN	++	++
CLE26p	RKVPRGDPPIHN	++	+
CLE1/4p	RLSPGGDPDRHH	-	-
CLE7p	RFSPGGDPQHH	-	-
CLE45p	RRVRRGSDPIHN	nd	(+)

**Table S2. Summary of mutations and phenotypes.** Mutations at position six in CLE or IDA peptides has little effect in the context P[S/T]mP (where m is a mutation to A or T), but produce a peptide with reduced activity in the context [P/R]RmP. nd, not determined.

## Chapter 2



## Molecular genetic framework for protophloem formation

Rodriguez-Villalon A, Gujas B, Kang YH, Breda AS, Cattaneo P, Depuydt S, Hardtke CS

Proc Natl Acad Sci U S A. 2014 Aug 5; 111 (31): 11551-6

### Highlights

- Exogenous applications of CLE45 boost BAM3 signalling, which inhibits protophloem specification by locking sieve elements precursors in their undifferentiated state.
- Gap cells might likely be the consequence of above-threshold activity of the CLE45-BAM3 module in CLE45G6T transgenic plants, and *brx-2* and *ops-2* mutants.
- Protophloem discontinuity might impair the transfer of growth-limiting metabolites and developmental signals such as auxin, affecting not only meristematic activity but also whole root system architecture.
- *BRX* and *OPS* positively regulate the rate and timing of protophloem differentiation, rather than a single event of specification.

### My contribution

I evaluated the root growth inhibiting activity of CLE45G6T by exogenous applications of peptide to seedlings. In addition, I described the effects induced by the modified peptide on protophloem formation, contributing to the notion that CLE45G6T is a weak form of the corresponding natural peptide. I provided datasets presented in Fig. 1K, L, M, N and S 1B.

# Molecular genetic framework for protophloem formation

Antia Rodriguez-Villalon, Bojan Gujas, Yeon Hee Kang, Alice S. Breda, Pietro Cattaneo, Stephen Depuydt, and Christian S. Hardtke<sup>1</sup>

Department of Plant Molecular Biology, University of Lausanne, CH-1015 Lausanne, Switzerland

Edited by Philip N. Benfey, Duke University, Durham, NC, and approved June 20, 2014 (received for review April 22, 2014)

The phloem performs essential systemic functions in tracheophytes, yet little is known about its molecular genetic specification. Here we show that application of the peptide ligand CLAVATA3/EMBRYO SURROUNDING REGION 45 (CLE45) specifically inhibits specification of protophloem in *Arabidopsis* roots by locking the sieve element precursor cell in its preceding developmental state. CLE45 treatment, as well as viable transgenic expression of a weak CLE45<sup>G6T</sup> variant, interferes not only with commitment to sieve element fate but also with the formative sieve element precursor cell division that creates protophloem and metaphloem cell files. However, the absence of this division appears to be a secondary effect of discontinuous sieve element files and subsequent systemically reduced auxin signaling in the root meristem. In the absence of the formative sieve element precursor cell division, metaphloem identity is seemingly adopted by the normally procambial cell file instead, pointing to possibly independent positional cues for metaphloem formation. The protophloem formation and differentiation defects in *brevis radix* (*brx*) and *octopus* (*ops*) mutants are similar to those observed in transgenic seedlings with increased CLE45 activity and can be rescued by loss of function of a putative CLE45 receptor, BARELY ANY MERISTEM 3 (*BAM3*). Conversely, a dominant gain-of-function *ops* allele or mild *OPS* dosage increase suppresses *brx* defects and confers CLE45 resistance. Thus, our data suggest that delicate quantitative interplay between the opposing activities of *BAM3*-mediated CLE45 signals and *OPS*-dependent signals determines cellular commitment to protophloem sieve element fate, with *OPS* acting as a positive, quantitative master regulator of phloem fate.

stem cell | division plane switching

The vascular tissues of higher plants are an important evolutionary invention that enabled their land conquest (1). At the heart of the plant vasculature, xylem tissue transports water and inorganic nutrients absorbed by the root system to aboveground organs, whereas phloem tissue distributes photosynthetic assimilates as well as systemic signals throughout the plant to coordinate its growth (1, 2). In *Arabidopsis thaliana* (*Arabidopsis*) roots, the vascular tissues are formed from stem cells located at the root tip, in the root meristem (1, 3). They create a bilaterally arranged vasculature, with central neighboring protoxylem and metaxylem cells that span the diameter of the stele, and two phloem poles that are located opposite of each other, flanking the xylem. Each phloem pole is composed of two distinct and intimately connected cell types: the sieve elements, which are the actual conductive cells of the phloem, and the companion cells, which provide essential metabolic functions for the enucleated sieve elements. Each phloem pole's sieve elements are ultimately derived from a single stem cell, which produces a daughter cell by anticlinal division (Fig. L4). This stem cell daughter (termed the sieve element procambium precursor cell here) then switches division plane to give rise to two cells by periclinal division. Whereas the inner cell forms a cell file of procambial character by subsequent anticlinal divisions, the outer cell (termed the sieve element precursor cell here) eventually divides periclinal once more. The cell file subsequently formed by the inner cell

eventually differentiates into metaphloem further up in the root to functionally replace the protophloem (1), which differentiates closer to the tip from the cell file emerging from the outer cell. Finally, as these cell files differentiate into sieve elements, the immediately neighboring cell files (which originate from different stem cells) synchronously differentiate into companion cells, although with a delay of two to four cells with respect to the sieve elements. In the *Arabidopsis* root meristem, the protophloem strands can be identified in confocal microscopy through their enhanced propidium iodide cell wall staining (Fig. 1B) (4).

Mutant analyses in *Arabidopsis* have identified various genes involved in the formation of vascular tissues (1, 3, 5–9). In addition to upstream regulators required for overall vascular morphogenesis, these screens have also identified factors that are specifically involved in xylem or phloem development. However, whereas various signaling pathway components and transcriptional regulators required for xylem development have been found, comparatively little is known about phloem development (1). The few identified specific regulators of phloem formation include the transcription factor ALTERED PHLOEM DEVELOPMENT (*APL*) (5) and OCTOPUS (*OPS*), a polar localized plasma membrane-associated protein of unknown biochemical function (10). *APL* is required for completion of protophloem and metaphloem differentiation, and its loss of function results in the replacement of functional phloem with cells that display xylem characteristics (1, 5). *OPS* loss of function has been reported to delay protophloem differentiation because in a stochastic manner, individual *ops* protophloem cells fail to undergo the nuclear degradation and cell wall thickening that characterizes sieve element formation (10). These undifferentiated cells (termed gap cells here) interrupt the protophloem sieve element strand integrity and, thus, likely source-to-sink transfer of growth-limiting metabolites and developmental signals, which eventually

## Significance

The emergence of vascular tissues played a central role in the plant conquest of land. Both xylem and phloem are essential for the development of flowering plants, yet little is known about the molecular genetic control of phloem specification and differentiation. Here we show that delicate quantitative interplay between two opposing signaling pathways determines cellular commitment to protophloem sieve element fate in root meristems of the model plant *Arabidopsis thaliana*. Our data suggest that a recently described phloem-specific protein is a positive, quantitative master regulator of phloem fate.

Author contributions: A.R.-V., B.G., Y.H.K., A.S.B., P.C., and C.S.H. designed research; A.R.-V., B.G., Y.H.K., A.S.B., and P.C. performed research; S.D. contributed new reagents/analytic tools; A.R.-V., B.G., Y.H.K., A.S.B., P.C., and C.S.H. analyzed data; and A.R.-V. and C.S.H. wrote the paper.

The authors declare no conflict of interest.

This article is a PNAS Direct Submission.

<sup>1</sup>To whom correspondence should be addressed. Email: christian.hardtke@unil.ch.

This article contains supporting information online at [www.pnas.org/lookup/suppl/doi:10.1073/pnas.1407337111/-DCSupplemental](http://www.pnas.org/lookup/suppl/doi:10.1073/pnas.1407337111/-DCSupplemental).

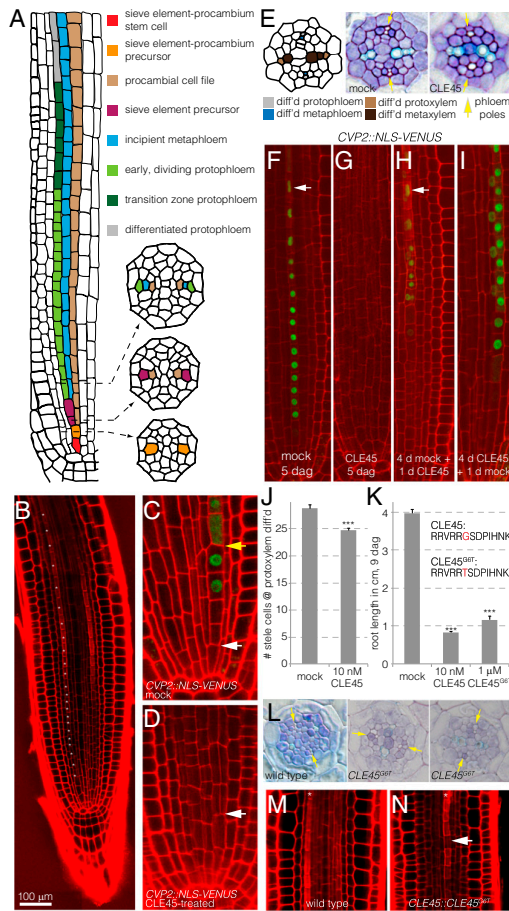


**Fig. 1.** Elevated CLE45 activity suppresses protophloem sieve element differentiation and the formative cell division of the sieve element precursor cell. (A) Schematic presentation of protophloem sieve element formation in the *Arabidopsis* root meristem. (B) Confocal microscopy image of a propidium iodide-stained root meristem. The developing protophloem strands (one of them marked by asterisks) stand out because of their enhanced propidium iodide cell wall staining, allowing their unequivocal identification. (C and D) Expression pattern of the *CVP2::NLS-VENUS* fluorescent reporter in 5-d-old wild-type roots on normal media (C) or when shifted onto media containing 10 nM CLE45 for 24 h after 4 d (D). (E) Toluidine blue-stained histological cross sections of mock- and CLE45-treated roots, taken at the level of advanced metaxylem differentiation. Differentiated protophloem and metaxylem sieve elements can be recognized by their position and by the absent staining. Note differentiated metaxylem, but not protophloem, in the CLE45-treated sample. (F–I) Effects of transient CLE45 application on protophloem differentiation, monitored in *CVP2::NLS-VENUS* plants. White arrowheads (F and H): advanced nuclear degradation in the most apical transition zone cells. (I, composite image). (J) Reduced stele cell number in CLE45-treated plants resulting from missing cell files, counted at the position of differentiated xylem. (K) Root growth inhibition by application of CLE45 or the CLE45<sup>G6T</sup> variant. (L) Cross-sections illustrating representative phenotypes of plants expressing a *CLE45::CLE45<sup>G6T</sup>* transgene with delayed protophloem differentiation (Center) or delayed protophloem differentiation and missing cell file (Right). (M and N) Occurrence of gap cells (arrowhead) in the protophloem transition zone of *CLE45::CLE45<sup>G6T</sup>* (N), but not wild type plants (M). \*\*\**P* < .001.

compromises root growth (10). A similar phenotype is observed in loss-of-function mutants of *BREVIS RADIX (BRX)* (11), another polar localized plasma membrane-associated protein that is also thought to act in the nucleus (11, 12). The *brx* short root phenotype is rescued by second site mutation in *BARELY ANY MERISTEM 3 (BAM3)*, which encodes a receptor-like kinase that is required for suppression of protophloem differentiation on treatment with the peptide ligand, CLAVATA3/EMBRYO SURROUNDING REGION 45 (CLE45) (13).

**Results and Discussion**

To better characterize CLE45 effects, we sought to establish a specific molecular marker for sieve element fate. The *COTYLEDON VASCULAR PATTERN 2 (CVP2)* gene, which is required for vascular morphogenesis (14), turned out to specifically mark the sieve element precursor cell and the subsequent protophloem cell file, as revealed by a nuclear localized fluorescent VENUS reporter protein expressed under control of the *CVP2* promoter (*CVP2::NLS-VENUS*) (Fig. 1C). In seedlings shifted onto media containing CLE45, *CVP2* expression disappeared concomitant with cell wall build-up (Fig. 1D and G), confirming that CLE45 suppresses protophloem differentiation (Fig. 1E–G) (13). Moreover, the periclinal division of the sieve element precursor cell did not occur, leading to a loss of the incipient metaxylem cell file (Fig. 1D, E, and J). Transient treatments revealed that CLE45 only acted on cells that had not yet started the differentiation process (Fig. 1H) and that its effects were reversible; that is, cells formed during CLE45 treatment started to express *CVP2* and differentiate into protophloem (as indicated by recovery of *APL* expression) once seedlings were shifted to CLE45-free media (Fig. 1I and Fig. S14). Thus, the data suggest that CLE45 treatment locks the sieve element precursor cell in its preceding developmental state, and thereby prevents protophloem differentiation.

Because we could not recover transgenic lines with increased CLE45 dosage (13), we constructed a weak CLE45 variant to verify these effects *in planta*. The amino acid at position 6 of CLE peptides is crucial for their activity (15), and indeed, replacement of the corresponding glycine by threonine yielded a CLE45 variant (CLE45<sup>G6T</sup>) that had identical effects as the wild-type version but required application of higher peptide concentrations (Fig. 1K). Plants that expressed a corresponding *CLE45::CLE45<sup>G6T</sup>* transgene could be recovered, and in all of these independent lines, root growth was impaired (Fig. S1B), the periclinal division of the sieve element precursor cell was frequently abolished, and protophloem differentiation was frequently delayed (Fig. 1L and Fig. S1C). Moreover, *CLE45::CLE45<sup>G6T</sup>* transgenics displayed stochastic occurrence of nondifferentiating protophloem cells, which were morphologically similar to the gap cells observed in *brx* and *ops* mutants (Fig. 1M and N). Thus, a mild increase in *CLE45-like* activity interfered both with the formative division that gives rise to the metaxylem and protophloem cell files and with protophloem differentiation.

These results supported the notion that the gap cell phenotype of *brx* mutants reflects stochastic above-threshold activity of the CLE45-BAM3 pathway (13). Further corroborating the phenotypic similarity between increased CLE45 dosage and *BRX* loss of function, closer inspection of *brx* mutants revealed a previously unrecognized phenotype; that is, the absence or severe delay of the sieve element precursor cell's periclinal division in the majority of phloem poles (Fig. 2A and C). The same phenotype, although at possibly lower penetrance, was also observed in *ops* mutants (Fig. 2B and C). In summary, *CLE45::CLE45<sup>G6T</sup>* plants, *brx* mutants, and *ops* mutants all displayed a similar phenotype spectrum that included frequently absent sieve element precursor division, the occurrence of gap cells, and an associated reduction in the number of early dividing protophloem cells, in root meristem size and root growth (Fig. 2D and E).

Notably, even in the absence of the incipient metaphloem cell file in the three genotypes, cells with metaphloem morphology appeared in the correct position, possibly because the normally procambial cell file adopted metaphloem identity.

Gap cells are located in the protophloem transition zone (Figs. 1A and 2E), and characterization of wild-type and the *ops* mutant has shown that this is where key events of protophloem sieve element differentiation take place, such as cell wall thickening and nuclear degradation (10, 16). To further characterize *brx* gap cells, we introduced a nuclear marker into the mutant, the stabilized fluorescent fusion protein mDII-VENUS, expressed under the constitutive 35S promoter (17). Investigation of these lines revealed that *brx* gap cells indeed displayed a persisting nucleus concomitant with the lack of cell wall thickening, similar to *ops* gap cells (Fig. 2F). Moreover, a fluorescent cytoskeleton marker, that is, FIMBRIN-GFP expressed under the constitutive

35S promoter (18), revealed a characteristic increase of actin filament abundance during protophloem differentiation, which did not occur in gap cells (Fig. 2G). Finally, the failure to form a continuous file of proper protophloem sieve elements possibly impinges on the differentiation of the neighboring companion cells because expression of the companion cell-specific *SUCROSE TRANSPORTER 2* (*SUC2*) gene, monitored by a fluorescent reporter (*SUC2::GFP*) (19), was frequently patchy or absent in *brx* phloem poles (Fig. 2H–K). Consistent with this observation, CLE45 treatment also suppressed *SUC2::GFP* expression (Fig. 2K and L).

The close relation between the action of *BRX* and *OPS* in protophloem formation was also underlined by our finding that one of the loci emerging from a *brx* second site suppressor screen (13) mapped to the *OPS* locus. The corresponding *ops* allele carries a glutamate to lysine mutation in position 319 (E319K), which segregated as a dosage-dependent semidominant suppressor locus (Fig. 3A and Fig. S1D). In the F1 obtained from crosses between the *ops* loss-of-function and the *ops*<sup>E319K</sup> mutant, the *ops* root growth defects were fully restored, suggesting that *ops*<sup>E319K</sup> is a genuine, fully active gain-of-function allele (Fig. 3B). Moreover, we observed dosage-dependent *OPS* action in plants expressing extra copies of wild-type *OPS* fused to GFP under control of the native *OPS* promoter (*OPS::OPS-GFP*); this transgene was functional, as indicated by its ability to rescue the *ops* mutant phenotype (Fig. 3C). When introduced into *brx* mutants, this construct rescued the root phenotype to varying extents, apparently correlating with *OPS-GFP* signal intensity in individual lines and frequently conferring near-wild-type levels of root growth (Fig. 3D). Concomitantly, the missing sieve element precursor division was restored (Fig. 3E) and gap cells were absent. When introduced into wild-type background, *OPS::OPS-GFP* transgene copies conferred resistance to CLE45 treatment (Fig. 3F), and the same was true for the *ops*<sup>E319K</sup> single mutant (Fig. 3G and H). Thus, an increase in *OPS* activity was sufficient to overcome the inhibitory effects of CLE45 treatment. This CLE45-resistance through enhanced *OPS* activity largely depended on the presence of functional *BRX* (Fig. 3F and Fig. S1D), suggesting that *BRX* conditions *OPS* action by keeping CLE45-BAM3 activity below a certain threshold level. Finally, corroborating this dose-dependent opposition between CLE45 and *OPS* action, *ops* root growth and protophloem differentiation defects were perfectly rescued in *bam3 ops* double mutants (Fig. 3I and J), similar to *bam3 brx* double mutants (13).

The highly specific meristematic reporter gene expression patterns of the five genes analyzed in this study matched a role in protophloem differentiation (Fig. 4A). *OPS* expression was also observed outside of the protophloem lineage, in the metaphloem, indicating that *OPS* may operate more generally during vascular development. The observation of the reporters' expression across a number of samples that represented various stages in the differentiation process (e.g., samples in which two or three sieve element precursors could be observed because they had not yet divided compared with samples in which this was only the case for one) allowed us to establish a spatiotemporal hierarchy of expression (Fig. 4B). *OPS* was thus expressed earliest and was consistently present in the sieve element procambium precursor cell, whereas *BRX*, *BAM3*, *CLE45*, and *CVP2* could only be detected in the sieve element precursor cell. However, although *CLE45* expression was typically observed immediately after its formation, *BRX* and *BAM3* were expressed with some delay, and *CVP2* even later. These expression patterns are consistent with the observed defects in protophloem differentiation but are also consistent with the absent formative division of the sieve element precursor cell. However, it appears unlikely that the acquisition of sieve element precursor fate includes an obligatory periclinal cell division, because in roots grown on CLE45-containing media for 4 d and then shifted onto

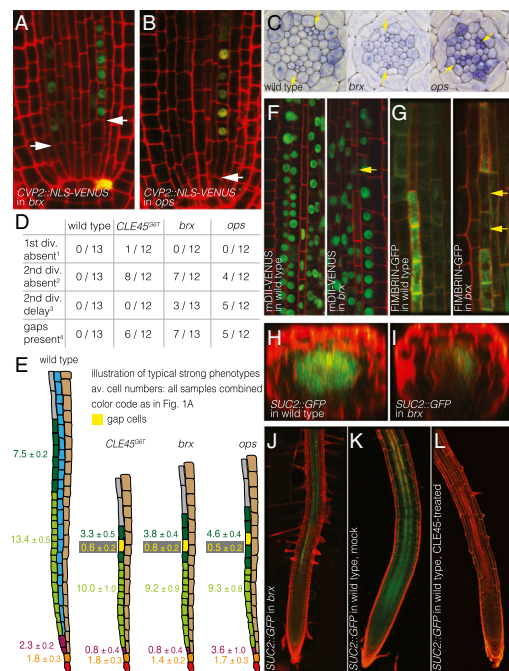
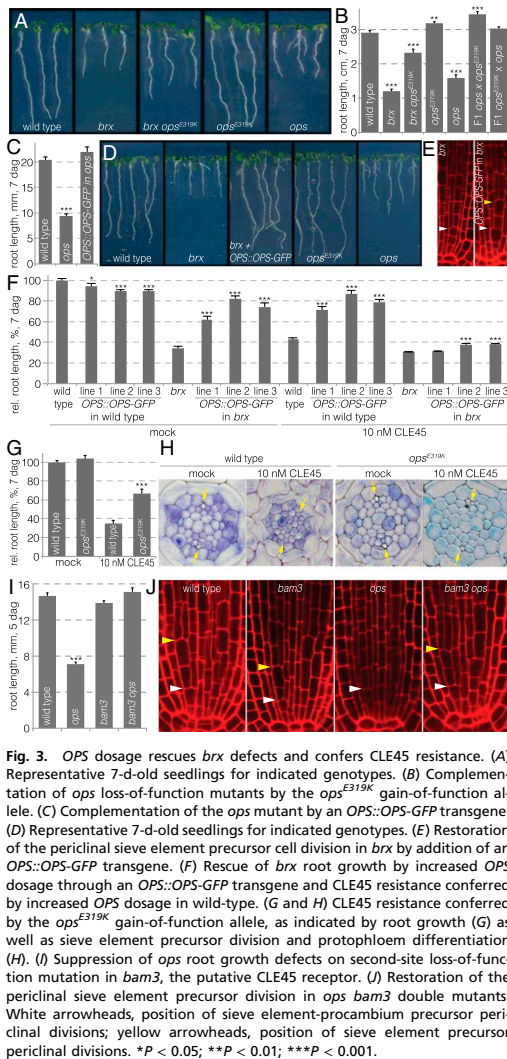


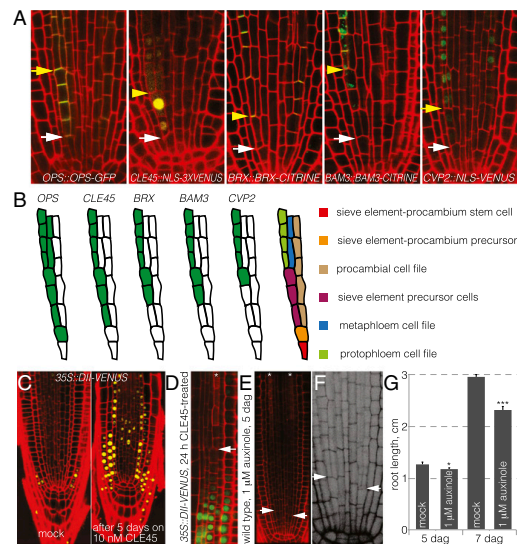
**Fig. 2.** Perturbed phloem formation in *CLE45::CLE45<sup>GFT</sup>* transgenic plants, *brx* mutants, and *ops* mutants. (A and B) Absence of the periclinal sieve element precursor cell division, but not the periclinal sieve element procambium precursor cell division (arrowhead), in *brx* (A) and *ops* (B). (C) Cross-sections show differentiated protophloem (arrowheads) in both phloem poles of wild-type at the level of differentiated protoxylem, but no differentiation in at least one pole in *brx* and *ops*. (D) Summary statistics of protophloem development defects in one typical experiment. (E) Illustration of the maximum penetrance phloem pole phenotypes, with average cell numbers across samples indicated. (F) Persistence of the nucleus in *brx* gap cells (arrowhead), as indicated by the nuclear mDII-VENUS marker. (G) Absence of the typical strong actin cytoskeleton signal in *brx* gap cells (arrowheads), as indicated by the FIMBRIN-GFP marker (composite image on the left). (H and I) Optical sections showing local and diffused GFP signal expressed under control of the companion cell-specific *SUC2* promoter, from both poles in wild-type (H) and from typically at most one pole in *brx* (I). (J–L) Patchy, interrupted *SUC2::GFP* expression in *brx* (J) compared with wild-type (K), and suppression of the signal in seedlings grown on CLE45-containing media (L).



CLE45-free media, protoxylem differentiation occurred within 20 h (as determined by *CVP2* expression, *APL* expression, and cell wall build-up). In contrast, the missing cell division had not yet been recovered at this point in most samples (Fig. 1I). Conversely, in roots grown on CLE45-free media for 4 d and then shifted onto CLE45-containing media, protoxylem differentiation was repressed within 20 h, whereas the periclinal sieve element precursor cell division was only fully suppressed in all samples after 30 h.

The frequent lack of this division in the *brx*, *ops*, and *CLE45::CLE45*<sup>G6T</sup> genotypes might therefore be an indirect effect of the interruption of protoxylem sieve element files by undifferentiated cells (Fig. S1E), which could interfere with the transport of metabolites and systemic signals, such as the plant

hormone auxin, to the meristem (1, 2, 10, 13). Because it has been suggested that threshold levels of auxin are necessary for periclinal cell divisions in the root meristem (20), and because higher auxin activity was detected in developing protoxylem compared with surrounding tissues (21) (Fig. S1F), we investigated whether a reduced meristematic auxin response, as indicated by the auxin sensor DII-VENUS (17), could be responsible for the absence of the sieve element precursor cell division. Consistent with these observations, CLE45 application resulted in reduced auxin response in the root meristem on prolonged, but not on short (i.e., a few hours), treatment (Fig. 4C). Observation of seedlings treated with CLE45 for 24 h also indicated coincidence of undetectable levels of DII-VENUS (i.e., high auxin activity) with the last periclinal sieve element precursor division before CLE45 application, and low auxin activity in cells formed thereafter (Fig. 4D). Moreover, treatment of seedlings with auxinole, a specific inhibitor of the nuclear auxin receptors, and thus auxin response (22, 23), abolished this division when applied at mild concentration (Fig. 4E and F), suggesting it is particularly sensitive to changes in auxin activity. Given that *BRX* has been implicated in potentiating auxin



hormone auxin, to the meristem (1, 2, 10, 13). Because it has been suggested that threshold levels of auxin are necessary for periclinal cell divisions in the root meristem (20), and because higher auxin activity was detected in developing protoxylem compared with surrounding tissues (21) (Fig. S1F), we investigated whether a reduced meristematic auxin response, as indicated by the auxin sensor DII-VENUS (17), could be responsible for the absence of the sieve element precursor cell division. Consistent with these observations, CLE45 application resulted in reduced auxin response in the root meristem on prolonged, but not on short (i.e., a few hours), treatment (Fig. 4C). Observation of seedlings treated with CLE45 for 24 h also indicated coincidence of undetectable levels of DII-VENUS (i.e., high auxin activity) with the last periclinal sieve element precursor division before CLE45 application, and low auxin activity in cells formed thereafter (Fig. 4D). Moreover, treatment of seedlings with auxinole, a specific inhibitor of the nuclear auxin receptors, and thus auxin response (22, 23), abolished this division when applied at mild concentration (Fig. 4E and F), suggesting it is particularly sensitive to changes in auxin activity. Given that *BRX* has been implicated in potentiating auxin

response (11, 24), this would also explain why the penetrance of the observed phenotypes was highest in *brx* mutants. Remarkably, however, root growth rate and meristem size were only mildly impaired in auxinole-treated roots, despite the absence of the incipient metaphloem cell file (Fig. 4G), and protophloem differentiation was not affected. This underlines the proposed essential function of the protophloem for root meristem growth in the early seedling and systemic performance of the root system later on (13, 25). Systemically reduced auxin activity could also account for the observation that on CLE45 treatment, and in *brx* or *ops* loss-of-function mutants, overall cell number was sometimes slightly reduced in the radial dimension beyond the two missing incipient metaphloem cell files (e.g., Fig. 1J).

In summary, our data suggest opposing activities of *BAM3*-mediated CLE45 signals on one side and *OPS*-dependent signals on the other. Their quantitative interplay is sensitive to both CLE45 and *OPS* dosage and determines the proper timing of protophloem specification and the progression of its differentiation. Our analyses suggest these pathways act specifically on sieve element precursors, although based on expression pattern *OPS* might even have an earlier role. Notably, both *brx* and *ops* loss-of-function mutants are, in principal, able to form sieve elements, although at a reduced frequency. Considering that CLE45 specifically blocks precursor cells from adopting sieve element fate, the main role of *BRX* and *OPS* is therefore apparently to promote the transition to this state and to maintain it. The existence of independent positional cues for sieve element differentiation is also suggested by our observation that even in the absence of the incipient metaphloem cell file in *brx* and *ops* mutants, cells with metaphloem morphology differentiated in the correct position, possibly because the normally procambial cell file apparently adopted metaphloem identity. Because CLE45 can fully suppress any protophloem differentiation, the gap cells in the protophloem transition zone of *brx* and *ops* mutants might reflect incompetence to respond to such cues because of stochastic above-threshold activity of the CLE45-BAM3 module. Finally, we describe a genetic framework that is specific for protophloem sieve element differentiation, which, however, is possibly also necessary for parallel differentiation of companion cells, and thus the formation of functional protophloem poles. However, because loss-of-function *brx bam3* or *ops bam3* double mutants appear to be wild-type, our data also indicate that neither of these genes is strictly required for protophloem formation. Thus, they might constitute an additional regulatory layer, which could, for instance, serve to convey environmental signals in conditions in which a shutdown of primary root growth might be advantageous. The associated systemic effects, for example, ref. 25, would support such a scenario.

## Materials and Methods

Plant tissue culture, CLE peptide treatments, plant transformation, histology, light microscopy, and confocal microscopy, as well as molecular biology experiments such as genomic DNA isolation, genotyping, or sequencing, were performed according to standard procedures, as described previously (11, 13).

- Lucas WJ, et al. (2013) The plant vascular system: Evolution, development and functions. *J Integr Plant Biol* 55(4):294–388.
- Ruiz-Medrano R, Xoconostle-Cázares B, Lucas WJ (2001) The phloem as a conduit for inter-organ communication. *Curr Opin Plant Biol* 4(3):202–209.
- Helariutta Y (2007) Cell signalling during vascular morphogenesis. *Biochem Soc Trans* 35(Pt 1):152–155.
- Truernit E, et al. (2008) High-resolution whole-mount imaging of three-dimensional tissue organization and gene expression enables the study of Phloem development and structure in Arabidopsis. *Plant Cell* 20(6):1494–1503.
- Bonke M, Thitamadee S, Mähönen AP, Hauser MT, Helariutta Y (2003) APL regulates vascular tissue identity in Arabidopsis. *Nature* 426(6963):181–186.
- De Rybel B, et al. (2013) A bHLH complex controls embryonic vascular tissue establishment and indeterminate growth in Arabidopsis. *Dev Cell* 24(4):426–437.
- Hardtke CS, Berleth T (1998) The Arabidopsis gene MONOPTEROS encodes a transcription factor mediating embryo axis formation and vascular development. *EMBO J* 17(5):1405–1411.

The *OPS* suppressor locus was identified by combined bulk segregant analysis and whole-genome sequencing, followed by confirmation through Sanger sequencing, as described (13).

**Plant Materials.** The *Arabidopsis* wild-type line used in this study was Columbia (Col-0), which was also the genetic background for the mutants and transgenic lines. The following null mutant alleles were used throughout: *brx-2* for *BRX*, *bam3-2* for *BAM3*, and *ops-2* for *OPS*. These mutants, as well as the transgenic reporter lines *35S::DII-VENUS*, *35S::mDII-VENUS*, and *35S::FIMBRIN-GFP*, have been described previously (10, 13, 17, 18).

**Transgenic Lines.** Reporter transgenes for plant transformation were created in suitable binary vectors and produced through standard molecular biology procedures and/or the Gateway Cloning Technology. The promoters or coding sequences for the *BAM3*, *BRX*, and *CLE45* reporter constructs have been described previously (13). For cloning of the *CVP2::NLS-VENUS* construct, a 1.5-kb genomic promoter fragment upstream of the initiation codon was amplified using the 5' to 3' oligonucleotides GGT TTG TGG CAA TTT GTA TCC and GCT TTT AAA TTC CAT GAA GAT GGG C. For cloning of the *SUC2::GFP* construct, a 2.3-kb genomic promoter fragment upstream of the initiation codon was amplified using the 5' to 3' oligonucleotides AGT CAT TAT CAA CTA GGG GTG CAT and ATT TGA CAA ACC AAG AAA GTA AGA AAA. For cloning of the *BAM3::BAM3-CITRINE* construct, the *BAM3* coding sequence was amplified using the 5' to 3' oligonucleotides ATG GCA GAC AAG ATC TTC AC and GAA AGT ATT AGG CTG TTT AG. For cloning of the *OPS::OPS-GFP* construct, a 1.9-kb *OPS* promoter fragment was amplified together with the (intron-free) *OPS* coding sequence using the 5' to 3' oligonucleotides GCG GTG TAA TCA TTA TTT CGT and TAT ACA GCC TCA TTA CAC TCC. To generate the *CLE45::CLE45<sup>567</sup>* construct, a replacement of the glycine in position 6 by threonine was introduced in the *CLE45* peptide coding sequence by amplification with the 5' to 3' oligonucleotides ATG TTG GGT TCC AGT ACA AGA and AGG ATC TGA TGT TCG TCT, followed by secondary amplification with the 5' to 3' oligonucleotides ATG TTG GGT TCC AGT ACA AGA and TTA AGA AAA TGG CTG AGC TT to introduce the mutation. All binary constructs were introduced into *Arabidopsis* backgrounds by Agrobacterium-mediated transformation following standard procedures. At least three independent transgenic lines were used for each construct to perform experiments and verify reproducibility.

**Genotyping.** Genotyping of mutant alleles was performed with the following 5' to 3' oligonucleotides: GTC AGT GTT TGC TTC CTC TCT ATG and TAT TTC CTT GTC TAG GTA AGA ATC C and TGA TCC ATG TAG ATT TCC CGG ACA TGA A in one reaction to genotype *brx-2* (wild-type band 240 bp; T-DNA insertion band 200 bp); CTG CAA CTT CTT CTC CGT TTG with CTG CAA CTT CTT CTC CGT TTG to genotype the *BAM3* wild-type allele (1.1 kb) and GAT TCC TTC GAA ACT CGG ATC with ATT TTG CCG ATT TCG GAA C (300 bp) to genotype the *bam3-2* T-DNA insertion allele; CAC ACC GTT GGT TTG GTT AAC with TCT TCC TCT AAA AAG CCT CCG to genotype the *OPS* wild-type allele (1.1 kb) and TCT TCC TCT AAA AAG CCT CCG with ATT TTG CCG ATT TCG GAA C (600 bp) to genotype the *ops-2* T-DNA insertion allele; and CTT CAG AAA TGG AGG CAG AAT and CAT ATC CGT AAT CAG CAA GCT to amplify a 145-bp *OPS* fragment that is cut into 124 and 21 bp on *Hin*III digest if the *ops<sup>E319K</sup>* mutation is present.

**ACKNOWLEDGMENTS.** We thank Prof. N. Geldner's group for providing vectors and F. Miseco for *BRX::BRX-CITRINE* seeds. This work was supported by Swiss National Science Foundation Grant 310030B\_147088 (to C.S.H.) and a European Molecular Biology Organization Long-Term Postdoctoral Fellowship (to A.R.-V.).

- Mähönen AP, et al. (2006) Cytokinin signaling and its inhibitor AHP6 regulate cell fate during vascular development. *Science* 311(5757):94–98.
- Mähönen AP, et al. (2000) A novel two-component hybrid molecule regulates vascular morphogenesis of the Arabidopsis root. *Genes Dev* 14(23):2938–2943.
- Truernit E, Bauby H, Belcram K, Barthélémy J, Palauqui JC (2012) OCTOPUS, a polarly localised membrane-associated protein, regulates phloem differentiation entry in Arabidopsis thaliana. *Development* 139(7):1306–1315.
- Scacchi E, et al. (2010) Spatio-temporal sequence of cross-regulatory events in root meristem growth. *Proc Natl Acad Sci USA* 107(52):22734–22739.
- Scacchi E, et al. (2009) Dynamic, auxin-responsive plasma membrane-to-nucleus movement of Arabidopsis BRX. *Development* 136(12):2059–2067.
- Depuydt S, et al. (2013) Suppression of Arabidopsis protophloem differentiation and root meristem growth by CLE45 requires the receptor-like kinase BAM3. *Proc Natl Acad Sci USA* 110(17):7074–7079.
- Carland FM, Nelson T (2004) Cotyledon vascular pattern2-mediated inositol (1,4,5) triphosphate signal transduction is essential for closed venation patterns of Arabidopsis foliar organs. *Plant Cell* 16(5):1263–1275.

15. Song XF, Guo P, Ren SC, Xu TT, Liu CM (2013) Antagonistic peptide technology for functional dissection of CLV3/ESR genes in *Arabidopsis*. *Plant Physiol* 161(3): 1076–1085.
16. Wu H, Zheng XF (2003) Ultrastructural studies on the sieve elements in root protoplasm of *Arabidopsis thaliana*. *Acta Bot Sin* 45(3):322–330.
17. Brunoud G, et al. (2012) A novel sensor to map auxin response and distribution at high spatio-temporal resolution. *Nature* 482(7383):103–106.
18. Wang YS, Motes CM, Mohamalawari DR, Blancaflor EB (2004) Green fluorescent protein fusions to *Arabidopsis* fimbrin 1 for spatio-temporal imaging of F-actin dynamics in roots. *Cell Motil Cytoskeleton* 59(2):79–93.
19. Ivashikina N, et al. (2003) Isolation of AtSUC2 promoter-GFP-marked companion cells for patch-clamp studies and expression profiling. *Plant J* 36(6):931–945.
20. Yoshida S, et al. (2014) Genetic control of plant development by overriding a geometric division rule. *Dev Cell* 29(1):75–87.
21. Santuari L, et al. (2011) Positional information by differential endocytosis splits auxin response to drive *Arabidopsis* root meristem growth. *Curr Biol* 21(22):1918–1923.
22. Dharmasiri N, et al. (2005) Plant development is regulated by a family of auxin receptor F box proteins. *Dev Cell* 9(1):109–119.
23. Hayashi K, et al. (2012) Rational design of an auxin antagonist of the SCF(TIR1) auxin receptor complex. *ACS Chem Biol* 7(3):590–598.
24. Depuydt S, Hardtke CS (2011) Hormone signalling crosstalk in plant growth regulation. *Curr Biol* 21(9):R365–R373.
25. Gujas B, Alonso-Blanco C, Hardtke CS (2012) Natural *Arabidopsis* brx loss-of-function alleles confer root adaptation to acidic soil. *Curr Biol* 22(20):1962–1968.

# Supporting Information

Rodriguez-Villalon et al. 10.1073/pnas.1407337111

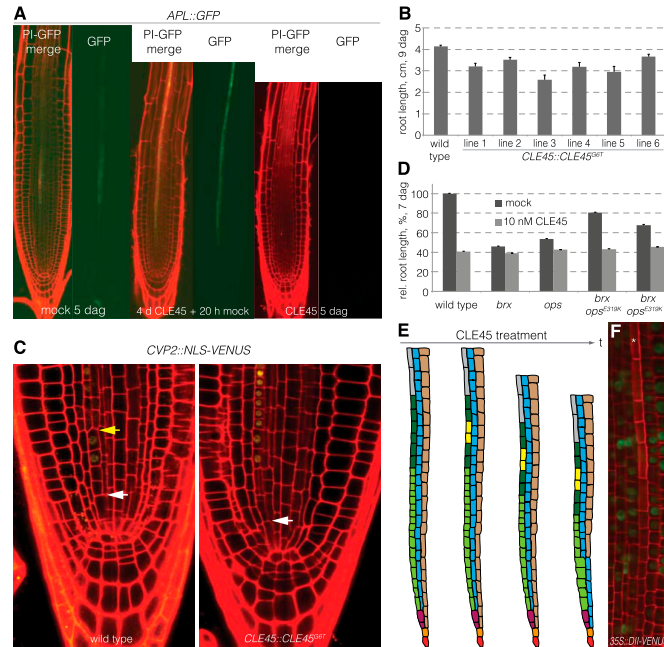
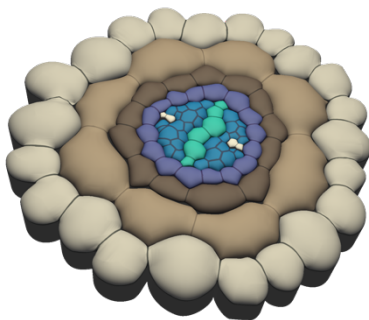


**Fig. 51.** (A) Expression of the *APL::GFP* fluorescent reporter in 5-d-old wild-type roots on normal media (Left), on media containing 10 nM CLE45 (Right), or after 20 h recovery on normal media after 4 d on media containing 10 nM CLE45 (Center). (B) Reduced root growth in *CLE45::CLE45<sup>G6T</sup>* transgenic plants. (C) Absence of the periclinal sieve element precursor cell division (yellow arrowhead in wild-type; Left), but not the periclinal sieve element-procambium precursor cell division (white arrowhead), in *CLE45::CLE45<sup>G6T</sup>* transgenic plants (Right). (D) Root growth of indicated genotypes on CLE45 compared with mock. Note mock difference between *brx* mutants carrying one or two copies of the *ops<sup>E319K</sup>* allele. (E) Schematic presentation of how impaired protophloem formation eventually feeds back on the formative sieve element precursor cell division; for example, on CLE45 treatment. Color code as in Fig. 1A. (F) Higher auxin activity in the protophloem (asterisk) compared with neighboring tissues, as indicated by the DII-VENUS reporter.

## Chapter 3



## Perception of root-active CLE peptides requires CORYNE function in the phloem vasculature

Hazak O, Brandt B, Cattaneo P, Santiago J, Rodriguez-Villalon A, Hothorn M and Hardtke CS

EMBO Rep. 2017 Aug; 18 (8):1367-1381

### Highlights

- Isolation of additional *bam3* loss-of-function alleles highlights the importance of both extracellular and cytoplasmic portions for the function of the receptor.
- Biochemical and genetics results ruled out SERK proteins to be a co-receptor for the BAM3-mediated CLE45 signalling.
- Experimental evidences identify protophloem as the site of action for root-active peptides, whereas CLV2 and CRN might probably control expression, localization and stability of LRR-RK signalling complexes.

### My contribution

I isolated new *bam3* loss-of-function alleles by genetic screening of *brx* suppressors. The different identified non-synonymous substitutions highlight the importance of both cytoplasmic and extra-cellular domains. I contributed the data in Fig. 1a and EV1A.

# Perception of root-active CLE peptides requires CORYNE function in the phloem vasculature

Ora Hazak<sup>1,†</sup>, Benjamin Brandt<sup>2,†</sup>, Pietro Cattaneo<sup>1</sup>, Julia Santiago<sup>2</sup>, Antia Rodriguez-Villalon<sup>1</sup>, Michael Hothorn<sup>2,\*</sup>  & Christian S Hardtke<sup>1,\*\*</sup> 

## Abstract

*Arabidopsis* root development is orchestrated by signaling pathways that consist of different CLAVATA3/EMBRYO SURROUNDING REGION (CLE) peptide ligands and their cognate CLAVATA (CLV) and BARELY ANY MERISTEM (BAM) receptors. How and where different CLE peptides trigger specific morphological or physiological changes in the root is poorly understood. Here, we report that the receptor-like protein CLAVATA 2 (CLV2) and the pseudokinase CORYNE (CRN) are necessary to fully sense root-active CLE peptides. We uncover BAM3 as the CLE45 receptor in the root and biochemically map its peptide binding surface. In contrast to other plant peptide receptors, we found no evidence that SOMATIC EMBRYOGENESIS RECEPTOR KINASE (SERK) proteins act as co-receptor kinases in CLE45 perception. CRN stabilizes BAM3 expression and thus is required for BAM3-mediated CLE45 signaling. Moreover, protophloem-specific CRN expression complements resistance of the *crn* mutant to root-active CLE peptides, suggesting that protophloem is their principal site of action. Our work defines a genetic framework for dissecting CLE peptide signaling and CLV/BAM receptor activation in the root.

**Keywords** CLAVATA; CLE45; MAKRS; receptor kinase; SERK

**Subject Categories** Development & Differentiation; Plant Biology; Signal Transduction

DOI 10.15252/embr.201643535 | Received 19 October 2016 | Revised 4 May 2017 | Accepted 5 May 2017 | Published online 12 June 2017

EMBO Reports (2017) 18: 1367–1381

## Introduction

Receptor kinases (RKs) are key regulators of growth and development in higher plants such as the model organism *Arabidopsis thaliana* (*Arabidopsis*). There are ~180 *Arabidopsis* RKs with extracellular leucine-rich repeat (LRR) domains, many of which can perceive peptide ligands, including members of the CLAVATA3/EMBRYO SURROUNDING REGION (CLE) peptide family [1,2]. CLE peptides are encoded endogenously and translated as

prepropeptides, which are secreted and processed to yield mature 12–13 amino acid, bioactive peptides [2–4]. In some cases, their activity is amplified by post-translational modifications, such as proline hydroxylation and additional arabinosylation [5,6]. *Arabidopsis* contains 32 CLE genes, some of which encode redundant peptides, thereby giving rise to 27 distinct CLE peptides [3,7,8]. Several of these peptides have been shown to play roles in root development, and chemically synthesized versions of many of them suppress *Arabidopsis* root growth in tissue culture when applied at nM to low μM concentrations (called root-active CLEs in the following) [9–11]. However, the perception mechanism for most CLE peptides in the root, including their receptors and co-receptors, remains unknown to date.

Genetic and biochemical studies have identified several LRR-RKs involved in the perception of individual CLE peptides. The outstanding, classic example is CLAVATA 1 (CLV1), which directly binds the CLV3 peptide to regulate stem cell homeostasis in the shoot apical meristem [4,12–17]. The CLV1-related LRR-RK BARELY ANY MERISTEM 3 (BAM3) is required to mediate the suppression of protophloem sieve element differentiation in the root meristem by CLE45 application [9,18,19]. PHLOEM INTERCALATED WITH XYLEM (PXY; a.k.a. TDIF RECEPTOR [TDR]) senses the redundant CLE41/44 peptides (a.k.a. TRACHEARY ELEMENT DIFFERENTIATION INHIBITORY FACTOR [TDIF]) to regulate vascular stem cell proliferation in secondary growth [20–25].

High-affinity ligand sensing and receptor activation of plant LRR-RKs relies on their interaction with shape-complementary co-receptor kinases [1,26–28]. For instance, the LRR-RK BRASSINOSTEROID INSENSITIVE 1 (BRI1) employs the SOMATIC EMBRYOGENESIS RECEPTOR KINASE (SERK) family co-receptors SERK1 and SERK3 to transmit the signal triggered by the small molecule ligand brassinosteroid [29]. The LRR-RK HAESA also relies on SERK proteins to transduce the signal triggered by the peptide ligand IDA, which is related to CLE peptides in structure [30,31]. Consistently, it was recently suggested that SERK1 also plays a role in PXY-mediated CLE41/44 signal transduction [25]. Thus, *Arabidopsis* SERKs have been implicated in multiple signaling pathways, comprising CLE as well as other peptide signals, hormonal cues, and pathogen-derived ligands [32,33]. Beyond PXY, however, it

<sup>1</sup> Department of Plant Molecular Biology, University of Lausanne, Lausanne, Switzerland

<sup>2</sup> Structural Plant Biology Laboratory, Department of Botany and Plant Biology, University of Geneva, Geneva, Switzerland

\*Corresponding author. Tel: +41 223793013; E-mail: michael.hothorn@unige.ch

\*\*Corresponding author. Tel: +41 216924251; E-mail: christian.hardtke@unil.ch

<sup>†</sup>These authors contributed equally to this work

remains unclear to what degree SERKs could be involved in the perception of CLE peptides.

For CLV1, different types of potential, context-dependent co-receptors have been described. In one scenario, CLV3 is perceived in association with CLV2, a receptor-like protein (RLP) that is comprised of extracellular LRRs and a transmembrane domain but lacks a kinase domain [12,34]. CLV2 in turn dimerizes with CORYNE (CRN), which consists of a transmembrane domain and an intracellular pseudo-kinase domain [35,36]. Other findings point to a CLV1-independent role of CLV2-CRN in CLV3 perception, possibly in conjunction with the CLV1-related LRR-RKs BAM1 and BAM2 [35,37,38]. Moreover, it was found that CLV2-CRN is required for the perception of many if not all root-active CLE peptides [11,35,39,40]. Finally, CLV1 has been implicated in stem cell homeostasis in the root meristem, where it presumably perceives CLE40 together with the non-LRR-RK ARABIDOPSIS CRINKLY 4 (ACR4) [41,42]. Likewise, BAM1 and RECEPTOR-LIKE PROTEIN KINASE 2 are also thought to play a role in CLE perception in the root [43]. In this study, we show that BAM3 is a *bona fide* CLE45 receptor, which appears to operate independent of SERK proteins. Moreover, we demonstrate that phloem-specific CRN expression is not only required for perception of CLE45, but of all root-active CLE peptides tested in this study, possibly by stabilizing expression of their receptors.

## Results

### BAM3 is a CLE45 receptor

Originally, we isolated *bam3* as a second-site suppressor of loss of function in *BREVIS RADIX* (*BRX*), which encodes a positive regulator of root protophloem sieve element differentiation, suggesting that *BRX* antagonizes the CLE45-BAM3 pathway [9,19]. Root protophloem differentiation (and thereby root growth) of *bam3* loss-of-function mutants is not impaired by exogenously applied CLE45 levels that suppress this process in wild-type plants, suggesting that BAM3 could act as a CLE45 receptor [9]. Subsequent results strengthened this notion [19,44] and also ruled out proposed alternative CLE45 receptors in the root [18]. However, direct evidence for CLE45-BAM3 interaction is still missing. We isolated additional CLE45-insensitive *bam3* loss-of-function alleles from our genetic screen [9] (Fig EV1A), including non-synonymous mutations leading to amino acid changes in the ligand-binding LRR and the cytoplasmic kinase domains (Fig 1A). Mutation of threonine 150 to isoleucine presumably interferes with proper folding of the BAM3 LRR domain, as does mutation of glycine 364 to arginine. Serine 303, however, maps to the inner face of the BAM3 LRR domain and is located in a surface region, which forms the peptide binding sites in the structurally related IDA receptor HAESA [30] and in the CLE41/44 receptor PXY [25] (Fig 1A and B). Two missense mutations in the BAM3 kinase domain (P883S, G901E) map to the core of the kinase C-lobe and may interfere with the proper folding or activity of the BAM3 kinase module. Together, our genetic analysis suggests that both the extracellular and cytoplasmic portions of BAM3 are important for the function of the receptor.

We produced the BAM3 LRR domain by secreted expression in insect cells and tested if the purified ectodomain interacts with a synthetic CLE45 peptide in isothermal titration calorimetry (ITC)

assays. We found that BAM3 bound CLE45 with a  $K_d$  of ~120 nM and with 1:1 stoichiometry (Fig 1C). The binding affinity for CLE45 to BAM3 was about 10-fold lower than CLE41/44 binding to the LRR ectodomain of PXY (Fig EV1B) [25]. BAM3 showed specific CLE45 binding, as the sequence-related CLV3 peptide, which is not expressed in the root [40], bound with much lower affinity ( $K_d$  ~10  $\mu$ M) (Fig EV1C). Importantly, N-terminal extension of CLE45 or CLV3 by a tyrosine residue (initially used to quantify the peptide concentrations) rendered the engineered peptides non-bioactive and drastically reduced binding to the BAM3 ectodomain (Fig EV1D-F). Prompted by our recent finding that the peptide hormone IDA is structurally related to CLE peptides, we created a BAM3 homology model based on the HAESA-IDA complex structure [30] to predict the CLE45 binding surface in BAM3 (Fig 1B). In our homology model, BAM3 residues Q226, Y228, and Y231 from the LRR domain form a part of the CLE45 binding surface. Consistently, binding of CLE45 to a purified BAM3 ectodomain in which Q226, Y228, and Y231 were mutated to alanines (BAM3<sup>QYY</sup>) was ~8 times weaker when compared to the wild-type LRR domain (Fig 1C).

To test the relevance of these mutations *in planta*, we re-created them in a full-length *BAM3* coding sequence to express the mutant protein as a CITRINE fusion (BAM3::BAM3<sup>QYY</sup>-CITRINE). First, we checked the subcellular localization of BAM3<sup>QYY</sup>-CITRINE and wild-type BAM3-CITRINE (BAM3::BAM3-CITRINE) in transient transformation of tobacco (*Nicotiana benthamiana*) leaf cells. In this system, both fusion proteins showed similar plasma membrane localization as well as some internal, likely endoplasmic reticulum signals (Fig EV2A). In *Arabidopsis*, BAM3<sup>QYY</sup>-CITRINE was specifically expressed in the protophloem, with a similar profile of subcellular (plasma membrane and internal) localization and abundance as wild-type BAM3-CITRINE (Figs 1D and EV2B). However, unlike BAM3-CITRINE, BAM3<sup>QYY</sup>-CITRINE was neither able to restore the *brx* phenotype when introduced into a *bam3 brx* double mutant (Fig 1E and F), nor able to restore CLE45 sensitivity when introduced into a *bam3* single mutant (Fig 1G and H). In summary, these data reinforce the view that BAM3 is the genuine CLE45 receptor in the context of the root protophloem [18].

### Individual SERKs are not necessary to perceive root-active CLE peptides

SERK proteins have recently been shown to act as co-receptors for the CLE41/44 receptor PXY [25,45] and for many other LRR-RKs [46]. In the case of the peptide receptor HAESA, complex formation with SERK1 allows for the specific and high-affinity sensing of IDA, and HAESA and SERK1 form stable, IDA-dependent heteromeric complexes *in vitro* [30]. To test whether SERK proteins could be involved in the sensing of other CLE peptides in the root, we surveyed the response of *serk* mutants to 14 root-active CLE peptides (CLV3, CLE8, CLE9/10, CLE11, CLE13, CLE14, CLE16, CLE18, CLE20, CLE21, CLE25, CLE26, CLE40, CLE45), which were selected for their significant, reproducible impact on root growth at 50 nM concentration. In general, the response of representative *serk* loss-of-function mutants (alleles *serk1-3*, *serk2-1*, *serk3-1*, *serk4-1*, and *serk5-1*) was largely similar to wild type (Fig 2A). Interestingly, another *serk1* allele, *serk1-1*, showed resistance to CLE45 application and was as insensitive as *bam3* (Fig EV2C). However, CLE45 resistance and the *serk1-1* mutation segregated freely in outcrosses

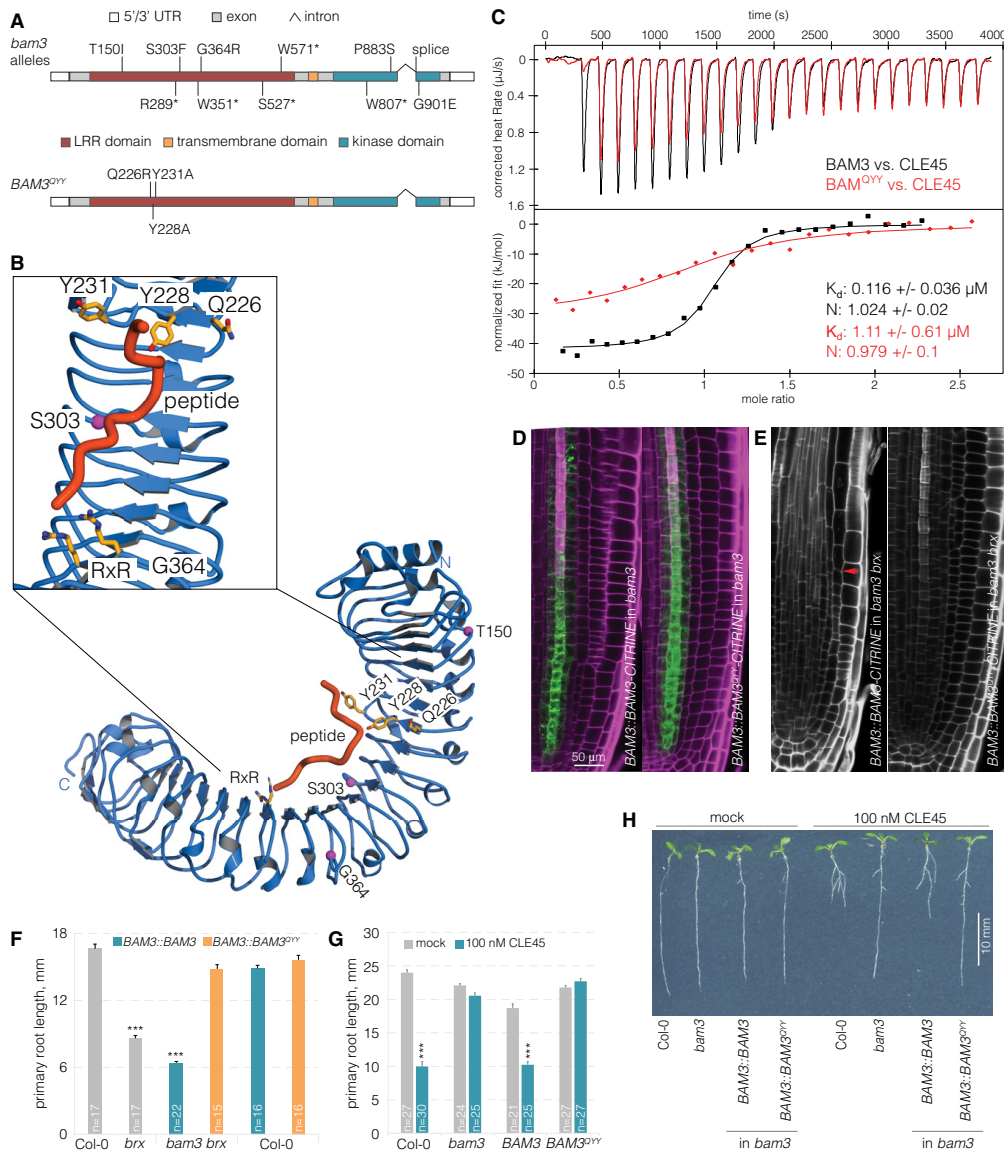


Figure 1.

to a *brx* mutant (i.e., only six out of 24 genotyped plants that were CLE45-resistant were also homozygous for *serk1-1*), suggesting that the CLE45 resistance resulted from an unlinked background mutation. Whole-genome sequencing of the *serk1-1* plants revealed a homozygous 28-bp deletion in *BAM3*, which would lead to a

frameshift after amino acid 699 and a premature stop codon six amino acids later, thereby deleting the kinase domain. Moreover, introduction of a transgenic *BAM3* copy restored CLE45 sensitivity of *serk1-1* (Fig EV2C). No complementation was observed with *SERK1* constructs that were reported to rescue the *serk1-1 serk2-1*

**Figure 1. BAM3 is a CLE45 receptor.**

- A Schematic overview of the *BAM3* gene structure. *bam3* loss-of-function mutations that were isolated as second-site suppressors of *brx* loss of function (top); amino acid point mutations predicted to disrupt BAM3-CLE45 interaction (bottom).
- B Ribbon diagram of a homology model of the BAM3 LRR ectodomain (in blue) based on the HAESA ectodomain (PDB-ID 5IXO). Magenta spheres indicate the position of genetic BAM3 missense mutations, and residues forming part of the predicted CLE45 binding site are shown in bonds representation (in yellow). The position of CLE45 has been inferred from an IDA-HAESA complex (PDB-ID 5IXQ).
- C Isothermal titration calorimetry (ITC) of purified BAM3 wild-type (black) or mutant BAM3<sup>QYY</sup> (red) extracellular domains vs. CLE45 peptide. N: stoichiometry,  $K_d$  dissociation constant. Shown are experimental values  $\pm$  fitting errors (95% confidence interval).
- D Expression of BAM3-CITRINE wild-type or mutant BAM3<sup>QYY</sup> fusion protein (green fluorescence) under control of the native *BAM3* promoter in root meristems of *bam3* mutants (magenta fluorescence: calcofluor white cell wall staining) (confocal microscopy).
- E Primary root meristems of *bam3 brx* double mutants carrying the indicated transgenes. Red arrow on the left panel indicates the approximate position of the final dividing cortex cell, which is out of range in the right panel.
- F Primary root length of 5-day-old seedlings of the indicated genotypes.
- G Primary root length of 7-day-old seedlings of the indicated genotypes in mock or CLE45 condition.
- H Representative 7-day-old seedlings of the indicated genotypes grown on standard mock or CLE45-containing media.
- Data information: Differences as compared to Col-0 (F) or mock (G) are not statistically significant unless indicated (Student's t-test); \*\*\* $P < 0.001$ ; mean  $\pm$  s.e.m.

double-mutant shoot phenotype [47] (Fig EV2D). Therefore, the *serk1-1* line should be considered a *bam3 serk1* double mutant.

#### SERK1 and SERK3 do not act as co-receptors in BAM3-mediated CLE45 signaling

In summary, none of the five *serk* mutants displayed CLE45 resistance. A signaling function of *SERK* genes in CLE45 perception might be masked by genetic redundancy, and therefore, the notion that SERK1 could be a BAM3 co-receptor still appeared attractive, especially given recently reported evidence that SERK1 cannot only interact with HAESA, but also with PXY, in a ligand-dependent manner [25,30]. However, although the BAM3 and SERK1 kinase domains were able to transphosphorylate each other in an *in vitro* kinase assay (Fig EV2E), neither SERK1 nor SERK3 formed CLE45-dependent complexes with BAM3 *in vitro* (Figs 2B and EV2F). In contrast, SERK1 formed CLE41/44-dependent heterodimers with PXY (Fig EV2G), corroborating earlier results [25,45]. Consistent with our gel filtration experiments, we could not detect binding of the SERK1-LRR domain to BAM3 in the presence of CLE45 in quantitative ITC assays (Fig 2C), while SERK1 bound to HAESA in the presence of IDA with low nanomolar affinity [30]. Finally, although *SERK1* has been reported to be expressed throughout the stele [48,49], closer inspection of a transgene driving expression of a SERK1-CITRINE fusion protein under control of the *SERK1* promoter (*SERK1::SERK1-CITRINE*) suggested that *SERK1* is not expressed in developing protophloem sieve elements (Fig EV2H). In summary, the results suggest that SERK1 (and based on our biochemical studies also SERK3) is not a co-receptor for BAM3-mediated CLE45 signaling.

#### CLV2 and CRN are necessary for full perception of root-active CLE peptides

Since our experiments did not support a role for SERK proteins in BAM3 receptor activation and CLE45 signal transduction, we assessed the relative contribution of other known CLV/BAM signaling components, CLV2 and CRN [11,35,37,39,50]. Both *CLV2* and *CRN* are expressed throughout most root tissues including the vascular cylinder [51]. We corroborated these findings by creating transgenic lines in which CITRINE fusions of CLV2 or CRN were

expressed under control of their native promoters (*CLV2::CLV2-CITRINE* and *CRN::CRN-CITRINE*). *CLV2::CLV2-CITRINE* displayed expression mostly in the stele (Fig EV3A), and *CRN::CRN-CITRINE* was expressed in the same domain (Fig EV3B). However, while *CLV2* appeared to be evenly expressed throughout the vascular cylinder of the root tip, *CRN* was apparently enriched in the phloem poles. To investigate *CRN* mutation in the same background as all other lines used in this study, we obtained a *crn* loss-of-function mutant in the Col-0 accession. In this CRISPR/Cas9-generated *crn* allele, a single nucleotide insertion in front of the 7<sup>th</sup> codon leads to a frameshift and three subsequent premature stop codons after amino acid 10 [52]. This *crn* mutant displayed complete insensitivity to CLE45 concentrations that strongly suppress protophloem differentiation and thus root growth in wild type (Fig 2A). A survey of other root-active CLE peptides revealed that this *crn* loss of function also conferred strong resistance to all of them (Fig 2A), corroborating the results for other *crn* alleles in different parental backgrounds [11]. As expected, we obtained very similar results when analyzing *clv2* loss-of-function mutants (Fig 2A). The *CLV2::CLV2-CITRINE* and *CRN::CRN-CITRINE* constructs complemented the respective mutants, indicating their functionality (Fig EV3C and D). Taken together, our experiments confirm that *CLV2* and *CRN* are necessary to mediate full sensitivity to all root-active CLE peptides monitored in this study.

#### The phloem is a crucial site of action for root-active CLE peptides

To test whether the CLE45 resistance of *crn* mutants reflects *CRN* activity in the developing protophloem, we expressed a transgenic *CRN-CITRINE* fusion under control of the *BAM3* promoter in *crn* mutants (Fig 3A–C). Interestingly, in these lines, we not only observed restored sensitivity to CLE45 (Fig 3D), but also to the similarly acting CLE26 [44] as well as other strongly root-active CLE peptides (Fig 3E). To monitor the CLE peptide effects in more detail, we transiently treated transgenic lines that expressed a nuclear localized fluorescent marker under control of the *COTYLEDON VASCULAR PATTERN 2* (*CVP2*) promoter (*CVP2::NLS-VENUS*) in wild-type background. *CVP2* is very specifically expressed in the developing sieve elements of the root meristem and is also a specific marker for their differentiation process [44]. Investigation of *CVP2::NLS-VENUS* seedlings after 24-h CLE peptide treatment indicated

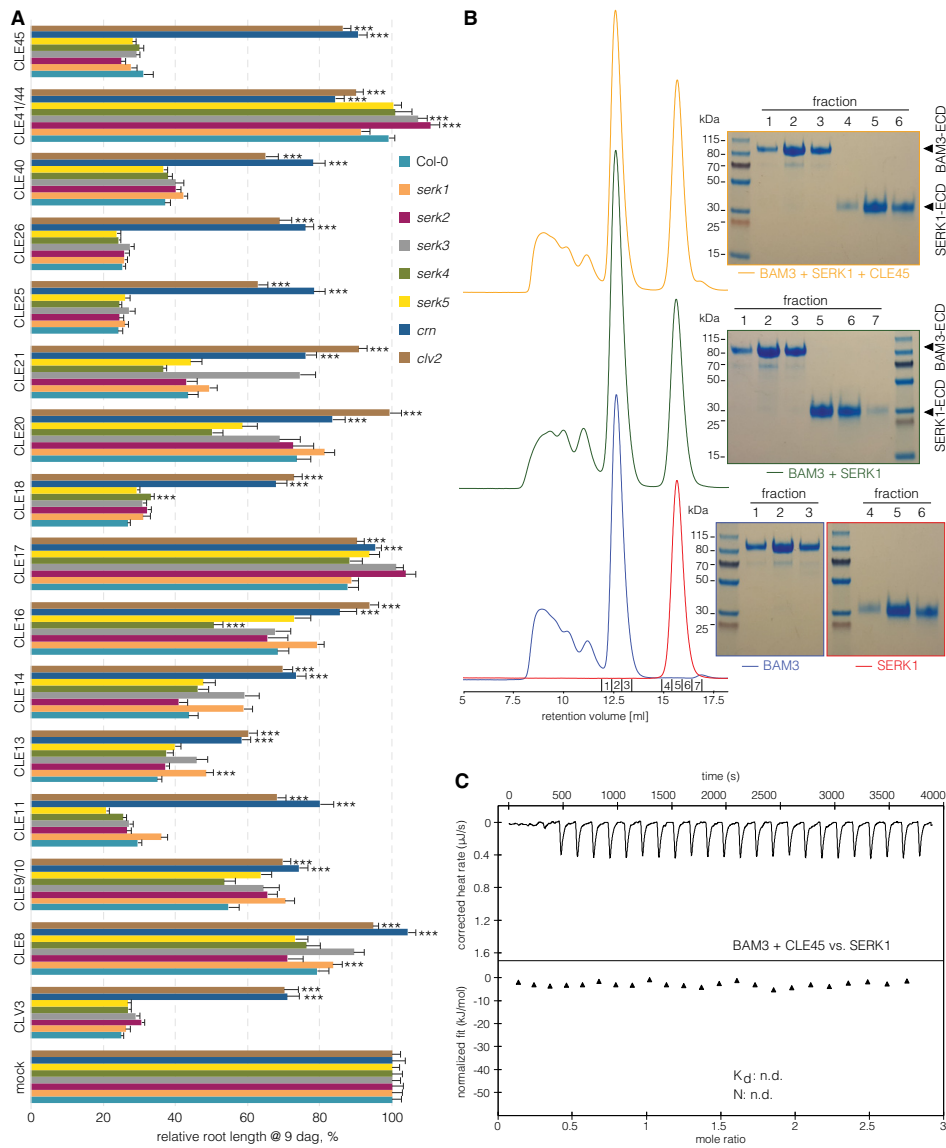


**Figure 2. Root growth CLE peptide resistance of mutants in potential co-receptors of CLE signaling pathways.**

**A** Primary root length of 9-day-old seedlings of indicated genotypes, grown on mock or 50 nM CLE peptide. Fourteen root-active peptides and two controls (CLE17 and CLE41/44) are shown.  $n \geq 12$  per column.

**B** Analytical size-exclusion chromatography. The BAM3 and SERK1 LRR domains elute as monomers when run stand-alone (blue and red traces), in combination (green trace), and in the presence of CLE45 (yellow trace). SDS-PAGE gels of the corresponding peak fractions are shown alongside.

**C** ITC of the purified BAM3 extracellular domain in the presence of CLE45 peptide titrated against the purified SERK1 extracellular domain. n.d.: not detectable.

Data information: Differences as compared to Col-0 (A) are not statistically significant unless indicated (Student's *t*-test); \*\*\* $P < 0.001$ ; mean  $\pm$  s.e.m.

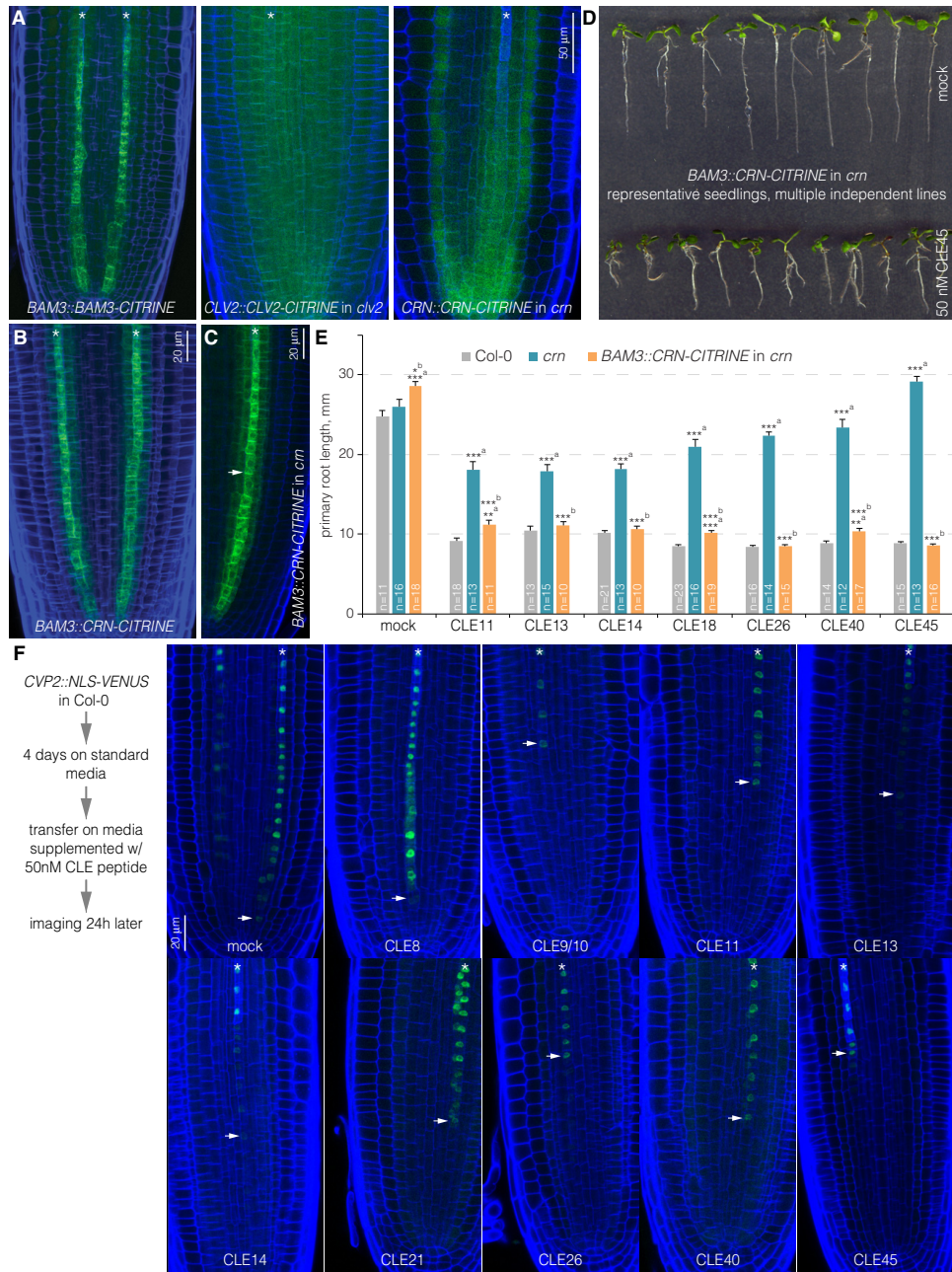


Figure 3.

**Figure 3. Protophloem-specific CRN action in the root meristem.**

- A Expression pattern of BAM3, CLV2, and CRN-CITRINE fusion proteins (green fluorescence) under control of their native promoters (blue fluorescence: calcofluor white cell wall staining) (confocal microscopy). Asterisks mark developing protophloem sieve element strands.
- B, C Expression pattern of CRN-CITRINE fusion protein under control of the *BAM3* promoter in Col-0 (B) or *crn* (C) background. Arrowhead in (C) highlights plasma membrane-localized CRN.
- D Representative 7-day-old *crn* seedlings expressing CRN-CITRINE fusion protein under control of the *BAM3* promoter grown on mock or CLE45.
- E Primary root length of 7-day-old seedlings of indicated genotypes, grown on mock or 50 nM of selected CLE peptides. Differences as compared to <sup>0</sup>: Col-0 or <sup>1</sup>: *crn* are not statistically significant unless indicated (Student's t-test); \**P* < 0.05; \*\**P* < 0.01; \*\*\**P* < 0.001; mean ± s.e.m.
- F Expression of nuclear localized, fluorescent VENUS protein under control of the *CVP2* promoter (which specifically marks developing protophloem sieve elements), 24 h after transfer from standard media to 50 nM of selected CLE peptides. Arrowheads indicate the cells closest to the tip in which *CVP2* expression was still detectable.

that indeed in practically all cases, protophloem development was perturbed to a large degree after CLE application (Fig 3F). While in some cases, a strong, immediate and specific suppression of protophloem differentiation was observed, in others the sieve element marker faded more gradually. However, in all cases, *CVP2* expression eventually disappeared toward the root tip. Together with the rescue of CLE peptide resistance through protophloem-specific *CRN* expression, these observations indicate that the developing phloem is a crucial site of action for root-active CLE peptides, even if some of them are not genuinely expressed in the root meristem and/or vasculature [53,54].

#### CRN promotes CLE45 sensitivity by enhancing BAM3 expression

To test whether CLV2-CRN might interact with BAM3, we next investigated these proteins in the cellular setting of the transient tobacco expression system. While BAM3 was mostly plasma membrane-localized (Fig EV4A), when expressed alone, CLV2 and CRN fusion proteins were mostly found inside cells and co-localized substantially with an endoplasmic reticulum marker (Figs 4A and B, and EV4B–D), in line with earlier findings [48,55]. Some plasma membrane localization could be observed at variable degrees in replicate experiments, which might be due to endogenous CLV2/CRN proteins, because as previously reported [55], co-expression of CLV2 and CRN resulted in increased delivery of both fusion proteins to the plasma membrane (Figs 4C and D, and EV4E and F). We confirmed these findings in the root vasculature of stable transgenic lines, by introducing the *BAM3::CRN-CITRINE* construct into the *clv2* mutant. While in wild type or the *crn* background CRN-CITRINE displayed substantial plasma membrane localization, it did not accumulate at the plasma membrane to the same extent in *clv2* mutants (Figs 4E and F, and EV3E). Conversely, CLV2-CITRINE fusion protein expressed under control of the *CLV2* promoter displayed some clear plasma membrane localization when expressed in the *clv2* mutant background, but mostly diffusive cytoplasmic localization when expressed in the *crn* mutant (Fig EV3F). Thus, as previously reported for the shoot, plasma membrane localization of CLV2 and CRN is largely interdependent in the root.

We next tested whether CLV2-CRN could interact with BAM3. We could not obtain the CLV2 ectodomain in sufficient quantity and quality for *in vitro* biochemical assays. In bimolecular fluorescence complementation (BiFC) experiments, we could not observe interaction of BAM3 with CRN, with the caveat that in this assay, CRN was supposedly not efficiently delivered to the plasma membrane. Also, in transient co-expression in tobacco, no co-localization was observed for CRN and BAM3 fusion proteins (Figs 4G and EV4G).

However, substantial co-localization occurred once a (non-fluorescent) HA-tagged CLV2 protein was co-expressed in addition (Figs 4H and EV4H and I). Co-localization of the three proteins was also observed when BiFC was performed for CLV2 and CRN in the presence of a fluorescent mTFPI-tagged BAM3 (Fig 4I). Moreover, a modest but robust BiFC interaction between BAM3 and CRN could be observed when (non-fluorescent) CLV2-HA was co-expressed as well (Fig 4J), as compared to a negative control (Fig 4K). Control experiments with BRI1 did not show such interaction (Fig 4L and M). Thus, it appears that in principle, BAM3 is capable of interaction with the CLV2-CRN dimer in a cellular setting. Such interaction could actually occur *in planta*, since both BAM3 and CRN displayed plasma membrane localization in developing sieve elements, which appeared to be mostly shootward for BAM3 (Fig 4N and O).

Despite the possibility for BAM3-CLV2/CRN interaction, it appears unlikely that CLV2-CRN acts in a capacity of co-receptor in CLE45 perception, since CRN is a pseudokinase [36]. To further investigate the role of CRN in CLE45 signaling, we thus conducted additional genetic experiments. Second-site loss of function in BAM3 or in its downstream signaling component MEMBRANE-ASSOCIATED KINASE REGULATOR 5 (MAKR5) suppresses *brx* mutant phenotypes [9,18]. Similarly, *clv2* or *crn* second-site mutation substantially rescued the protophloem differentiation, root meristem size and root growth defects of *brx* mutants (Fig 5A and B). The phenotype of *brx crn* double mutants qualified *crn* as a strong but partial *brx* suppressor, with overall rescue roughly comparable to *brx makr5* double mutants [18], but less penetrant than in *bam3 brx* double mutants [9]. Thus, *crn* loss of function dampens CLE45 signaling in the *brx* background, where the CLE45-BAM3 pathway is apparently hyperactive [9,18]. Another feature of CLE45 perception is the accumulation of MAKR5-GFP fusion protein in developing protophloem sieve elements upon CLE45 treatment [18]. This response, which appears to be triggered by post-translational events since it still takes place in the presence of cycloheximide (Fig 5C), is abolished in *bam3* mutants and was likewise undetectable in *crn* mutants (Fig 5D). Therefore, CRN is required for CLE45 signaling as judged by all established criteria. To investigate whether *crn* loss of function can affect the expression or subcellular localization of BAM3, we introduced the *BAM3::BAM3-CITRINE* construct into the *crn* mutant background. Indeed, we observed substantially reduced overall BAM3-CITRINE abundance in the *crn* mutant, especially at later stages of protophloem development (Fig 5E and F). Since BAM3 gene expression was not affected in *crn* root tips (Fig 5G), this apparently reflected post-translational regulation. We verified this observation by crossing individual *BAM3::BAM3-CITRINE* lines in *crn* background with a *crn*

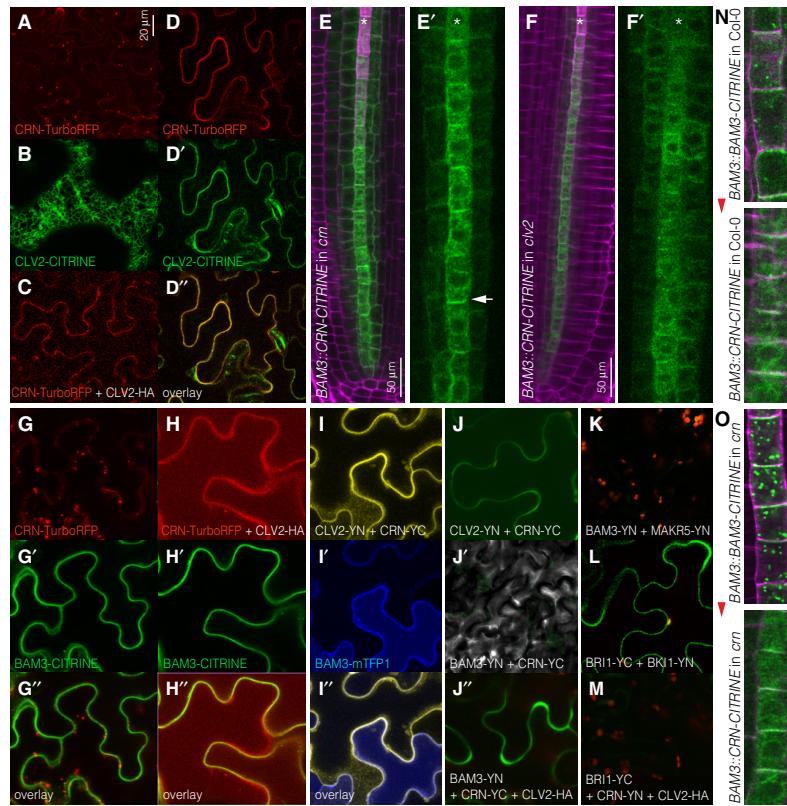


**Figure 4. Co-localizations and interactions of BAM3, CRN, and CLV2.**

- A Transient expression of CRN-TurboRFP fusion protein (red fluorescence) in tobacco (*Nicotiana benthamiana*) leaf epidermal cells, under control of a constitutive promoter (confocal microscopy).
- B Transient expression of CLV2-CITRINE fusion protein (green fluorescence) in tobacco leaf epidermal cells.
- C Transient co-expression of CRN-TurboRFP fusion protein and (non-fluorescent) CLV2-HA fusion protein in tobacco leaf epidermal cells.
- D Transient co-expression of CRN-TurboRFP and CLV2-CITRINE fusion proteins in tobacco leaf epidermal cells. Red fluorescent and green fluorescent channels are shown separately and in overlay.
- E, F Expression pattern of CRN-CITRINE fusion protein (green fluorescence) under control of the *BAM3* promoter in *crn* (E) or *clv2* mutant (F), with corresponding close-ups (magenta fluorescence: calcofluor white cell wall staining). Asterisks mark developing protophloem sieve element strands. Arrowhead in (E) highlights plasma membrane-localized CRN-CITRINE.
- G Transient co-expression of CRN-TurboRFP and BAM3-CITRINE fusion proteins in tobacco leaf epidermal cells. Red fluorescent and green fluorescent channels are shown separately and in overlay.
- H Transient co-expression of CRN-TurboRFP, BAM3-CITRINE, and (non-fluorescent) CLV2-HA fusion proteins in tobacco leaf epidermal cells. Red fluorescent and green fluorescent channels are shown separately and in overlay.
- I Bimolecular fluorescence complementation (BiFC) between transiently co-expressed CLV2 and CRN proteins fused to one half each of YFP (yellow fluorescence) in the presence of co-expressed BAM3-mTFP1 fusion protein (blue fluorescence). Yellow fluorescent and blue fluorescent channels are shown separately and in overlay.
- J BiFC between transiently co-expressed BAM3 and CRN proteins fused to one half each of YFP (green fluorescence) in the presence of co-expressed (non-fluorescent) CLV2-HA fusion protein in tobacco leaf epidermal cells (J'). Parallel control experiments for BiFC between CLV2 and CRN (J) and BAM3 and CRN (J') are shown.
- K BiFC between transiently co-expressed BAM3 and MAKRS5 proteins fused to one half each of YFP (red: chloroplast autofluorescence).
- L BiFC between transiently co-expressed BRI1 and BKI1 proteins fused to one half each of YFP (green fluorescence).
- M BiFC between transiently co-expressed BRI1 and CRN proteins fused to one half each of YFP in the presence of co-expressed (non-fluorescent) CLV2-HA fusion protein in tobacco leaf epidermal cells (red: chloroplast autofluorescence).
- N, O Expression of BAM3-CITRINE or CRN-CITRINE fusion proteins (green fluorescence) under control of the *BAM3* promoter in the developing sieve element cells close to the stem cells in Col-0 (N) or *crn* (O) background (magenta fluorescence: calcofluor white cell wall staining). Red arrowhead indicates rootward direction.

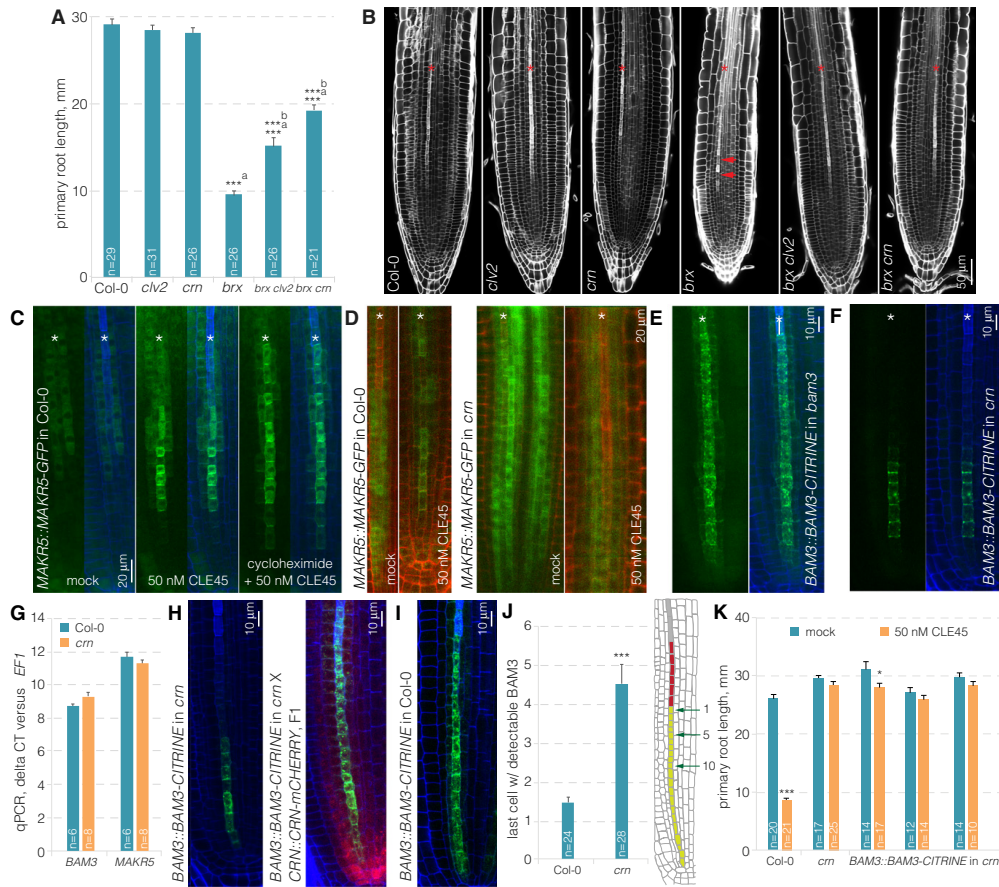


**Figure 5. Genetic interactions between CRN, BRX, and MAKRS.**

**A** Primary root length of 9-day-old seedlings of indicated genotypes.  
**B** Root meristems of indicated genotypes (white fluorescence: calcofluor white cell wall staining) (confocal microscopy). Red arrowheads indicate the "gap" cells in *brx*.  
**C** MAKRS-GFP fusion protein (green fluorescence) expressed under control of the native *MAKR5* promoter in response to CLE45 application in the presence or absence of cycloheximide (blue fluorescence: calcofluor white cell wall staining). Green channel is shown separately (left) and in overlay with blue channel (right).  
**D** Response of MAKRS-GFP fusion protein to CLE45 application in *crn* mutant background as compared to Col-0 control (red fluorescence: propidium iodide cell wall staining).  
**E, F** Expression of BAM3-CITRINE fusion protein under control of the *BAM3* promoter in developing protophloem of *bam3* (E) or *crn* (F).  
**G** qPCR of *BAM3* expression in Col-0 or *crn* root tips, with *MAKR5* as control, relative to the *EF1* housekeeping gene, representing the average for 2–3 technical replicates of three biological replicates, mean  $\pm$  s.e.m. Differences were not statistically significant between Col-0 and *crn* (Student's *t*-test;  $P = 0.096$  for *BAM3*,  $P = 0.273$  for *MAKR5*).  
**H** Expression of BAM3-CITRINE fusion protein (green fluorescence) under control of the *BAM3* promoter in developing protophloem of *crn* (left panel) and in an F1 plant derived from a cross of the same line to a *crn* mutant complemented by a *CRN::CRN-mCHERRY* (red fluorescence) transgene (right panel).  
**I** Expression of BAM3-CITRINE fusion protein (green fluorescence) in Col-0, as a parallel control for panel (J).  
**J** Quantification of the last proliferating protophloem cell (light green cells in the root schematic) with detectable BAM3-CITRINE signal, with respect to the beginning of the protophloem transition zone (red cells).  
**K** Primary root length of 7-day-old seedlings of indicated genotypes on mock or CLE45 media, and several independent transgenic lines are shown.  
 Data information: Differences as compared to <sup>a</sup> Col-0 or <sup>b</sup> *brx* (A), mock (M), are not statistically significant unless indicated (Student's *t*-test); \* $P < 0.05$ ; \*\*\* $P < 0.001$ ; mean  $\pm$  s.e.m. Asterisks in (B–F) mark developing protophloem sieve element strands.

line that was complemented by a *CRN::CRN-mCHERRY* construct. In corresponding F1 plants that thus carried both hemizygous *BAM3::BAM3-CITRINE* and *CRN::CRN-mCHERRY* transgenes in homozygous *crn* background, *BAM3-CITRINE* expression was restored to its wild-type levels (Fig 5H and I). This included expression throughout the developing sieve element cell file, which was one feature that could be easily quantified. While *BAM3-CITRINE* signal could practically always be observed up to the last cell before the protophloem transition zone in wild type, the signal was already completely absent in *crn* roots much earlier (Fig 5J). Finally, because increase in *BAM3* dosage through *BAM3::BAM3-CITRINE* could not overcome the CLE45 resistance of *crn* (Fig 5K), it appears that CRN is essential for CLE45 perception because it is required for efficient *BAM3* protein expression and its maintenance during sieve element development.

## Discussion

Plant LRR-RKs are central signaling hubs that can sense diverse ligands to control various facets of the plant life cycle, from plant-pathogen interactions to intrinsic developmental processes. Many of the currently known LRR-RKs require shape-complementary co-receptor kinases for receptor activation [46]. For instance, LRR-RKs of the SERK family can serve as co-receptors for BRI1 in brassinosteroid sensing [29], for FLAGELLIN INSENSITIVE 2 in innate immunity [56,57], for ERRECTA and related RKs in stomata development [58], and for HAESA in abscission [30]. More recently, SERKs have also been implicated in CLE peptide sensing, as co-receptors of PXY as well as PXY-LIKE LRR-RKs [25,45]. In the case of the LRR-RK HAESA, the presence of SERK1 strongly increases the binding affinity for the IDA peptide (a ~60-fold increase from 20  $\mu$ M to 350 nM) [30]. Consequently, while there is no detectable binding of the SERK1 ectodomain to HAESA in the absence of ligand, IDA-bound HAESA senses SERK1 with 75 nM affinity [30]. Structural comparison of the HAESA-IDA-SERK1 ternary complex with a CLE receptor complex containing PXY-CLE41/44-SERK2 revealed that both complexes are highly similar (root-mean-square deviation, r.m.s.d., is 2.3 Å comparing 782 C<sub>α</sub> atoms) (Fig EV5A and B). However, in contrast to HAESA, the isolated PXY ectodomain binds CLE41/44 with nanomolar (10–30 nM), not micromolar, affinity (Fig EV1B) [25]. Interestingly, the SERK1 ectodomain binds relatively weakly to CLE41/44-bound PXY, suggesting that, despite their structural similarities, the activation mechanisms for HAESA and PXY may differ [30,45].

Our system-wide analysis of root-active CLE peptides in *Arabidopsis* suggests that only few CLE-sensing complexes may critically involve SERK co-receptor kinases or that CLE resistance phenotypes in *serk* mutants are caused by secondary effects. However, in our study, we did not investigate genetic redundancy between *SERK* genes. It appears possible that an array of higher order *serk* mutants will uncover fully redundant, overlapping roles of *SERKs* in CLE peptide sensing. Such analyses are substantially complicated by the dwarf and short root phenotypes of higher order *serk* mutants, however [59]. Moreover, despite their overall high sequence similarity, SERK proteins have diversified sufficiently to adopt potentially separate signaling roles [60]. Thus, their potential genetic requirement in CLE perception might be determined by a

combination of differential expression patterns and levels as well as protein structure variation.

Importantly, we could not find biochemical, genetic, or cell biological evidence that would support a role for SERKs in *BAM3*-mediated CLE45 sensing and signaling. While we could demonstrate CLE45 binding by *BAM3* *in vitro* and observe matching *in planta* evidence, SERK1 or SERK3 did neither form CLE45-dependent or CLE45-independent complexes with *BAM3*, nor did *serk* mutants display CLE45-resistant phenotypes. Moreover, our finding that the *serk1-1* allele carries a *bam3* background mutation that confers CLE45 resistance emphasizes that full-scale analysis of *serk* mutant redundancy could only be considered reliable in conjunction with transgenic rescue. Reported phenotypes for *serk* multiple mutants that involve the *serk1-1* allele should thus be carefully considered in light of CLE45 resistance, especially with respect to vascular phenotypes [45]. Indeed, it appears possible that *BAM3* also has a role in secondary growth [61].

Compared to *SERK* genes, the genetic requirement for *CLV2* and *CRN* in the full-scale sensing of all root-active CLE peptides that we investigated in this study was absolute. The results point to a generic rate-limiting role of *CLV2-CRN* in CLE receptor activity, for which multiple scenarios could be envisaged. In this respect, a classic role as co-receptor appears least likely, because *CRN* does not possess an active kinase domain and *CLV2* is very different in size and sequence from *SERK* proteins [36]. Nevertheless, *CLV2-CRN* might participate as a component in receptor complexes, for instance to stabilize them or to recruit downstream components. Such a role would not be mutually exclusive with another possibility, a role of *CLV2-CRN* in promoting the plasma membrane delivery of LRR-RKs, or in enhancing their plasma membrane localization indirectly, for instance through molecular crowding. Our observations of reduced *BAM3* abundance in *crn* mutants support the latter ideas, and it remains to be seen whether this will also apply to other, yet to be identified CLE peptide receptors in the root. So far, a conceptually similar role of *CRN* was not observed in the shoot [62]. However, such a function might be masked by the observed compensatory transcriptional cross-regulation between redundantly acting receptors [63], a scenario that apparently does not exist for *BAM3* in the root [9,18].

Our most surprising finding is the observation that *CRN* activity in the developing protophloem was sufficient to restore sensitivity to all root-active CLE peptides investigated in this study. This observation is consistent with the more or less penetrant effect of all of these peptides on protophloem differentiation, irrespective of additional effects on root development that could be observed for individual CLEs. Thus, the results reinforce the emerging notion of the protophloem as a limiting, systemic organizer of overall root meristem development [9,19,64]. What remains enigmatic, however, is why *crn* mutants do not display an apparent morphological root phenotype if none of the root-efficient CLE peptides can be sensed properly? One possibility is that observations obtained from external CLE application might at least in part be misleading with regard to the genuine role of those peptides. Yet the *CLV2/CRN* module could function in certain conditions that upregulate CLE peptide levels and thereby might be crucial for root growth adaptation. Alternatively, it could also mean that most CLE peptide signaling is not essential for root development, at least in tissue culture conditions, or that compensatory, possibly non-peptide-mediated mechanisms

exist. It is important to note, however, that *crn* loss of function does not confer complete CLE peptide resistance, as exemplified by the strong, yet partial CLE45 resistance of *crn* as compared to *bam3*. Therefore, it appears possible that partially redundant CRN-related functions exist. Identification of additional genuine CLE peptide receptors in the root context might enable us to address this topic systematically in future studies.

In summary, we present a genetic framework for CLE peptide sensing in the *Arabidopsis* root that assigns distinct functions to various known receptor pathway components. Our data suggest that SERK proteins are involved in some, but not in the majority of the root CLE-sensing membrane signaling complexes, or alternatively act in a highly redundant manner. Instead, we provide evidence that CLV2 and CRN are part of root-active CLE peptide signaling pathways, possibly by controlling the expression, proper membrane localization, and/or stability of LRR-RK signaling complexes. Finally, our data suggest that the root protophloem is the crucial site of action of root-active CLE peptides. Nevertheless, they are apparently perceived by several distinct receptor complexes, many of which remain to be identified. The data presented in this study could serve as a resource to facilitate this task.

## Materials and Methods

Plant tissue culture, plant transformation, and common molecular biology procedures such as genomic DNA isolation, genotyping, sequencing, and peptide or inhibitor treatments were performed according to standard procedures as previously described [9,19,44,65].

### Sequence analysis of the *serk1-1* mutant

Whole-genome sequencing and data analysis of *serk1-1* mutants were performed as described [9]. The data and experimental details can be retrieved from the NCBI Short Read Archive at <https://www.ncbi.nlm.nih.gov/Traces/study/?acc=SRP104341> [accessions: STUDY: PRJNA383544 (SRP104341); SAMPLE: serk1-1 (SRS2134599); EXPERIMENT: A\_ (SRX2748469); RUN: serk1-1\_R1\_fused.fastq.gz (SRR5460456)].

### Plant materials, growth conditions, and physiological assays

All mutant and transgenic lines were in the *Arabidopsis* Columbia-0 (Col-0) background. The following previously described mutant alleles were used throughout: *brx-2*, *bam3-2*, *brx-2 bam3*, *clv2-1*, *serk1-1* and *serk1-3*, *serk2-1*, *serk3-1*, *serk4-1*, *serk5-1* [9,47,59,66–68]. The *crn* loss-of-function mutant allele (*crn-10*) carries a single nucleotide insertion in front of the 7<sup>th</sup> codon, which leads to a frameshift and three subsequent premature stop codons after amino acid 10 [52]. Observations with transgene constructs were confirmed in multiple independent transgenic lines.

### Transgenic constructs and lines

The *BAM3::BAM3-CITRINE*, *MAKR5::MAKR5-GFP*, and *CVP2::NLS-VENUS* constructs and transgenic lines have been described before [18,19,44]. The transgenic lines created for this study are summarized in Table EV1. All constructs used in this study were created

with the multi-site GATEWAY cloning system according to standard protocols (Invitrogen). The constructs are listed in Table EV2. Oligonucleotides used in cloning procedures or for genotyping are listed in Table EV3.

### qRT-PCR

For qRT-PCR (qPCR), RNA was prepared from root tips of 7-day-old Col-0 and *crn* seedlings, and *BAM3* and *MAKR5* expressions were quantified relative to the *EF1* housekeeping gene on an Applied Biosystems Quantstudio 3 instrument as previously described [9,18].

### Transient expression and BiFC assays

For transient expression experiments, we used the 4<sup>th</sup> to 6<sup>th</sup> leaves of *N. benthamiana* plants. Infiltrations, co-localization, and BiFC analyses were essentially performed as previously described [69].

### Confocal imaging

Confocal images were obtained with Zeiss 700 or Zeiss 780 inverted confocal microscopes. All dual-color images were acquired by sequential line switching, allowing the separation of channels by both excitation and emission.

### Root counter staining

In some experiments, we used calcofluor white instead of standard propidium iodide (PI) staining for visualizing cell walls. To this end, 4- to 6-day-old seedlings were fixed in 4% paraformaldehyde in PBS for 45 min. After washing with PBS, seedlings were cleared with ClearSee solution [70] overnight. After incubation in 0.2% calcofluor white in ClearSee solution, seedlings were transferred to fresh ClearSee solution for 2–24 h before imaging.

### Peptides

Peptides were obtained at the 1–4 mg scale, > 75% pure (GenScript USA Inc.). The peptide sequences were as follows. CLV3: RTVPSGPDPLHH; CLE8: RRVPTGPNPLHH; CLE9/10: RLVPSGPNPLHN; CLE11: RVVPSGPNPLHH; CLE13: RLVPSGPNPLHH; CLE14: RLVPKGPNPLHN; CLE16: RLVHTGPNPLHN; CLE17: RVVHTGPNPLHN; CLE18: RQIPTGPDPLHN; CLE20: RRVKVTGSNPLHN; CLE21: RSIPTGPNPLHN; CLE25: RRVKPNGDPPIHN; CLE26: RRVKPRGDPPIHN; CLE40: RQVPTGSDPLHH; CLE41/44: HEVPSGPNPISN; CLE45: RRVRRGSDPIHN. N-terminally tyrosine-modified CLV3, CLE41/44, and CLE45 peptides were used as standards for quantification. Peptides for biochemical assays were synthesized by Peptide Specialty Laboratories, Heidelberg, Germany (see below).

### Protein homology modeling

Structural homologs of the BAM3 LRR (residues 30–651) and kinase (residues 699–903) domains were identified using the program HHpred [71], and homology modeling was done in Modeller [72] using the isolated LRR domain of HAESA (PDB-ID 5XIO) [30] and the kinase domain of BRI1 (PDB-ID 5LPB) [73] as templates.

### Protein expression and isolation of LRR-RLK ectodomains

The coding sequences for BAM3 (amino acids 30–651), PXY/TDR (30–647), SERK1 (24–213), and SERK3 (1–220) ectodomains were amplified out of *Arabidopsis* Col-0 cDNA using the PfuX7 polymerase (Norholm). The point mutations Q226A, Y228A, and Y231A for the BAM3<sup>QYY</sup>-ECD were introduced by site-directed mutagenesis. All DNA fragments were cloned into a modified pFastBac1 vector (Geneva Biotech), fusing BAM3-, PXY-, and SERK1-ECD coding sequences with an N-terminal azurocidin signal peptide. To all ectodomain sequences, a C-terminal StrepII-9xHIS tandem affinity purification tag was added, and all constructs were confirmed by sequencing. Bacmids were generated by transforming the plasmids into *Escherichia coli* DH10MultiBac (Geneva Biotech), isolated, transformed into *Spodoptera frugiperda* Sf9 with Profectin transfection reagent (AB Vector) followed by viral amplification. Secreted protein was expressed by infecting *Trichoplusia ni* Tnao38 cells or for PXY-ECD *S. frugiperda* Sf9 with a viral multiplicity of 1, and incubation for 3 days post-infection. Cells were separated by centrifugation at  $5,000 \times g$  for 30 min, and the supernatant was filtered through 0.45  $\mu$ m filters. The proteins were isolated from the medium by Ni<sup>2+</sup> (HisTrap excel; GE Healthcare) and subsequent StrepII (Strep-Tactin Superflow high capacity, IBA) affinity chromatography and further purified by size-exclusion chromatography (Superdex Increase 200) with 20 mM citrate pH 5 and 150 mM NaCl for BAM3 and SERK1/3 as buffer. For PXY and also one preparation of SERK1, the gel filtration was carried out with 10 mM Bis-Tris and 100 mM NaCl [45]. Molecular weights of all purified proteins were determined by MALDI-TOF mass spectroscopy (BAM3-ECD: 94,586 Da; PXY-ECD: 92,519 Da; SERK1-ECD: 27,551 Da; SERK3-ECD: 29,951 Da), and concentrations were measured via the absorption at 280 nm (corrected with the extinction coefficient for each protein).

### Gel filtration experiments

For each gel filtration experiment, 100  $\mu$ g of SERK1-ECD or SERK3-ECD and equimolar amounts of either BAM3-ECD or PXY-ECD as well as 25  $\mu$ M of CLE45 (RRVRRGSDPIHN), and 25  $\mu$ M CLE41/44 (HEV-Hyp-SG-Hyp-NPISN) were used in the combinations indicated in the figures, incubated for 10 min after mixing and then subjected to gel filtration on a Superdex Increase 200 equilibrated with 20 mM citrate pH 5 and 150 mM NaCl, except for the gel filtration with PXY + SERK1 + CLE41/44, for which the column was equilibrated in 10 mM Bis-Tris and 100 mM NaCl [45]. The concentration of peptides modified N-terminally with a tyrosine (Y-peptides) was determined by their absorbance at 280 nm (corrected by the extinction coefficient). The concentrations for the peptides without tyrosine modification were determined by a quantitative colorimetric peptide assay (Pierce) using the respective Y-peptides as standards. The elution of proteins from the gel filtration column was monitored by absorption at 280 nm. Fractions indicated in the figures were separated on Bis-Tris polyacrylamide gels.

### Isothermal titration calorimetry

Isothermal titration calorimetry assays were run on a Nano ITC (1 ml standard cell; 250  $\mu$ l syringe; TA Instruments) at 25°C in 20 mM sodium citrate pH 5 and 150 mM NaCl for all ITCs with

BAM3 and 10 mM Bis-Tris pH 6 and 100 mM NaCl for the ITC with PXY. CLE41/44 (HEVPSGPNPISN), CLE45 (RRVRRGSDPIHN), CLV3 (RTV-HYP-SG-HYP-DPLHHH), and Y-CLV3 (YRTV-HYP-SG-HYP-DPLHH) were dissolved in the respective ITC buffer (20 mM sodium citrate pH 5 and 150 mM NaCl for CLE45, Y-CLE45, CLV3, and Y-CLV3; 10 mM Bis-Tris pH 6 and 100 mM NaCl for CLE41/44), and the following concentrations were used in the assays: BAM3-ECD vs. CLE45: 10 and 80  $\mu$ M; BAM3-ECD vs. Y-CLE45: 9 and 154.5  $\mu$ M; BAM3<sup>QYY</sup> vs. CLE45: 8.6 and 80  $\mu$ M; BAM3-ECD vs. CLV3: 10 and 400  $\mu$ M; BAM3-ECD vs. Y-CLV3: 8.6 and 175  $\mu$ M; PXY-ECD vs. CLE41/44: 7.5 and 75  $\mu$ M; BAM3-ECD + CLE45 vs. SERK1-ECD: 8.2 + 25  $\mu$ M and 82  $\mu$ M, respectively. For each experiment, 10  $\mu$ l was repetitively injected into the cell in 150 s time intervals. The measured heat rates for the BAM3-ECD vs. CLE45, BAM3<sup>QYY</sup> vs. CLE45, BAM3-ECD vs. Y-CLE45, BAM3-ECD vs. CLV3, BAM3-ECD vs. Y-CLV3, and PXY-ECD vs. CLE41/44 were corrected by subtracting the heat rates measured for injecting CLE45, Y-CLE45, CLV3, Y-CLV3, or CLE41/44 into the ITC buffer, respectively. The data for the BAM3-ECD + CLE45 vs. SERK1-ECD measurement was corrected by subtracting heat rates acquired by injecting SERK1-ECD into a cell containing CLE45. Data analyses and modeling were carried out using the software supplied by the manufacturer (NanoAnalyze, version 3.5).

### Kinase domain protein expression and isolation as well as *in vitro* kinase assays

Kinase domain protein production and *in vitro* kinase assays were carried out as previously described [30]. In brief, the coding sequence for the cytosolic part of BAM3 (679–992; BAM3-KD) was amplified from *Arabidopsis* Col-0 cDNA. The DNA for the cytosolic region of SERK1 (264–625; SERK1-KD) was synthesized and codon-optimized for expression in *E. coli*. Both were inserted into an expression vector based on pET (Novagen) that gives rise to an N-terminal tag consisting of 8xHis-StrepII-Thioredoxin, which can be cleaved by a TEV-protease. Per site-directed mutagenesis point mutations were introduced into both coding sequences, resulting in inactive kinase domains for SERK1-KD (D447 to N; mSERK1-KD) and BAM3-KD (D854 to N; mBAM3-KD) [73]. All constructs were confirmed by sequencing and transformed into *E. coli* Rosetta 2 (Novagen). The bacteria were grown to an OD<sub>600</sub> = 0.6, and protein expression was induced by adding IPTG to a final concentration of 0.5 mM followed by incubation for 18 h at 16°C. Cells were harvested by centrifugation at  $5,000 \times g$  and 4°C for 15 min, resuspended in buffer A (20 mM Tris-HCl pH 8, 500 mM NaCl, 4 mM MgCl<sub>2</sub>, and 2 mM  $\beta$ -mercaptoethanol) to which 15 mM imidazole and 0.1% (v/v) Igepal were added, and lysed by sonication. The sample was then centrifuged at  $35,000 \times g$  and 4°C for 30 min, and the supernatant was used for a Co<sup>2+</sup> affinity purification. Co<sup>2+</sup> resin (His-Select Cobalt Affinity Gel, Sigma) was incubated with the cell lysate for 60 min at 4°C, subjected to a gravity flow column (Pierce), and washed twice with buffer A (+15 mM imidazole). Recombinant proteins were eluted in buffer A (+250 mM imidazole) and dialyzed in buffer B (20 mM Tris-HCl pH 8, 250 mM NaCl, 4 mM MgCl<sub>2</sub>, and 0.5 mM TCEP). To BAM3-KD and BAM3<sup>QYY</sup>-KD, TEV-protease was added before dialyses and then removed after dialyses by a second Co<sup>2+</sup> HIS-affinity purification (during this step, the cut tag was also removed). The proteins were then subjected to

gel filtration on a Superdex Increase 200 column using buffer B, collected, and concentrated in Amicon Ultra devices (10,000 MWCO cutoff).

To perform *in vitro* kinase assays, 1 µg of each kinase domain, in the combination indicated in the figure, was added in a total volume of 20 µl (buffer B). To start the reaction, 5 µCi of [ $\gamma$ - $^{32}$ P]-ATP (Perkin-Elmer) was added and the reaction was carried out for 45 min at room temperature before being terminated by the addition of 4 µl of 6× SDS-loading dye and immediate incubation at 95°C for 7 min. SDS-PAGE in 4–15% gradient gels (TGX, Bio-Rad) separated the proteins, and the gels were subsequently stained with Instant Blue (Expedeon). Gel pictures were taken, and subsequently, an X-ray film was exposed to the gel in order to detect the radioactive signals of  $^{32}$ P.

**Expanded View** for this article is available online.

### Acknowledgements

We would like to thank Dr. Zachary Nimchuk for the *crn-10* mutant allele and Drs. N. Geldner and S. Yalovsky for vector plasmids. This work was supported by Swiss National Science Foundation grants 31003A\_166394 (awarded to C.S.H.) and 31003A\_156920 (awarded to M.H.), German Research Foundation (DFG) grant CRC 1101-D01 (awarded to M.H.), a Human Frontier Science Program Career Development Award (M.H.), and the European Molecular Biology Organization (EMBO) Young Investigator program (M.H.). A.R.V., J.S., and B.B. were supported by EMBO long-term post-doctoral fellowships.

### Author contributions

OH, BB, MH, and CSH designed the study and wrote the paper together. OH, BB, PC, JS, and AR-V performed experiments.

### Conflict of interest

The authors declare that they have no conflict of interest.

## References

- Katsir L, Davies KA, Bergmann DC, Laux T (2011) Peptide signaling in plant development. *Curr Biol* 21: R356–R364
- Cock JM, McCormick S (2001) A large family of genes that share homology with CLAVATA3. *Plant Physiol* 126: 939–942
- Ito Y, Nakanomyo I, Motose H, Iwamoto K, Sawa S, Dohmae N, Fukuda H (2006) Dodeca-CLE peptides as suppressors of plant stem cell differentiation. *Science* 313: 842–845
- Kondo T, Sawa S, Kinoshita A, Mizuno S, Kakimoto T, Fukuda H, Sakagami Y (2006) A plant peptide encoded by CLV3 identified by *in situ* MALDI-TOF MS analysis. *Science* 313: 845–848
- Matsubayashi Y (2011) Small post-translationally modified peptide signals in *Arabidopsis*. *Arabidopsis Book* 9: e0150
- Ohyama K, Shinohara H, Ogawa-Ohnishi M, Matsubayashi Y (2009) A glycopeptide regulating stem cell fate in *Arabidopsis thaliana*. *Nat Chem Biol* 5: 578–580
- Goad DM, Zhu C, Kellogg EA (2016) Comprehensive identification and clustering of CLV3/ESR-related (CLE) genes in plants finds groups with potentially shared function. *New Phytol* <https://doi.org/10.1111/nph.14348>
- Strabala TJ, O'Donnell PJ, Smit AM, Ampomah-Dwamena C, Martin EJ, Netzler N, Nieuwenhuizen NJ, Quinn BD, Foote HC, Hudson KR (2006) Gain-of-function phenotypes of many CLAVATA3/ESR genes, including four new family members, correlate with tandem variations in the conserved CLAVATA3/ESR domain. *Plant Physiol* 140: 1331–1344
- Depuydt S, Rodriguez-Villalon A, Santuari L, Wyser-Rmili C, Ragni L, Hardtke CS (2013) Suppression of *Arabidopsis* protophloem differentiation and root meristem growth by CLE45 requires the receptor-like kinase BAM3. *Proc Natl Acad Sci USA* 110: 7074–7079
- Kinoshita A, Nakamura Y, Sasaki E, Kyojuka J, Fukuda H, Sawa S (2007) Gain-of-function phenotypes of chemically synthetic CLAVATA3/ESR-related (CLE) peptides in *Arabidopsis thaliana* and *Oryza sativa*. *Plant Cell Physiol* 48: 1821–1825
- Miwa H, Betsuyaku S, Iwamoto K, Kinoshita A, Fukuda H, Sawa S (2008) The receptor-like kinase SOL2 mediates CLE signaling in *Arabidopsis*. *Plant Cell Physiol* 49: 1752–1757
- Brand U, Fletcher JC, Hobe M, Meyerowitz EM, Simon R (2000) Dependence of stem cell fate in *Arabidopsis* on a feedback loop regulated by CLV3 activity. *Science* 289: 617–619
- Clark SE, Running MP, Meyerowitz EM (1995) CLAVATA3 is a specific regulator of shoot and floral meristem development affecting the same processes as CLAVATA1. *Development* 121: 2057–2067
- Clark SE, Williams RW, Meyerowitz EM (1997) The CLAVATA1 gene encodes a putative receptor kinase that controls shoot and floral meristem size in *Arabidopsis*. *Cell* 89: 575–585
- Ogawa M, Shinohara H, Sakagami Y, Matsubayashi Y (2008) *Arabidopsis* CLV3 peptide directly binds CLV1 ectodomain. *Science* 319: 294
- Rojo E, Sharma VK, Kovaleva V, Raikhel NV, Fletcher JC (2002) CLV3 is localized to the extracellular space, where it activates the *Arabidopsis* CLAVATA stem cell signaling pathway. *Plant Cell* 14: 969–977
- Fletcher JC, Brand U, Running MP, Simon R, Meyerowitz EM (1999) Signaling of cell fate decisions by CLAVATA3 in *Arabidopsis* shoot meristems. *Science* 283: 1911–1914
- Kang YH, Hardtke CS (2016) *Arabidopsis* MAKR5 is a positive effector of BAM3-dependent CLE45 signaling. *EMBO Rep* 17: 1145–1154
- Rodriguez-Villalon A, Gujas B, Kang YH, Breda AS, Cattaneo P, Depuydt S, Hardtke CS (2014) Molecular genetic framework for protophloem formation. *Proc Natl Acad Sci USA* 111: 11551–11556
- Etchells JP, Turner SR (2010) The PXY-CLE41 receptor ligand pair defines a multifunctional pathway that controls the rate and orientation of vascular cell division. *Development* 137: 767–774
- Fisher K, Turner S (2007) PXY, a receptor-like kinase essential for maintaining polarity during plant vascular-tissue development. *Curr Biol* 17: 1061–1066
- Hirakawa Y, Kondo Y, Fukuda H (2010) TDIF peptide signaling regulates vascular stem cell proliferation via the WOX4 homeobox gene in *Arabidopsis*. *Plant Cell* 22: 2618–2629
- Hirakawa Y, Shinohara H, Kondo Y, Inoue A, Nakanomyo I, Ogawa M, Sawa S, Ohashi-Ito K, Matsubayashi Y, Fukuda H (2008) Non-cell-autonomous control of vascular stem cell fate by a CLE peptide/receptor system. *Proc Natl Acad Sci USA* 105: 15208–15213
- Morita J, Kato K, Nakane T, Kondo Y, Fukuda H, Nishimasu H, Ishitani R, Nureki O (2016) Crystal structure of the plant receptor-like kinase TDR in complex with the TDIF peptide. *Nat Commun* 7: 12383
- Zhang H, Lin X, Han Z, Qu LJ, Chai J (2016) Crystal structure of PXY-TDIF complex reveals a conserved recognition mechanism among CLE peptide-receptor pairs. *Cell Res* 26: 543–555
- Hazak O, Hardtke CS (2016) CLAVATA 1-type receptors in plant development. *J Exp Bot* 67: 4827–4833

27. Li J, Tax FE (2013) Receptor-like kinases: key regulators of plant development and defense. *J Integr Plant Biol* 55: 1184–1187
28. Brandt B, Hothorn M (2016) SERK co-receptor kinases. *Curr Biol* 26: R225–R226
29. Santiago J, Henzler C, Hothorn M (2013) Molecular mechanism for plant steroid receptor activation by somatic embryogenesis co-receptor kinases. *Science* 341: 889–892
30. Santiago J, Brandt B, Wildhagen M, Hohmann U, Hothorn LA, Butenko MA, Hothorn M (2016) Mechanistic insight into a peptide hormone signaling complex mediating floral organ abscission. *Elife* 5: e15075
31. Meng X, Zhou J, Tang J, Li B, de Oliveira MV, Chai J, He P, Shan L (2016) Ligand-induced receptor-like kinase complex regulates floral organ abscission in *Arabidopsis*. *Cell Rep* 14: 1330–1338
32. Schwessinger B, Rathjen JP (2015) Changing SERKs and priorities during plant life. *Trends Plant Sci* 20: 531–533
33. Torii KU (2012) Mix-and-match: ligand-receptor pairs in stomatal development and beyond. *Trends Plant Sci* 17: 711–719
34. Jeong S, Trotochaud AE, Clark SE (1999) The *Arabidopsis* CLAVATA2 gene encodes a receptor-like protein required for the stability of the CLAVATA1 receptor-like kinase. *Plant Cell* 11: 1925–1934
35. Muller R, Bleckmann A, Simon R (2008) The receptor kinase CORYNE of *Arabidopsis* transmits the stem cell-limiting signal CLAVATA3 independently of CLAVATA1. *Plant Cell* 20: 934–946
36. Nimchuk ZL, Tarr PT, Meyerowitz EM (2011) An evolutionarily conserved pseudokinase mediates stem cell production in plants. *Plant Cell* 23: 851–854
37. Guo Y, Han L, Hymes M, Denver R, Clark SE (2010) CLAVATA2 forms a distinct CLE-binding receptor complex regulating *Arabidopsis* stem cell specification. *Plant J* 63: 889–900
38. Shinohara H, Matsubayashi Y (2015) Reevaluation of the CLV3-receptor interaction in the shoot apical meristem: dissection of the CLV3 signaling pathway from a direct ligand-binding point of view. *Plant J* 82: 328–336
39. Meng X, Feldman LJ (2010) CLE14/CLE20 peptides may interact with CLAVATA2/CORYNE receptor-like kinases to irreversibly inhibit cell division in the root meristem of *Arabidopsis*. *Planta* 232: 1061–1074
40. Fiers M, Golemic E, Xu J, van der Geest L, Heidstra R, Stiekema W, Liu CM (2005) The 14-amino acid CLV3, CLE19, and CLE40 peptides trigger consumption of the root meristem in *Arabidopsis* through a CLAVATA2-dependent pathway. *Plant Cell* 17: 2542–2553
41. De Smet I, Vassileva V, De Rybel B, Levesque MP, Grunewald W, Van Damme D, Van Noorden G, Naudts M, Van Isterdael G, De Clercq R et al (2008) Receptor-like kinase ACR4 restricts formative cell divisions in the *Arabidopsis* root. *Science* 322: 594–597
42. Stahl Y, Grabowski S, Bleckmann A, Kuhnemuth R, Weidtkamp-Peters S, Pinto KG, Kirschner GK, Schmid JB, Wink RH, Hulsewede A et al (2013) Moderation of *Arabidopsis* root stemness by CLAVATA1 and ARABIDOPSIS CRINKLY4 receptor kinase complexes. *Curr Biol* 23: 362–371
43. Shimizu N, Ishida T, Yamada M, Shigenobu S, Tabata R, Kinoshita A, Yamaguchi K, Hasebe M, Mitsumasa K, Sawa S (2015) BAM1 and RECEPTOR-LIKE PROTEIN KINASE 2 constitute a signaling pathway and modulate CLE peptide-triggered growth inhibition in *Arabidopsis* root. *New Phytol* 208: 1104–1113
44. Rodríguez-Villalón A, Gujas B, van Wijk R, Munnik T, Hardtke CS (2015) Primary root protophloem differentiation requires balanced phosphatidylinositol-4,5-bisphosphate levels and systemically affects root branching. *Development* 142: 1437–1446
45. Zhang H, Lin X, Han Z, Wang J, Qu LJ, Chai J (2016) SERK family receptor-like kinases function as a co-receptor with PXY for plant vascular development. *Mol Plant* 10: 1406–1414
46. Hohmann U, Lau K, Hothorn M (2017) The structural basis of ligand perception and signal activation by receptor kinases. *Annu Rev Plant Biol* 68: 109–137
47. Colcombet J, Boisson-Dernier A, Ros-Palau R, Vera CE, Schroeder JI (2005) *Arabidopsis* SOMATIC EMBRYOGENESIS RECEPTOR KINASES 1 and 2 are essential for tapetum development and microspore maturation. *Plant Cell* 17: 3350–3361
48. Somssich M, Ma Q, Weidtkamp-Peters S, Stahl Y, Felekyan S, Bleckmann A, Seidel CA, Simon R (2015) Real-time dynamics of peptide ligand-dependent receptor complex formation in planta. *Sci Signal* 8: ra76
49. Kwaaitaal MA, de Vries SC (2007) The SERK1 gene is expressed in procambium and immature vascular cells. *J Exp Bot* 58: 2887–2896
50. Pallakias H, Simon R (2014) The CLE40 and CRN/CLV2 signaling pathways antagonistically control root meristem growth in *Arabidopsis*. *Mol Plant* 7: 1619–1636
51. Somssich M, Bleckmann A, Simon R (2016) Shared and distinct functions of the pseudokinase CORYNE (CRN) in shoot and root stem cell maintenance of *Arabidopsis*. *J Exp Bot* 67: 4901–4915
52. Nimchuk ZL (2017) CLAVATA1 controls distinct signaling outputs that buffer shoot stem cell proliferation through a two-step transcriptional compensation loop. *PLoS Genet* 13: e1006681
53. Hobe M, Muller R, Grunewald M, Brand U, Simon R (2003) Loss of CLE40, a protein functionally equivalent to the stem cell restricting signal CLV3, enhances root waving in *Arabidopsis*. *Dev Genes Evol* 213: 371–381
54. Jun J, Fiume E, Roeder AH, Meng L, Sharma VK, Osmont KS, Baker C, Ha CM, Meyerowitz EM, Feldman LJ et al (2010) Comprehensive analysis of CLE polypeptide signaling gene expression and overexpression activity in *Arabidopsis*. *Plant Physiol* 154: 1721–1736
55. Bleckmann A, Weidtkamp-Peters S, Seidel CA, Simon R (2010) Stem cell signaling in *Arabidopsis* requires CRN to localize CLV2 to the plasma membrane. *Plant Physiol* 152: 166–176
56. Chinchilla D, Zipfel C, Robatzek S, Kemmerling B, Nurnberger T, Jones JD, Felix G, Boller T (2007) A flagellin-induced complex of the receptor FLS2 and BAK1 initiates plant defence. *Nature* 448: 497–500
57. Kemmerling B, Schwedt A, Rodriguez P, Mazzotta S, Frank M, Qamar SA, Mengiste T, Betsuyaku S, Parker JE, Mussig C et al (2007) The BRI1-associated kinase 1, BAK1, has a brassinolide-independent role in plant cell-death control. *Curr Biol* 17: 1116–1122
58. Meng X, Chen X, Mang H, Liu C, Yu X, Gao X, Torii KU, He P, Shan L (2015) Differential function of *Arabidopsis* SERK family receptor-like kinases in stomatal patterning. *Curr Biol* 25: 2361–2372
59. Albrecht C, Russinova E, Kemmerling B, Kwaaitaal M, de Vries SC (2008) *Arabidopsis* SOMATIC EMBRYOGENESIS RECEPTOR KINASE proteins serve brassinosteroid-dependent and -independent signaling pathways. *Plant Physiol* 148: 611–619
60. Aan den Toorn M, Albrecht C, de Vries S (2015) On the origin of SERKs: bioinformatics analysis of the somatic embryogenesis receptor kinases. *Mol Plant* 8: 762–782
61. Lehmann F, Hardtke CS (2016) Secondary growth of the *Arabidopsis* hypocotyl-vascular development in dimensions. *Curr Opin Plant Biol* 29: 9–15
62. Nimchuk ZL, Tarr PT, Ohno C, Qu X, Meyerowitz EM (2011) Plant stem cell signaling involves ligand-dependent trafficking of the CLAVATA1 receptor kinase. *Curr Biol* 21: 345–352

63. Nimchuk ZL, Zhou Y, Tarr PT, Peterson BA, Meyerowitz EM (2015) Plant stem cell maintenance by transcriptional cross-regulation of related receptor kinases. *Development* 142: 1043–1049
64. Kang YH, Breda A, Hardtke CS (2017) Brassinosteroid signaling directs formative cell divisions and protophloem differentiation in *Arabidopsis* root meristems. *Development* 144: 272–280
65. Scacchi E, Salinas P, Gujas B, Santuari L, Krogan N, Ragni L, Berleth T, Hardtke CS (2010) Spatio-temporal sequence of cross-regulatory events in root meristem growth. *Proc Natl Acad Sci USA* 107: 22734–22739
66. DeYoung BJ, Bickle KL, Schrage KJ, Muskett P, Patel K, Clark SE (2006) The CLAVATA1-related BAM1, BAM2 and BAM3 receptor kinase-like proteins are required for meristem function in *Arabidopsis*. *Plant J* 45: 1–16
67. Deyoung BJ, Clark SE (2008) BAM receptors regulate stem cell specification and organ development through complex interactions with CLAVATA signaling. *Genetics* 180: 895–904
68. Rodrigues A, Santiago J, Rubio S, Saez A, Osmont KS, Gadea J, Hardtke CS, Rodriguez PL (2009) The short-rooted phenotype of the *brevis radix* mutant partly reflects root abscisic acid hypersensitivity. *Plant Physiol* 149: 1917–1928
69. Bracha-Drori K, Shichrur K, Katz A, Oliva M, Angelovici R, Yalovsky S, Ohad N (2004) Detection of protein-protein interactions in plants using bimolecular fluorescence complementation. *Plant J* 40: 419–427
70. Kurihara D, Mizuta Y, Sato Y, Higashiyama T (2015) ClearSee: a rapid optical clearing reagent for whole-plant fluorescence imaging. *Development* 142: 4168–4179
71. Soding J, Biegert A, Lupas AN (2005) The HHpred interactive server for protein homology detection and structure prediction. *Nucleic Acids Res* 33: W244–W248
72. Sali A, Blundell TL (1993) Comparative protein modelling by satisfaction of spatial restraints. *J Mol Biol* 234: 779–815
73. Bojar D, Martinez J, Santiago J, Rybin V, Bayliss R, Hothorn M (2014) Crystal structures of the phosphorylated BRI1 kinase domain and implications for brassinosteroid signal initiation. *Plant J* 78: 31–43



**License:** This is an open access article under the terms of the Creative Commons Attribution 4.0 License, which permits use, distribution and reproduction in any medium, provided the original work is properly cited.

## Expanded View Figures

**Figure EV1. BAM3-CLE45 control experiments and *bam3* alleles.**

- A Relative primary root length of indicated genotypes at 9 dag, in response to increasing amounts of CLE45 in the media.  $n = 12$  for each genotype, mean  $\pm$  s.e.m. All differences as compared to wild type were statistically significant (Student's *t*-test) with  $P < 0.001$  for 15 and 50 nM, and  $P < 0.05$  for 100 nM.
- B ITC of purified PXY extracellular domain vs. CLV41/44 peptide. n.d.: not detectable. N: stoichiometry,  $K_d$  dissociation constant. Shown are experimental values  $\pm$  fitting errors (95% confidence interval).
- C ITC of purified BAM3 extracellular domain vs. CLV3 peptide.
- D ITC of purified BAM3 extracellular domain vs. an N-terminally tyrosine-modified CLV3 peptide.
- E ITC of purified BAM3 extracellular domain vs. an N-terminally tyrosine-modified CLE45 peptide.
- F Representative 9-day-old Col-0 seedlings grown on mock or in presence of indicated peptides.

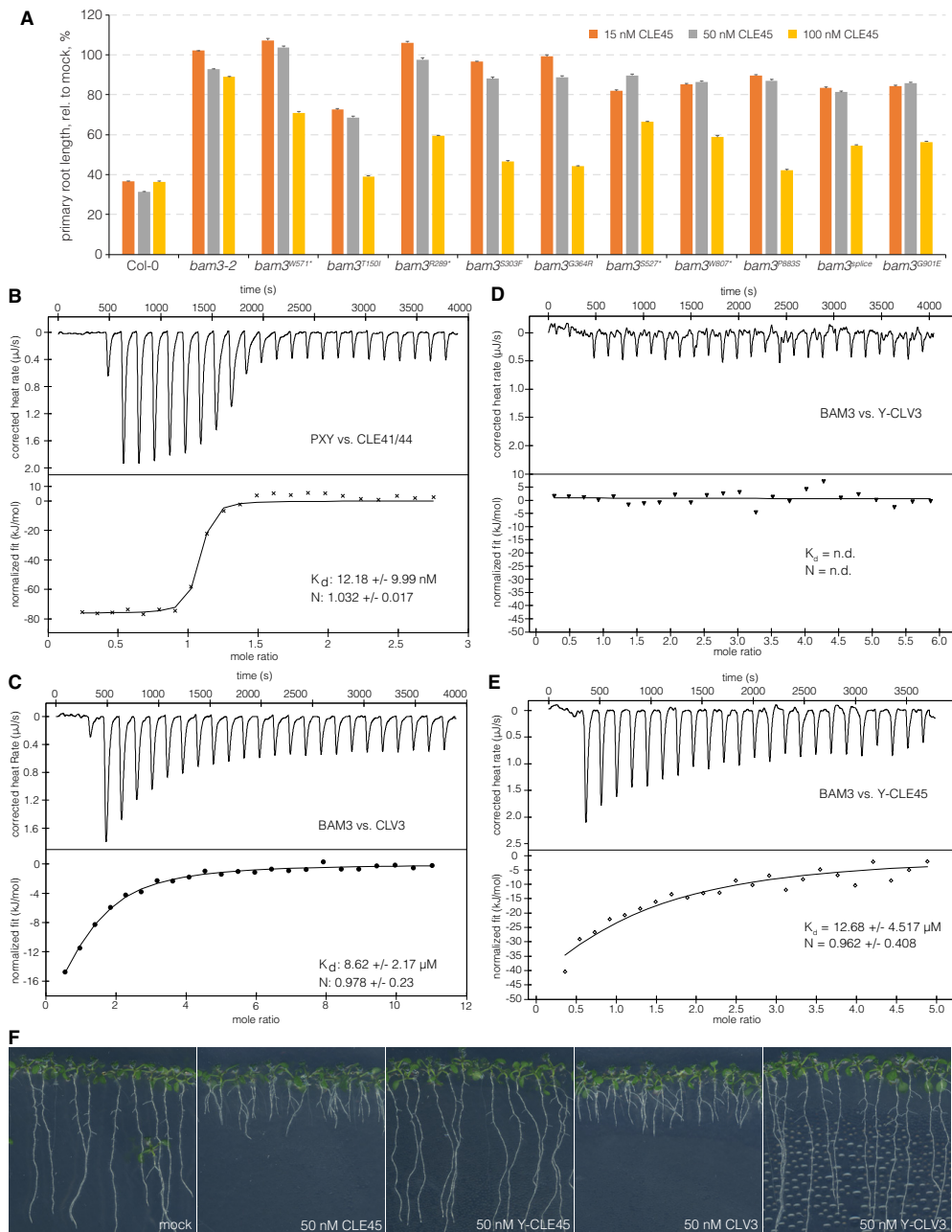


Figure EV1.

**Figure EV2. BAM3 localization and biochemical control experiments.**

- A Transient expression of BAM3 wild-type or mutant BAM3<sup>QYY</sup> CITRINE fusion proteins (green fluorescence) in tobacco leaf epidermal cells, under control of a constitutive promoter (confocal microscopy).
- B Close-up of developing protophloem sieve element cell files expressing BAM3 wild-type or mutant BAM3<sup>QYY</sup> CITRINE fusion proteins (green fluorescence).
- C, D Primary root length of 7-day-old seedlings of indicated genotypes on mock or CLE45 media, several independent lines per transgene construct are shown. Differences as compared to mock are not statistically significant unless indicated (Student's t-test); \* $P < 0.05$ ; \*\* $P < 0.01$ ; \*\*\* $P < 0.001$ ; mean  $\pm$  s.e.m.
- E Transphosphorylation kinase assays with purified BAM3 kinase domain (BAM3-KD) or SERK1 kinase domain (SERK1-KD) as well as kinase dead point mutant versions (mBAM3-KD & mSERK1-KD) alone and in combination.
- F Analytical size-exclusion chromatography of purified BAM3 and SERK3 extracellular domains in the presence of CLE45 peptide reveals no ligand-induced complex formation between BAM3 and SERK3.
- G Analytical size-exclusion chromatography of purified PXY and SERK1 extracellular domains in the presence of CLE41/44 peptide reveals CLE41/44-induced binding of SERK1 to the PXY ectodomain.
- H Expression of SERK1-CITRINE fusion protein (green fluorescence) under control of the native *SERK1* promoter (blue fluorescence: calcofluor white cell wall staining). Green channel is shown separately (left) and in overlay with blue channel (right). Asterisk indicates the developing sieve element cell file.

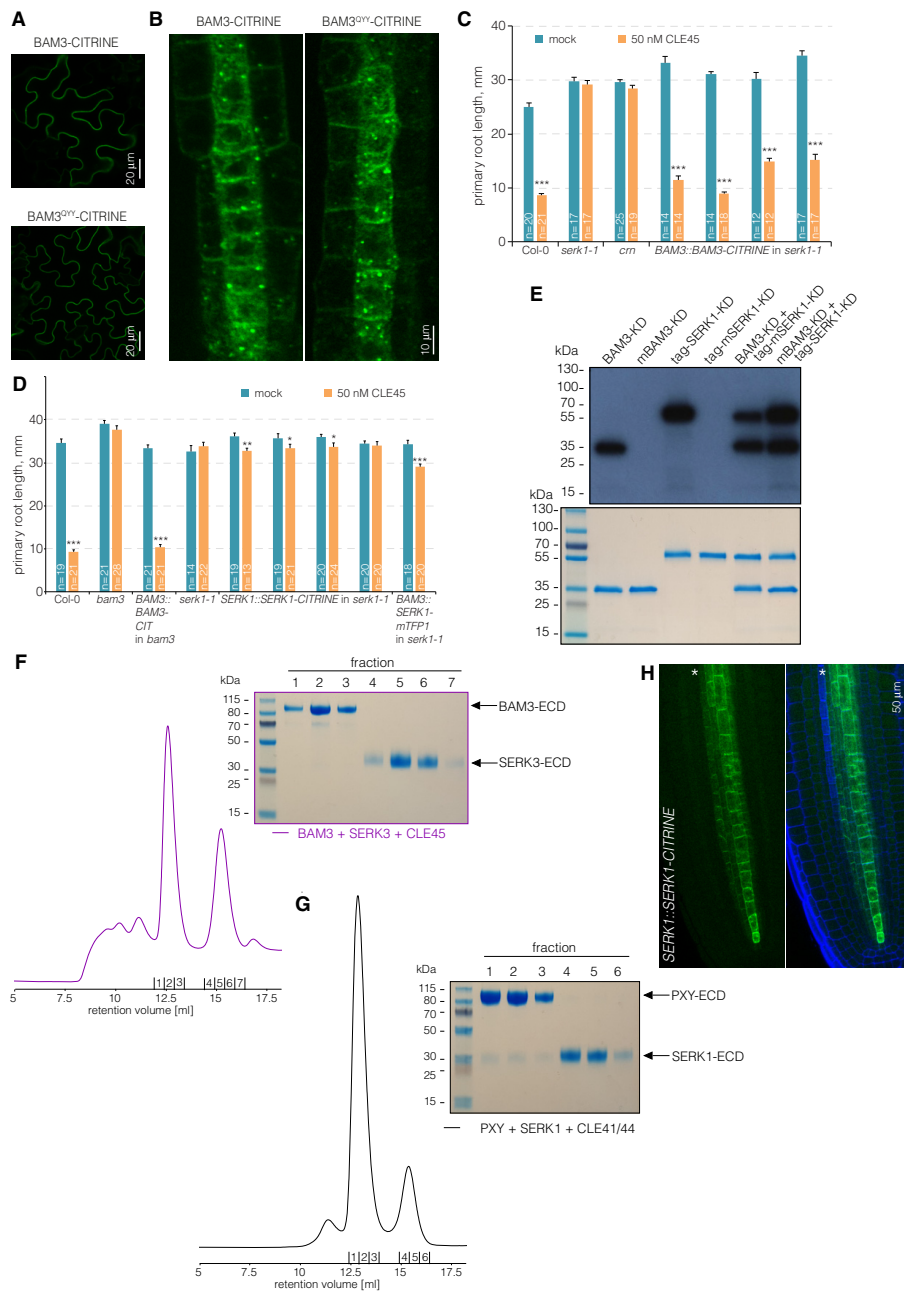
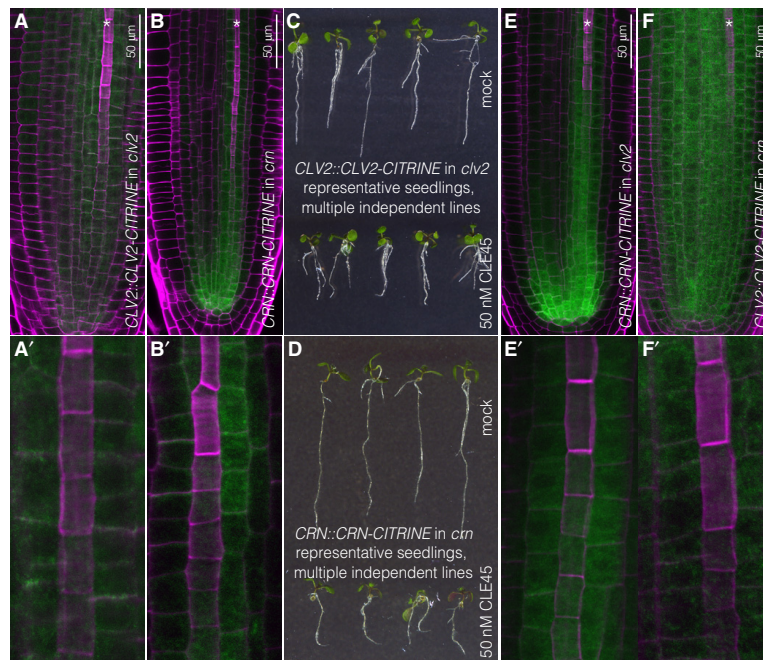
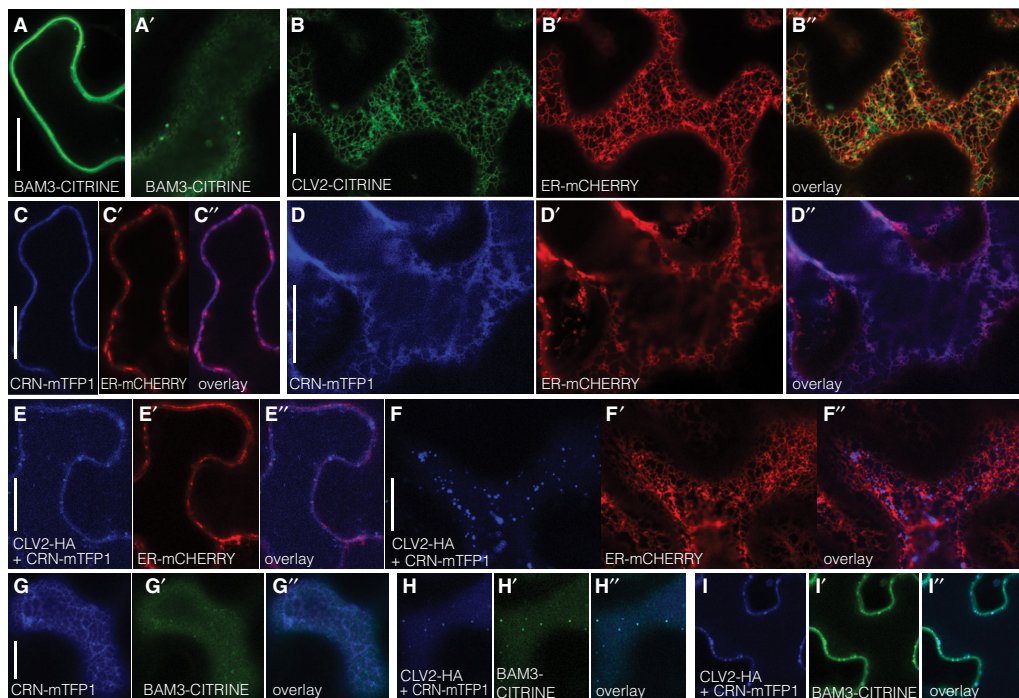


Figure EV2.



**Figure EV3. CLV2 and CRN localizations in *Arabidopsis* roots.**

- A Expression of CLV2-CITRINE fusion protein (green fluorescence) under control of the native promoter in *clv2* root meristems (magenta fluorescence: calcofluor white cell wall staining) (confocal microscopy). Asterisk marks developing protophloem sieve element strand. Close-up (A') with developing protophloem at the center is shown.
- B Same as in (A), for CRN-CITRINE fusion protein under control of the native promoter in *crn* root meristems.
- C Representative 5-day-old *clv2* seedlings expressing CLV2-CITRINE fusion protein under control of its native promoter grown on mock or CLE45.
- D Representative 5-day-old *crn* seedlings expressing CRN-CITRINE fusion protein under control of its native promoter grown on mock or CLE45.
- E Same as in (A), for CRN-CITRINE fusion protein under control of the native promoter in *clv2* root meristems.
- F Same as in (A), for CLV2-CITRINE fusion protein under control of the native promoter in *crn* root meristems.



**Figure EV4. Tobacco co-localization, additional, and control experiments.**

- A Transient expression of BAM3-CITRINE fusion protein (green fluorescence) in tobacco (*Nicotiana benthamiana*) leaf epidermal cells, under control of a constitutive promoter (confocal microscopy), optical section through cell center. Panel (A'): same in cell surface view.
- B Transient co-expression of CLV2-CITRINE fusion protein (green fluorescence) and an endoplasmic reticulum marker (ER-mCHERRY, red fluorescence).
- C Transient co-expression of CRN-mTFP1 fusion protein (blue fluorescence) and the ER-mCHERRY marker (red fluorescence), optical section through cell center.
- D Same as (C), in cell surface view.
- E, F Corresponding to (C) and (D), in the additional presence of (non-fluorescent) CLV2-HA fusion protein.
- G Transient co-expression of CRN-mTFP1 (blue fluorescence) and BAM3-CITRINE (green fluorescence) fusion proteins, in cell surface view.
- H, I Transient co-expression of CRN-mTFP1 (blue fluorescence) and BAM3-CITRINE (green fluorescence) fusion proteins, in the additional presence of (non-fluorescent) CLV2-HA fusion protein. Panel (H): cell surface view. Panel (I): optical section through cell center.

Data information: Scale bars are 20  $\mu$ m.

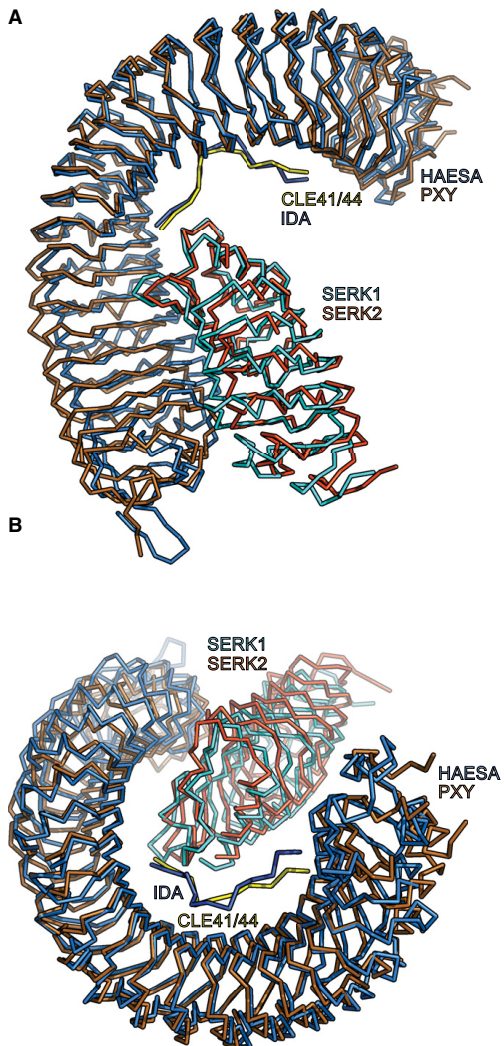


**Figure EV5. Structure comparison of HAESA-IDA-SERK1 and PXY-CLE41-SERK2 signaling complexes.**

A, B Structural superposition of HAESA-IDA-SERK1 (PDB-ID 5IYX, HAESA in light blue, IDA in dark blue, and SERK1 in cyan) (Santiago et al<sup>[30]</sup>) with a PXY-CLE41/44-SERK2 complex (PDB-ID 5GQR, PXY in gold, IDA in yellow, and SERK2 in orange) (Zhang et al<sup>[45]</sup>). The complexes closely align with an r.m.s.d. of 2.3 Å comparing 770 C<sub>α</sub> atoms.

Table EV1. Transgenic and mutant lines created in this study

Number	Name	Method
1	<i>BAM3::BAM3-CITRINE</i> in <i>wt</i> , <i>bam3-2</i> , <i>brx-2 bam3</i> , <i>serk1-1</i> and <i>crn-10</i>	transformation
2	<i>BAM3::bam3<sup>QYY</sup>-CITRINE</i> in <i>bam3-2</i> , <i>brx-2 bam3</i>	transformation
3	<i>BAM3::CRN-CITRINE</i> in <i>wt</i> , <i>crn-10</i> , <i>clv2-1</i>	transformation
4	<i>BAM3::SERK1-mTFP1</i> in <i>serk1-1</i>	transformation
5	<i>SERK1::SERK1-CITRINE</i> in <i>wt</i> and <i>serk1-1</i>	transformation
6	<i>CRN::CRNg-CITRINE</i> in <i>crn-10</i> and <i>clv2-1</i>	transformation
7	<i>CLV2::CLV2g-CITRINE</i> in <i>clv2-1</i> and <i>crn-10</i>	transformation
8	<i>MAKR5::MAKR5-GFP</i> in <i>crn-10</i> and <i>clv2-1</i>	transformation
9	<i>crn-10 brx-2</i>	cross
10	<i>serk1-1 brx-2</i>	cross
11	<i>clv2-1 brx-2</i>	cross

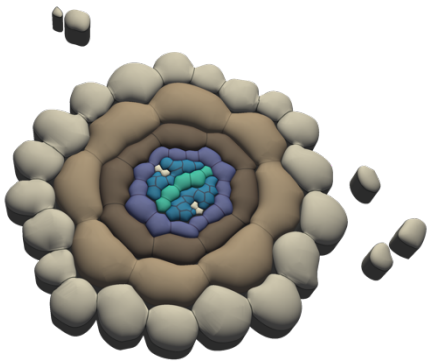
Table EV2. Constructs used in this study

Number	Name	Source
IH_p42	<i>pH7-m34GW-35S::BAM3-YN</i>	This study
IH_p43	<i>pH7-m34GW-35S::BAM3-YC</i>	This study
IH_p48	<i>pH7-m34GW-35S::CLV2-YN</i>	This study
IH_p49	<i>pH7-m34GW-35S::CLV2-YC</i>	This study
IH_p50	<i>pH7-m34GW-35S::CRN-YN</i>	This study
IH_p51	<i>pH7-m34GW-35S::CRN-YC</i>	This study
IH_p52	<i>pH7-m34GW-35S::BRI1-YN</i>	This study
IH_p53	<i>pH7-m34GW-pBAM3::BAM3-CITRINE</i>	Rodriguez-Villalon et al, 2014
IH_p54	<i>pH7-m34GW-pBAM3::bam3<sup>QYY</sup>-CITRINE</i>	This study
IH_p55	<i>pH7-m34GW-pSERK1::SERK1-CITRINE</i>	This study
IH_p56	<i>pH7-m34GW-pMAKR5::MAKR5-GFP</i>	Kang and Hardtke, 2016
IH_p57	<i>pH7-m34GW-pBAM3::CRN-CITRINE</i>	This study
IH_p58	<i>pH7-m24GW-pCLV2CLV2g-CITRINE</i>	This study
IH_p59	<i>pH7-m24GW-pCRNCRNg-CITRINE</i>	This study
IH_p60	<i>pH7-m34GW-pUBQ10::BAM3-CITRINE</i>	This study
IH_p61	<i>pH7-m34GW-35S::BAM3-mTFP1</i>	This study
IH_p62	<i>pH7-m34GW-35S::BRI1-mTFP1</i>	This study
IH_p63	<i>pH7-m34GW-35S::CLV2-HA</i>	This study
IH_p64	<i>pH7-m34GW-35S::SERK1-TurboRFP</i>	This study
IH_p65	<i>pH7-m34GW-35S::CRN-TurboRFP</i>	This study
IH_p66	<i>pH7-m34GW-35S::SERK1-TurboRFP</i>	This study
IH_p67	<i>pH7-m34GW-35S::CLV2-CITRINE</i>	This study
IH_p68	<i>pH7-m34GW-pBAM3::SERK1-mTFP1</i>	This study
IH_69	<i>pH7-m34GW-35S::CRN-mTFP1</i>	This study
IH_70	<i>pH7-m34GW-35S::BRI1-YC</i>	This study
IH_71	<i>pH7-m34GW-35S::BK11-YN</i>	This study
p1	<i>pFastBac1-Az-BAM3-ECD (30-651)</i>	This study
p2	<i>pFastBac1-Az-PXY-ECD (30-647)</i>	This study
p3	<i>pFastBac1-Az-SERK1-ECD (24-213)</i>	This study
p4	<i>pFastBac1-Az-SERK3-ECD (22-220)</i>	This study
p5	<i>pET-TH-BAM3-KD (679-992)</i>	This study
p6	<i>pET-TH-SERK1 (264–625)</i>	This study

Table EV3. Primers used in this study

Number	Name	Sequence	Comments
1	CLV2attb1F1	GTA CAA AAA AGC AGG CTC CAT GAT AAA GAT TGC AGA TTT CAC TC	Cloning CLV2 cds into pENTRY221
2	CLV2attb1F2	GGG GAC AAG TTT GTA CAA AAA AGC AGG CTC CAT GAT AAA GA	Cloning CLV2 cds into pENTRY221
3	CLV2attb2R1	TTG TAC AAG AAA GCT GGG TAA GCT TTG GTC TGA AGA ATA TAA CTA C	Cloning CLV2 cds into pENTRY221
4	CLV2attb2R2	GGG GAC CAC TTT GTA CAA GAA AGC TGG GTA AGC TTT GGT CTG A	Cloning CLV2 cds into pENTRY221
5	CRNattb1F1	GTA CAA AAA AGC AGG CTC CAT GAA GCA AAG AAG AAG AAG AAA	Cloning CRN cds into pENTRY221
6	CRNattb1F2	GGG GAC AAG TTT GTA CAA AAA AGC AGG CTC CAT GAA GCA AAG A	Cloning CRN cds into pENTRY221
7	CRNattb2R1	TTG TAC AAG AAA GCT GGG TAA AAG CTG TGC AGT TGT GTA GCA	Cloning CRN cds into pENTRY221
8	CRNattb2R2	GGG GAC CAC TTT GTA CAA GAA AGC TGG GTA AAA GCT GTG CAG	Cloning CRN cds into pENTRY221
9	pCLV2CLV2g_ attb4F	GGG GAC AAC TTT GTA TAG AAA AGT TGC ATA TTA GAT CTA GGG TTT AGA TAC CAT T	Cloning full genomic pCLV2- CLV2
10	pCLV2CLV2g_ attb1R	GGG GAC TGC TTT TTT GTA CAA ACT TGG AGC TTT GGT CTG AAG AAT ATA AC	Cloning full genomic pCLV2- CLV2
11	pCRNCRNg_ attb4F	GGG GAC AAC TTT GTA TAG AAA AGT TGC AAT TTT GGT TTT GAA TCT GTG TC	Cloning full genomic pCRN- CRN
12	pCRNCRNg_ attb1R	GGG GAC TGC TTT TTT GTA CAA ACT TGG AAA GCT GTG CAG TTG TGT AAG	Cloning full genomic pCRN- CRN
13	pSERK1 KpnI F	TGG TAC CCG TTT CTC TTT CAT AAC AAG GTA GC	Cloning SERK1 promoter
14	pSERK1 SmaI R	TCC CGG GTT CAA ACA ACA ATG CTA AAT TTC G	Cloning SERK1 promoter
15	cm F	GTA GAA GCA GCA ATG AAG CAA AGA AGA AGGTG	Genotyping of <i>cm</i> mutant (PCR product was later cut with HphI)
16	cm R	GTT GAA GTT GTG GAT AAG TG	Genotyping of <i>cm</i> mutant

## Chapter 4



# **BIG BROTHER uncouples cell proliferation from elongation in the *Arabidopsis* primary root**

Cattaneo P and Hardtke CS

Plant Cell Physiol. 2017 Sep 1; 58 (9):1519-1527

## **Highlights**

- A second site null-mutation in the gene *BIG BROTHER* partially rescues the *brx* and *ops* reduced meristematic activity, although not the impaired transfer of growth-limiting metabolites and developmental signals along the protophloem.
- Dissection of *bb* meristem growth over time reveals a significant enhancement of dividing cell number. Additional observations revealed no differences in cell elongation and overall root length compared to wild type.
- Consequences on macroscopic *bb* root growth might be circumvented by the extra formative division in the vascular cylinder.

## **My contribution**

I designed and performed all experiments included in this chapter.

# BIG BROTHER Uncouples Cell Proliferation from Elongation in the Arabidopsis Primary Root

Pietro Cattaneo and Christian S. Hardtke\*

Department of Plant Molecular Biology, University of Lausanne, Biophore Building, CH-1015 Lausanne, Switzerland

\*Corresponding author: E-mail, christian.hardtke@unil.ch; Fax, +41-21-692-4150.

(Received April 4, 2017; Accepted June 25, 2017)

Regular Paper

Plant organ size is sensitive to environmental conditions, but is also limited by hardwired genetic constraints. In *Arabidopsis*, a few organ size regulators have been identified. Among them, the *BIG BROTHER* (*BB*) gene has a prominent role in the determination of flower organ and leaf size. *BB* loss-of-function mutations result in a prolonged proliferation phase during leaf(-like) organ formation, and consequently larger leaves, petals and sepals. Whether *BB* has a similar role in root growth is unknown. Here we describe a novel *bb* allele which carries a P235L point mutation in the *BB* RING finger domain. This allele behaves similarly to described *bb* loss-of-function alleles and displays increased root meristem size due to a higher number of dividing, meristematic cells. In contrast, mature cell length is unaffected. The increased meristematic activity does not, however, translate into overall enhanced root elongation, possibly because *bb* mutation also results in an increased number of cell files in the vascular cylinder. These extra formative divisions might offset any growth acceleration by extra meristematic divisions. Thus, although *BB* dampens root cell proliferation, the consequences on macroscopic root growth are minor. However, *bb* mutation accelerates overall root growth when introduced into sensitized backgrounds. For example, it partially rescues the short root phenotypes of the *brevis radix* and *octopus* mutants, but does not complement their phloem differentiation or transport defects. In summary, we provide evidence that *BB* acts conceptually similarly in leaf(-like) organs and the primary root, and uncouples cell proliferation from elongation in the root meristem.

**Keywords:** Auxin • DA1 • DA1-RELATED 1 • DA1-RELATED 2 • DA2 • PLETHORA.

**Abbreviations:** BAM3, BARELY ANY MERISTEM 3; BB, BIG BROTHER; BRX, BREVIS RADIX; CFDA, carboxyfluorescein diacetate; CLE45, CLAVATA3/EMBRYO SURROUNDING REGION 45; DAR1, DA1-RELATED 1; DAR2, DA1-RELATED 2; GFP, green fluorescent protein; OPS, OCTOPUS; PLT, PLETHORA; UIM, ubiquitin interaction motif.

## Introduction

Plant organ size can vary as a function of environmental conditions; however, this variation operates within the limits set by genetic constraints. The underlying genetic factors can be

revealed in standardized growth conditions that even out plant ontogeny. Moreover, they are most evident in structures whose size shows comparatively little variation in response to the environment, such as seeds or flower organs of the model plant *Arabidopsis thaliana* (*Arabidopsis*). Through a forward genetic screen, the *BIG BROTHER* (*BB*) gene of *Arabidopsis* has been identified as a negative regulator of petal size (Disch et al. 2006). *BB* loss-of-function mutations result in bigger petals, and *BB* gain of function, through ectopic overexpression, induces the opposite phenotype (Disch et al. 2006, Vanhaeren et al. 2017). In the loss-of-function scenario, final cell size is not affected, while in the gain-of-function scenario, a slight, possibly compensatory cell size increase could be observed. Nevertheless, a priori the organ size variation can be explained by differences in cell number. For instance, in *bb* loss-of-function mutants, cell number is increased. However, this is not due to an accelerated cell cycle, but rather due to a delay in the transition from proliferation to elongation (Disch et al. 2006, Li et al. 2008, Vanhaeren et al. 2017).

*BB* encodes an E3 ubiquitin ligase with a RING finger domain that is essential for its activity (Disch et al. 2006). Another RING finger-type E3 ligase, *DA2*, plays a similar role to *BB* in organ size determination (Xia et al. 2013). *bb* and *da2* mutants enhance each other's phenotype in an additive manner, suggesting that the two genes work genetically independently of each other. They also enhance the phenotype of another, dominant-negative mutant with increased organ size due to a prolonged cell proliferation phase, *da1-1* (Li et al. 2008, Xia et al. 2013, Du et al. 2014, Vanhaeren et al. 2017). A recent study has demonstrated that both *BB* and *DA2* ubiquitinate *DA1*, a peptidase with ubiquitin interaction motifs (UIMs), which thereby becomes activated (Dong et al. 2017). Although this apparently destabilizes *BB* and *DA2* in turn, *DA1* might be required for efficient target recognition and/or degradation by *BB* and *DA2*, which would explain the similar phenotypes of the three loss-of-function mutants and their mutual enhancement (Dong et al. 2017).

*DA1* acts partially redundantly with one of its homologs, *DA1-RELATED 1* (*DAR1*) (Li et al. 2008, Dong et al. 2017). Interestingly, loss of function in another homolog, *DAR2*, has been reported to affect root meristem activity, however in an opposite sense, as would be expected from the *da1/dar1* precedence (Peng et al. 2013). *dar2* mutants display reduced cell proliferation in the root meristem and increased mature cell length which, however, do not compensate each other and lead

*Plant Cell Physiol.* 58(9): 1519–1527 (2017) doi:10.1093/pcp/pcx091, Advance Access publication on 30 June 2017,

available online at [www.pcp.oxfordjournals.org](http://www.pcp.oxfordjournals.org)

© The Author 2017. Published by Oxford University Press on behalf of Japanese Society of Plant Physiologists.

This is an Open Access article distributed under the terms of the Creative Commons Attribution Non-Commercial License (<http://creativecommons.org/licenses/by-nc/4.0/>), which permits non-commercial re-use, distribution, and reproduction in any medium, provided the original work is properly cited. For commercial re-use, please contact [journals.permissions@oup.com](mailto:journals.permissions@oup.com)

to substantially reduced root growth (Peng et al. 2013). Thus, DAR2 mutation appears to accelerate the transition from root cell proliferation to differentiation–elongation. However, unlike DA1 or DAR1, DAR2 does not contain UIMs (Peng et al. 2013), and therefore its biochemical function might be distinct. Whether *da1*, *bb* or *dar1* mutants display root phenotypes has not been reported; however, *BB* is expressed in the root (Disch et al. 2006). Here we demonstrate that *BB* has a conceptually similar role in the root and in the shoot. *bb* mutants display increased root meristem size in terms of cell number, in both the longitudinal and radial dimensions. Although the impact of this phenotype on overall, macroscopic root growth is minor, it gains in importance in sensitized backgrounds.

## Results

Arabidopsis mutants in the *BREVIS RADIX* (*BRX*) gene display a short root phenotype (Mouchel et al. 2004), which is the consequence of impaired protophloem development in the root meristem of *brx* mutants (Rodríguez-Villalón et al. 2014). The occurrence of sieve element precursors that do not undergo differentiation presumably leads to interrupted sieve tubes in *brx* mutants and is associated with a number of systemic effects, such as reduced auxin activity throughout the root meristem and increased lateral root branching (Mouchel et al. 2006, Gujas et al. 2012, Rodríguez-Villalón et al. 2015). At the morphological level, the *brx* short root phenotype can be explained by a combination of strongly reduced meristematic activity and lightly reduced cell elongation (Mouchel et al. 2004). In an attempt to isolate second site genetic modifiers of this phenotype, we have conducted a suppressor screen for mutants which fully or partially restore *brx* root growth vigor (Depuydt et al. 2013, Rodríguez-Villalón et al. 2014, Rodríguez-Villalón et al. 2015, Kang and Hardtke 2016). One of the lines isolated displayed an intermediate phenotype of partial yet substantial suppression of impaired *brx* root growth. Genetic mapping by whole-genome sequencing of bulked segregants (Depuydt et al. 2013) pointed to a mutation in the *BB* gene (At3g63530) as probably causative. This C to T change gives rise to an amino acid substitution, P235L, directly C-terminal to the penultimate cysteine of the *BB* RING finger domain (Fig. 1A).

To verify independently whether *BB* mutation could indeed be responsible for the second site suppression, we obtained the *bb-2* allele, which is in the same Columbia-0 (Col-0) background and carries a T-DNA insertion in the *BB* 5' region that leads to a strong down-regulation of *BB* expression (Disch et al. 2006). In the F<sub>2</sub> of crosses to the *brx* mutant, the segregation of short root vs. intermediate root length individuals suggested that *bb-2* can suppress the *brx* phenotype (Supplementary Fig. S1A), which was eventually confirmed in subsequently isolated *bb-2 brx* double mutants (Fig. 1B, C). Therefore, although the residue corresponding to P235 in *BB* is typically not conserved across RING finger domains (Kosarev et al. 2002), it is apparently important for *BB* activity, because the P235L mutation leads to a loss of function. In summary, our data show that *bb*

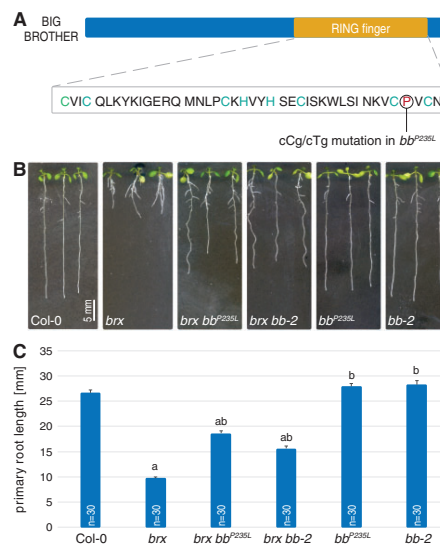


**Fig. 1** Second site mutation in *BB* partially suppresses reduced *brx* root growth. (A) Schematic presentation of the *BB* protein, and the position and sequence of the RING finger domain, highlighting the mutation leading to the P235L amino acid change. (B) Representative seedlings of the indicated genotypes, at 7 d after germination (dag). (C) Average primary root length of the indicated genotypes, at 7 dag. Differences as compared with the Col-0 wild-type background (a) or *brx* mutant background (b) are statistically significant as indicated (Student's *t*-test;  $P < 0.001$ ; mean  $\pm$  SEM).

loss-of-function mutations are second site suppressors of the *brx* root phenotype.

To determine whether *brx* suppression by *bb* reflects a role for *BB* in phloem development, we analyzed *bb brx* double mutants in further detail. A key feature of *brx* mutants is the occurrence of non-differentiated, so-called gap cells in the protophloem transition zone (Rodríguez-Villalón et al. 2014) (Fig. 2A). Perfect *brx* suppressors, such as loss of function in *BARELY ANY MERISTEM 3* (*BAM3*) (Depuydt et al. 2013), do not only fully rescue the short root phenotype, but also fully restore proper sieve element differentiation. In *bb brx* double mutants, this was not the case (Fig. 2B). Consistently, impaired phloem sap delivery to the root meristem (a consequence of the gap cells) was not rescued either, as illustrated by the strongly reduced phloem-mediated translocation of carboxyfluorescein diacetate (CFDA) dye from the cotyledons to the root phloem unloading zone (Fig. 2C–E). Moreover, *bb brx* as well as *bb* mutants were fully sensitive to the *BAM3* ligand *CLAVATA3/EMBRYO SURROUNDING REGION 45* (*CLE45*) (Fig. 2F). Thus, *BB* apparently does not affect *CLE45* perception, which negatively regulates protophloem formation through *BAM3* (Depuydt et al. 2013). Also, auxin activity, as judged from the abundance of the *DII-VENUS* reporter (Santuari et al. 2011), was

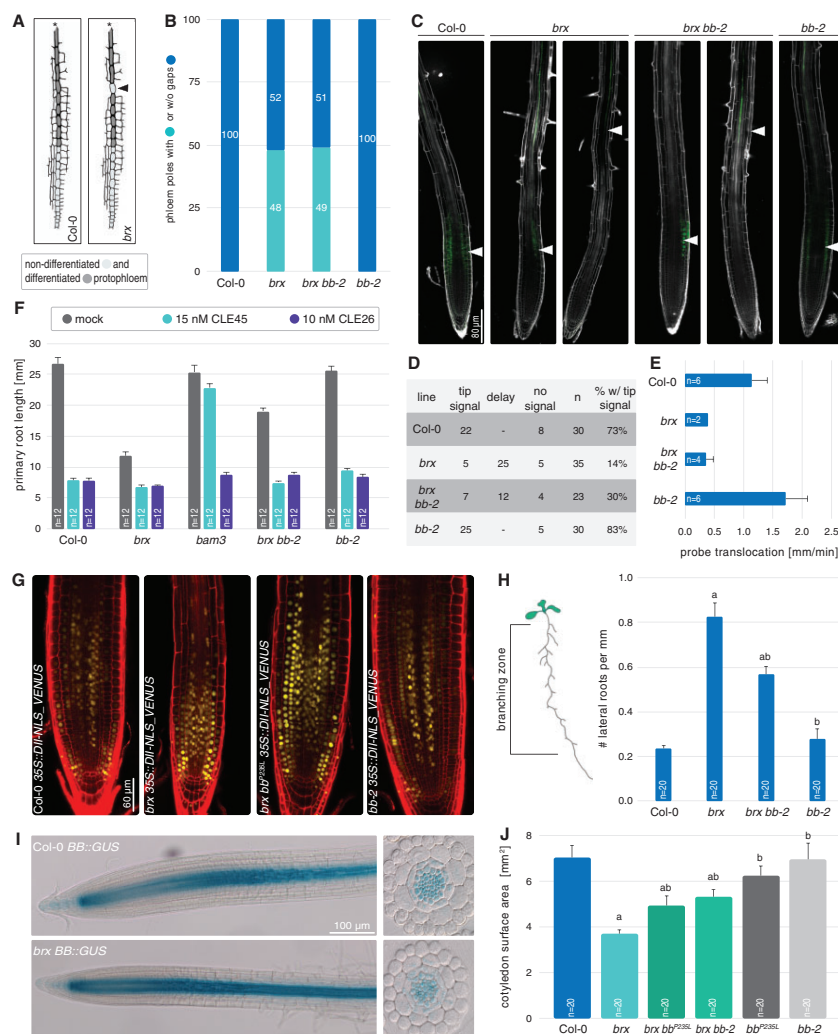


**Fig. 2** Evaluation of local and systemic phenotypes in *bb brx* double mutant roots. (A) Schematic overview of developing protophloem sieve element strands, highlighting the occurrence of undifferentiated ‘gap’ cells (arrowhead) in *brx* mutants. (B) Quantification of gap cell frequency in the indicated genotypes at 7 d after germination (dag). Differences between Col-0 and *bb-2* vs. *brx* and *bb-2 brx* were statistically significant ( $P < 0.001$ , Fisher’s exact test), but not within those pairs. (C) Phloem-mediated translocation of CFDA dye (green fluorescence, arrowheads) into the phloem unloading zone of the root tip, 45 min after CFDA application to the cotyledons of 4-day-old seedlings. Representative seedlings for the indicated phenotypes [white fluorescence: propidium iodide (PI) cell wall staining] are shown. (D) Corresponding classification of the CFDA signal at the end of the experiment. (E) CFDA translocation velocity *in vivo* measurements, based exclusively on seedlings in which it reached the root tip. (F) Primary root growth response of the indicated genotypes to the presence of CLE peptides in the medium at 7 dag. All treatments were statistically significant as compared with mock treatment ( $P < 0.001$ , Student’s *t*-test), except for *bam3* on CLE45. (G) Auxin activity in the indicated genotypes at 7 dag as monitored by the DII-VENUS inverse reporter (yellow fluorescence), composite images (red fluorescence: PI staining). (H) Lateral root density in the indicated genotypes at 12 dag. (I) GUS reporter staining of BB expression in the indicated genotypes at 7 dag. (J) Cotyledon surface area in the indicated genotypes at 9 dag. Differences as compared with the Col-0 wild-type background (a) or *brx* mutant background (b) are statistically significant as indicated (Student’s *t*-test;  $P < 0.01$ ; mean  $\pm$  SEM).



not markedly increased in *bb brx* mutants as compared with *brx* single mutants (Fig. 2G). However, we noticed a slight reduction in lateral root density (Fig. 2H), which could also reflect the observation that mature cell length was partially rescued (see below). Finally, we confirmed that *BB* is expressed in the root, in the vascular cylinder (Disch et al. 2006). We also verified that *bb* loss of function does not suppress *brx* because of an effect of *BRX* loss of function on *BB* expression, i.e. *BB* is not overexpressed in a *brx* background (Fig. 2I).

In summary, although *bb* mutation substantially rescued the reduced root growth of *brx*, this does not appear to be due to a specific *BB* function in protophloem development, but rather to a generic effect on root growth. In support of this, we also observed rescue of the reduced cotyledon size of *brx* (Beuchat et al. 2010) (Fig. 2J), and restoration of *brx* root meristem size to nearly wild-type levels, as indicated by the number of meristematic cortex cells (Fig. 3A, B). To verify whether *bb* mutation already has an effect on root growth by itself, we investigated the *bb-2* mutant as well as the *bb<sup>P235I</sup>* mutant (recovered from crosses of the suppressor line to Col-0) in more detail. Neither of the two alleles displayed any significant difference from the wild type in terms of root growth vigor (Fig. 1C). This was also true when *bb* root growth was monitored on other, suboptimal growth media (e.g. without sucrose) (Supplementary Fig. S1B). However, surprisingly, in both mutants the meristems were clearly larger than in the wild type (Fig. 3A, B). Nevertheless, an impact on root growth could also not be detected over an extended time period (Fig. 3C). The larger *bb* meristem was also obvious in the cumulative cortex cell lengths along the meristem (Fig. 3D), which allowed us to calculate the switching point between cell proliferation and the transition to differentiation–elongation (Supplementary Fig. S1C). This switch point was consistently later in *bb* than in the wild type (Fig. 3E). However, the apparently prolonged cell proliferation phase had no marked effect on cell size, because the length of both proliferating and mature cortex cells was similar in *bb* and Col-0 (Fig. 3F, G). Thus, *bb* mutation apparently permits a longer phase of cell proliferation before cell expansion in the root meristem, similar to its role in the shoot. While these observations suggest that despite their larger meristem, *bb* roots do not grow overall faster than those of the wild type, the effects of *BB* loss of function apparently manifest in sensitized backgrounds such as *brx*. Consistent with the partially rescued *brx* root growth, *bb* second site mutation not only normalized root meristem size, but also recovered the switch point, as well as, in part, mature cell length (Fig. 3B–G).

Potential discrepancies between meristem size, mature cell length and overall root growth vigor can sometimes be explained by altered frequency of formative divisions, which give rise to root cell files. For example, the short root phenotype of brassinosteroid receptor mutants can be explained quantitatively by a combination of reduced mature cell size and a slowing down of root growth by supernumerary formative cell divisions (Kang et al. 2017). Indeed, cross-sections of *bb* mutants revealed a marked increase in cell file number in the *BB* expression domain, i.e. the endodermis, the pericycle and the vascular cylinder (Fig. 4A, B). Thus, cell number was not

only increased in the longitudinal, but also in the radial dimension of *bb* root meristems. Notably, the supernumerary formative divisions did not impinge on vascular tissue organization. Moreover, they did not substantially increase the vascular cylinder area (Fig. 4C), but rather resulted in smaller cells (in the radial dimension) and therefore presumably more anisotropic cells (Fig. 4D). This effect was also observed in the respective *bb brx* double mutants, again indicating that *BB* acts independently of *BRX* in root development.

To verify this notion in an independent scenario, we also crossed the *bb-2* mutant to a loss-of-function allele of *OCTOPUS* (*OPS*), another positive regulator of protophloem development (Truernit et al. 2012, Rodriguez-Villalon et al. 2014). The *brx* and *ops* mutant root phenotypes are essentially identical, including the systemic effects (Truernit et al. 2012, Rodriguez-Villalon et al. 2014, Rodriguez-Villalon et al. 2015, Kang et al. 2017). Similar to *bb brx* double mutants, the reduced root growth of *ops* mutants was partially compensated by *bb* second site mutation (Fig. 5A, B). However, again the more specific defects of *ops* were not complemented (Fig. 5C–E), while cell number was increased in both the longitudinal and radial dimensions (Fig. 5F, G). Therefore, *BB* also appears to act independently of *OPS* in root development, corroborating its generic role as a growth repressor.

## Discussion

Within the limits of constraints dictated by environmental factors, plant organ size is genetically determined (Breuninger and Lenhard 2010, Gonzalez and Inze 2015). This is most conspicuous in organs whose size is comparatively invariable, such as petals. The *BB* gene was indeed originally identified because of the effect of its loss of function on petal size, but it soon became clear that it also affected the size of other leaf(-like) organs (Disch et al. 2006, Li et al. 2008). Kinetic analyses of leaf development suggest that this phenotype is due to a role for *BB* in limiting the cell proliferation phase, and promoting the transition to differentiation and cell expansion (Disch et al. 2006, Li et al. 2008, Vanhaeren et al. 2017). This appears to be a general theme in organ size determination, since a similar role has been described for other pertinent factors (Krizek, 1999, Mizukami and Fischer 2000, Hu et al. 2003), which presumably act in parallel to the *BB*–*DA1*–*DA2* network (Disch et al. 2006, Dong et al. 2017). Here we found that *BB* has a conceptually similar role in the determination of primary root meristem size. *bb* loss-of-function alleles display increased meristematic cell number, but no alteration in mature cell length. This phenotype is remarkable, given reports that a shift in the relative size of the root meristem's proliferation or differentiation–elongation zones is typically associated with altered mature cell length (Moubayidin et al. 2010, Scacchi et al. 2010, Depuydt and Hardtke 2011, Perilli et al. 2012, Peng et al. 2013, Mahonen et al. 2014). The phenotype of *bb* mutants is therefore more similar to that obtained by ectopic overexpression of *PLETHORA* (*PLT*) transcription factors, which promote the expression of cell proliferation genes, but suppress the expression

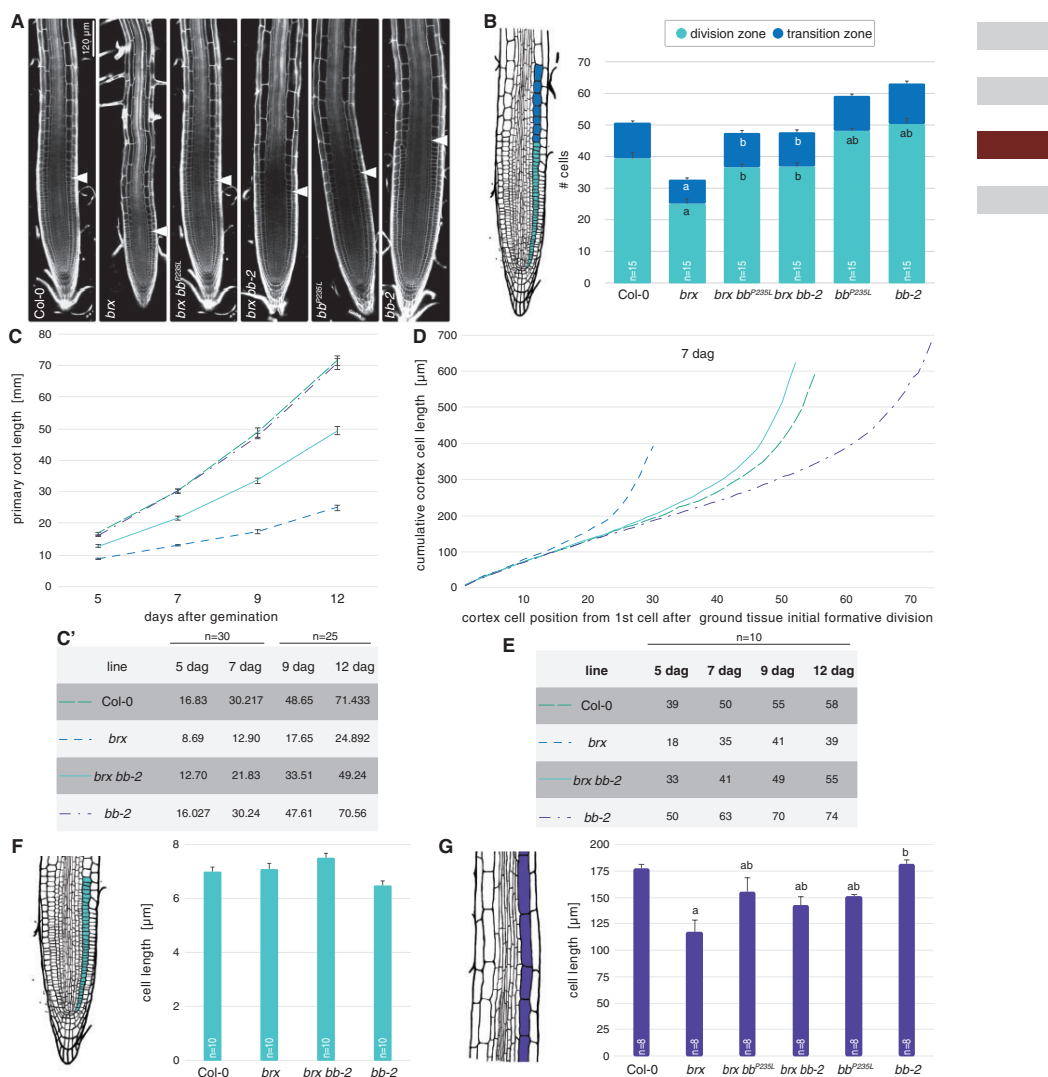


**Fig. 3** Cell proliferation in *bb* root meristems. (A) Representative root meristems of the indicated genotypes at 7 d after germination (dag), confocal microscopy [white fluorescence: propidium iodide (PI) staining]. Arrowheads indicate the approximate location of the proliferation to differentiation–elongation switch. (B) Quantification of cortex cell number in the division zone and transition zone of 7-day-old seedlings of the indicated genotypes. (C) Root growth progression in the indicated phenotypes over time. Differences between *brx* and *brx bb-2*, and between those two genotypes and Col-0 and *bb-2* were statistically significant ( $P < 0.001$ ; Student's *t*-test) at every time point (C': data for individual time points). (D) Progression of cortex cell elongation along the meristems of 7-day-old roots of the indicated genotypes. (E) Calculations for the switch between proliferation and transition in cortex cell files of the indicated genotypes, with respect to the first cell after the formative ground tissue division. (F) Length of proliferating cortex cells in the indicated genotypes at 7 dag. Average of the average for 10 roots, with 20–45 cells scored per root. (G) Length of mature cortex cells in the indicated genotypes at 7 dag. Average of the average for eight roots, with approximately 10 cells scored per root. Differences as compared with the Col-0 wild-type background (a) or *brx* mutant background (b) are statistically significant as indicated (Student's *t*-test;  $P < 0.05$ ; mean  $\pm$  SEM).

1523

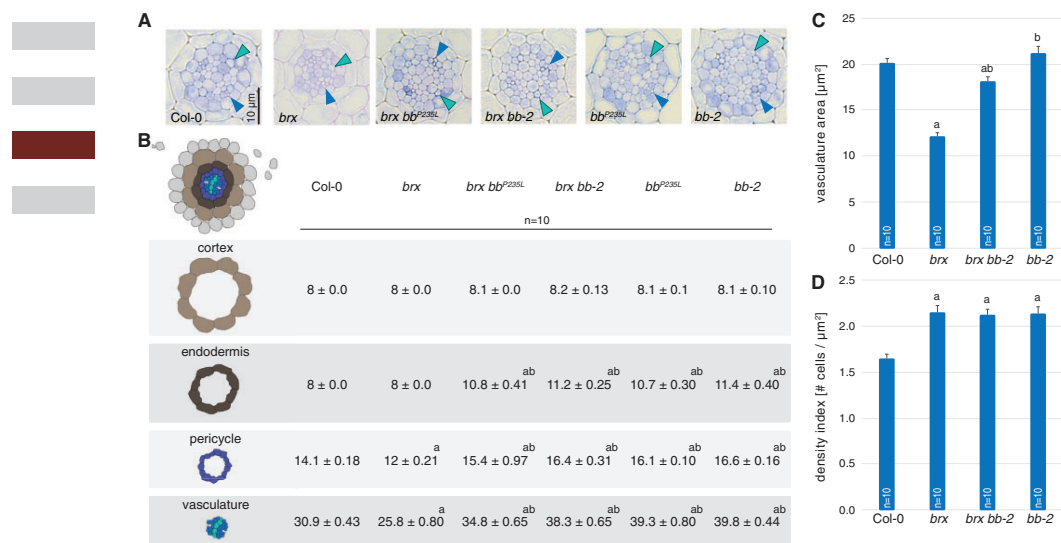


**Fig. 4** Formative divisions in *bb* root meristems. (A) Representative histological cross-sections of 6-day-old roots of the indicated genotypes, taken at the position where protoxylem (green arrowheads) has differentiated (blue arrowheads: protophloem). (B) Quantification of cell file number in roots of the indicated genotypes at 6 d after germination (dag). (C) Quantification of vascular cylinder area in roots of the indicated genotypes at 6 dag. (D) Quantification of cell file density in the vascular cylinder in roots of the indicated genotypes at 6 dag. Differences as compared with the Col-0 wild-type background (a) or *brx* mutant background (b) are statistically significant as indicated (Student's *t*-test;  $P < 0.01$ ; mean  $\pm$  SEM).

of genes involved in differentiation (Mahonen et al. 2014, Santuari et al. 2016). However, whether *PLT* gain of function also affects mature cell size has not been reported in detail. In summary, our results suggest that *bb* mutation prolongs the cell proliferation phase in the root meristem, but does not affect mature cell length, thereby uncoupling root meristematic activity from cell elongation. Because this effect is observed in the cortex cell layer, where *BB* does not appear to be expressed, it also suggests co-ordination of growth between layers through non-cell-autonomous signals, as previously observed (Kang et al. 2017).

Surprisingly, the increased cell proliferation in *bb* meristems did not translate into enhanced overall root growth in our standard conditions, with a limit of observation at 12 d after germination. Therefore, within the limits of our experimental set-up, *BB* mutation had no macroscopic effect on root growth. On the one hand, this might in part be explained by the increased number of formative cell divisions in the stele, which could lead to a temporal slowing down of root growth as observed in other, similar scenarios (De Rybel et al. 2013, Kang et al. 2017). On the other hand, unchanged overall root growth and mature cell size suggest an unchanged overall output of differentiated cells by the *bb* meristem. This in turn implies that the division rate of each individual cell might be reduced (Beemster and Baskin 1998, Beemster et al. 2002). However, a stimulatory effect of *bb*

second site mutation was observed in the *brx* and *ops* backgrounds, in which root growth is strongly reduced because of impaired protophloem differentiation (Truernit et al. 2012, Rodriguez-Villalon et al. 2014, Rodriguez-Villalon et al. 2015). Notably, the partial rescue of *brx* or *ops* by *bb* was not associated with a marked restoration of reported systemic defects, such as reduced auxin activity or phloem sap delivery. This is consistent with the persistence of the protophloem differentiation defects in *bb brx* or *bb ops* double mutants. The only exception was the reduced density of lateral roots, which scaled with the rescue of primary root growth however, and could also be simply explained by the partially rescued mature cell length. Thus, *bb* mutation can influence cell elongation; however, it appears that this only becomes evident in genetic backgrounds in which the cell proliferation phase is severely shortened and cell differentiation is accelerated (Mouchel et al. 2004, Truernit et al. 2012). Moreover, the slightly reduced number of formative divisions in the *brx* and *ops* vascular cylinders (Rodriguez-Villalon et al. 2015) was overcompensated by *bb* second site mutation, corroborating that *BB* appears to act locally and largely independently of systemic inputs. In line with this notion, *BB* was for instance not found among the *PLT* target genes (Santuari et al. 2016).

In summary, we demonstrate that *bb* loss-of-function mutations prolong the cell proliferation phase in the root

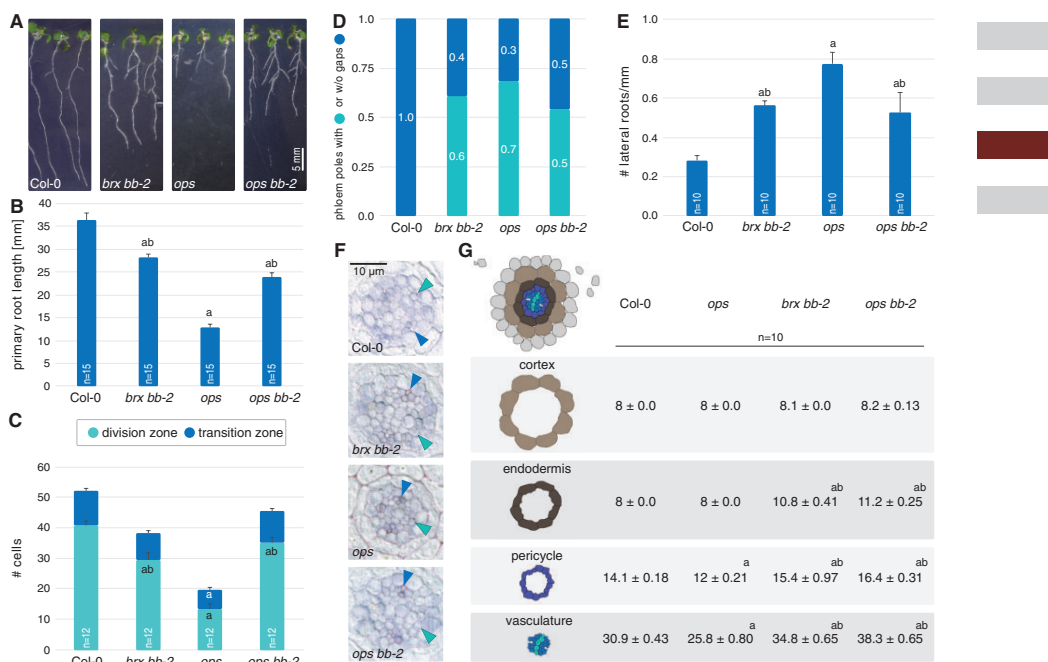


**Fig. 5** Second site mutation in *BB* partially suppresses *ops* phenotypes. (A) Representative seedlings of the indicated genotypes at 7 d after germination (dag). (B) Average primary root length of the indicated genotypes at 7 dag. (C) Quantification of cortex cell number in the division zone and transition zone of 7-day-old seedlings of the indicated genotypes. (D) Quantification of gap cell frequency in the indicated genotypes at 5 dag. Differences between Col-0 and all other genotypes were statistically significant ( $P < 0.001$ , Fisher's exact test), but not between *brx-2*, *ops* and *bb-2 ops*. (E) Lateral root density in the indicated genotypes at 12 dag. (F) Representative histological cross-sections of 6-day-old roots of the indicated genotypes, taken at the position where protoxylem (green arrowheads) has differentiated (blue arrowheads: protophloem). (G) Quantification of cell file number in roots of the indicated genotypes at 6 dag. Differences as compared with the Col-0 wild-type background (a) or *ops* mutant background (b) are statistically significant as indicated (Student's *t*-test;  $P < 0.05$ ; mean  $\pm$  SEM).

meristem and uncouple root meristematic activity from cell differentiation and elongation. It will be interesting to investigate whether mutations in *BB* homologs have a similar effect in other species, or whether such mutations could be exploited to boost root growth generically, for instance in crops.

## Materials and Methods

### Plant materials, growth conditions and physiological assays

Plant tissue culture, plant transformation and common molecular biology procedures such as genomic DNA isolation, plant transformation, genotyping, (whole-genome) sequencing and peptide treatments were performed according to standard procedures as previously described (Kang and Hardtke 2016, Kang et al. 2017). For plant tissue culture, seeds were surface-sterilized, germinated and grown vertically on half-strength Murashige and Skoog (MS) agar medium with or without 0.3% sucrose under continuous light of approximately

120  $\mu$ E intensity at 22°C. All mutants were in the Arabidopsis Col-0 wild-type background, i.e. the described *brx-2*, *ops-2* and *bb-2* alleles (Disch et al. 2006, Rodrigues et al. 2009, Truernit et al. 2012), as well as the newly isolated *bb<sup>92351</sup>* allele. To produce *BB::GUS* plants, the *BB* promoter (At3g63530) was amplified using oligonucleotides 5'-GGG GAC AAG TTT GTA CAA AAA AGC AGG CTT CGA AGA AGA AGA CGG AGA AGG-3' and 5'-GGG GAC CAC TTT GTA CAA GAA AGC TGG GTT TTC AGC TAC TGC AAT CGA GA-3' (note: including the attB1 and attB2 sites, respectively, for GATEWAY cloning), and cloned into the pMDC163 vector. Arabidopsis Col-0 and *brx-2* plants were transformed with the construct and lines with single insertions were selected in the  $T_2$  generation. Homozygous plants for analysis were obtained in the  $T_3$  generation. All quantitative data shown are from single, representative replicate experiments, with genotypes assayed in parallel.

### Probe unloading measurements

To measure phloem translocation rate, CFDA stock solution (10 mg ml<sup>-1</sup> in dimethylsulfoxide) was diluted 1:100 (v/v) in ddH<sub>2</sub>O and 1  $\mu$ l was applied to wounded cotyledons at 4 d post-germination. Transport along sieve tubes was monitored after 45 min. using an epifluorescence microscope with a green fluorescent protein (GFP) filter. Seedlings were then mounted in propidium

iodide and imaged by confocal laser scanning microscopy (Zeiss LSM700) using a GFP filter.

### Probe translocation speed assay

Arabidopsis plants were grown for 4 d, the plates were scanned, root lengths were measured using ImageJ software, and seedlings were subsequently used for CFDA loading. Plants were mounted in a plastic chamber, below a slice of solid 0.7% medium enriched with propidium iodide. CFDA was applied as described above, and the protophloem unloading zone was subsequently imaged by confocal laser scanning microscopy (Zeiss 880). Probe translocation speed was calculated by dividing the root length by the time it took CFDA to reach the root meristem unloading zone.

### Division–elongation switch point calculation

Arabidopsis seedlings were grown for 5, 7, 9 and 12 d after germination. Samples were mounted in propidium iodide, and root meristems were imaged by confocal laser scanning microscopy. Cumulative cortex cell length (starting from the first cell after the ground tissue initial formative division) was measured using ImageJ software. Ten roots were used for each line to calculate the average. The linear function representing the division zone was calculated by considering the second to 20th cells (except for *brx* at 5 d after germination, where the second and 10th cells were used because the meristem was still too small). The linear function representing the elongation phase was calculated considering the third from last and last cells. The two functions were then used to calculate the intersection point, i.e. the cortex cell where the switch between division and elongation phase occurs. Details are displayed in Supplementary Fig. S1C.

### Supplementary data

Supplementary data are available at PCP online.

### Funding

This work was supported by the Swiss National Science Foundation [grant 31003A\_166394 awarded to C.S.H.].

### Acknowledgments

We would like to thank Dr. Y.-H. Kang for initiation of the project, Dr. M. Lenhard for *bb-2* mutant seeds, and the Genomic Technologies Facility of the University of Lausanne for support in whole-genome sequencing.

### Disclosures

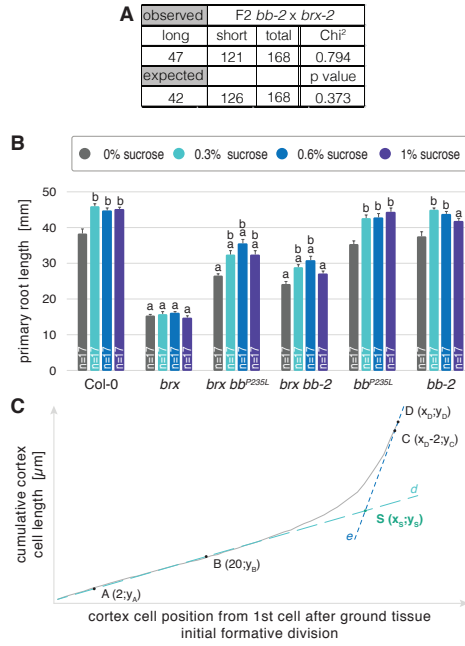
The authors have no conflicts of interest to declare.

### References

- Beemster, G.T. and Baskin, T.I. (1998) Analysis of cell division and elongation underlying the developmental acceleration of root growth in *Arabidopsis thaliana*. *Plant Physiol.* 116: 1515–1526.
- Beemster, G.T., De Vusser, K., De Tavernier, E., De Bock, K. and Inze, D. (2002) Variation in growth rate between *Arabidopsis* ecotypes is correlated with cell division and A-type cyclin-dependent kinase activity. *Plant Physiol.* 129: 854–864.
- Beuchat, J., Scacchi, E., Tarkowska, D., Ragni, L., Strnad, M. and Hardtke, C.S. (2010) BRX promotes *Arabidopsis* shoot growth. *New Phytol.* 188: 23–29.
- Breuninger, H. and Lenhard, M. (2010) Control of tissue and organ growth in plants. *Curr. Top. Dev. Biol.* 91: 185–220.
- De Rybel, B., Moller, B., Yoshida, S., Grabowicz, I., Barbier de Reuille, P., Boeren, S., et al. (2013) A bHLH complex controls embryonic vascular tissue establishment and indeterminate growth in *Arabidopsis*. *Dev. Cell* 24: 426–437.
- Depuydt, S. and Hardtke, C.S. (2011) Hormone signalling crosstalk in plant growth regulation. *Curr. Biol.* 21: R365–R373.
- Depuydt, S., Rodriguez-Villalon, A., Santuari, L., Wyser-Rmili, C., Ragni, L. and Hardtke, C.S. (2013) Suppression of *Arabidopsis* protophloem differentiation and root meristem growth by CLE45 requires the receptor-like kinase BAM3. *Proc. Natl. Acad. Sci. USA* 110: 7074–7079.
- Disch, S., Anastasiou, E., Sharma, V.K., Laux, T., Fletcher, J.C. and Lenhard, M. (2006) The E3 ubiquitin ligase *BIG BROTHER* controls *Arabidopsis* organ size in a dosage-dependent manner. *Curr. Biol.* 16: 272–279.
- Dong, H., Dumenil, J., Lu, F.H., Na, L., Vanhaeren, H., Naumann, C., et al. (2017) Ubiquitylation activates a peptidase that promotes cleavage and destabilization of its activating E3 ligases and diverse growth regulatory proteins to limit cell proliferation in *Arabidopsis*. *Genes Dev.* 31: 197–208.
- Du, L., Li, N., Chen, L., Xu, Y., Li, Y., Zhang, Y., et al. (2014) The ubiquitin receptor DA1 regulates seed and organ size by modulating the stability of the ubiquitin-specific protease UBP15/SOD2 in *Arabidopsis*. *Plant Cell* 26: 665–677.
- Gonzalez, N. and Inze, D. (2015) Molecular systems governing leaf growth: from genes to networks. *J. Exp. Bot.* 66: 1045–1054.
- Gujas, B., Alonso-Blanco, C. and Hardtke, C.S. (2012) Natural *Arabidopsis* *brx* loss-of-function alleles confer root adaptation to acidic soil. *Curr. Biol.* 22: 1962–1968.
- Hu, Y., Xie, Q. and Chua, N.H. (2003) The *Arabidopsis* auxin-inducible gene ARGOS controls lateral organ size. *Plant Cell* 15: 1951–1961.
- Kang, Y.H., Breda, A. and Hardtke, C.S. (2017) Brassinosteroid signaling directs formative cell divisions and protophloem differentiation in *Arabidopsis* root meristems. *Development* 144: 272–280.
- Kang, Y.H. and Hardtke, C.S. (2016) *Arabidopsis* MAKRS is a positive effector of BAM3-dependent CLE45 signaling. *EMBO Rep.* 17: 1145–1154.
- Kosarev, P., Mayer, K.F. and Hardtke, C.S. (2002) Evaluation and classification of RING-finger domains encoded by the *Arabidopsis* genome. *Genome Biol.* 3: RESEARCH0016.
- Krizek, B.A. (1999) Ectopic expression of *AINTEGUMENTA* in *Arabidopsis* plants results in increased growth of floral organs. *Dev. Genet.* 25: 224–236.
- Li, Y., Zheng, L., Corke, F., Smith, C. and Bevan, M.W. (2008) Control of final seed and organ size by the DA1 gene family in *Arabidopsis thaliana*. *Genes Dev.* 22: 1331–1336.
- Mahonen, A.P., ten Tusscher, K., Siligato, R., Smetana, O., Diaz-Trivino, S., Salojarvi, J., et al. (2014) PLETHORA gradient formation mechanism separates auxin responses. *Nature* 515: 125–129.
- Mizukami, Y. and Fischer, R.L. (2000) Plant organ size control: *AINTEGUMENTA* regulates growth and cell numbers during organogenesis. *Proc. Natl. Acad. Sci. USA* 97: 942–947.
- Moubayidin, L., Perilli, S., Dello Iorio, R., Di Mambro, R., Costantino, P. and Sabatini, S. (2010) The rate of cell differentiation controls the *Arabidopsis* root meristem growth phase. *Curr. Biol.* 20: 1138–1143.
- Mouchel, C.F., Briggs, G.C. and Hardtke, C.S. (2004) Natural genetic variation in *Arabidopsis* identifies BREVIS RADIX, a novel regulator of cell proliferation and elongation in the root. *Genes Dev.* 18: 700–714.
- Mouchel, C.F., Osmont, K.S. and Hardtke, C.S. (2006) BRX mediates feedback between brassinosteroid levels and auxin signalling in root growth. *Nature* 443: 458–461.
- Peng, Y., Ma, W., Chen, L., Yang, L., Li, S., Zhao, H., et al. (2013) Control of root meristem size by DA1-RELATED PROTEIN2 in *Arabidopsis*. *Plant Physiol.* 161: 1542–1556.
- Perilli, S., Di Mambro, R. and Sabatini, S. (2012) Growth and development of the root apical meristem. *Curr. Opin. Plant Biol.* 15: 17–23.
- Rodrigues, A., Santiago, J., Rubio, S., Saez, A., Osmont, K.S., Gadea, J., et al. (2009) The short-rooted phenotype of the *brevis radix* mutant partly reflects root abscisic acid hypersensitivity. *Plant Physiol.* 149: 1917–1928.

- Rodríguez-Villalon, A., Gujas, B., Kang, Y.H., Breda, A.S., Cattaneo, P., Depuydt, S., et al. (2014) Molecular genetic framework for protophloem formation. *Proc. Natl. Acad. Sci. USA* 111: 11551–11556.
- Rodríguez-Villalon, A., Gujas, B., van Wijk, R., Munnik, T. and Hardtke, C.S. (2015) Primary root protophloem differentiation requires balanced phosphatidylinositol-4,5-bisphosphate levels and systemically affects root branching. *Development* 142: 1437–1446.
- Santuari, L., Sanchez-Perez, G.F., Luijten, M., Rutjens, B., Terpstra, I., Berke, L., et al. (2016) The PLETHORA gene regulatory network guides growth and cell differentiation in Arabidopsis roots. *Plant Cell* 28: 2937–2951.
- Santuari, L., Scacchi, E., Rodríguez-Villalon, A., Salinas, P., Dohmann, E.M., Brunoud, G., et al. (2011) Positional information by differential endocytosis splits auxin response to drive Arabidopsis root meristem growth. *Curr. Biol.* 21: 1918–1923.
- Scacchi, E., Salinas, P., Gujas, B., Santuari, L., Krogan, N., Ragni, L., et al. (2010) Spatio-temporal sequence of cross-regulatory events in root meristem growth. *Proc. Natl. Acad. Sci. USA* 107: 22734–22739.
- Truernit, E., Bauby, H., Belcram, K., Barthelemy, J. and Palauqui, J.C. (2012) OCTOPUS, a polarly localised membrane-associated protein, regulates phloem differentiation entry in Arabidopsis thaliana. *Development* 139: 1306–1315.
- Vanhaeren, H., Nam, Y.J., De Milde, L., Chae, E., Storme, V., Weigel, D., et al. (2017) Forever young: the role of ubiquitin receptor DA1 and E3 ligase BIG BROTHER in controlling leaf growth and development. *Plant Physiol.* 173: 1269–1282.
- Xia, T., Li, N., Dumenil, J., Li, J., Kamenski, A., Bevan, M.W., et al. (2013) The ubiquitin receptor DA1 interacts with the E3 ubiquitin ligase DA2 to regulate seed and organ size in Arabidopsis. *Plant Cell* 25: 3347–3359.

Figure S1



Linear functions describing *differentiation* (*d*) and *elongation* (*e*) are:

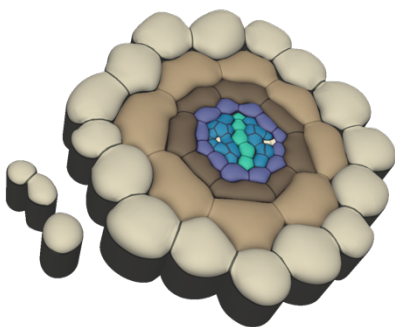
$$e: y = \frac{(y_B - y_A)}{(20 - 2)} x + \frac{20y_A - 2y_B}{(20 - 2)}$$

$$d: y = \frac{(y_D - y_C)}{(x_D - (x_D - 2))} x + \frac{x_D y_C - (x_D - 2)y_D}{(x_D - (x_D - 2))}$$

The switching point  $S(x_s, y_s)$  is given by solving the system:

$$\begin{cases} y = \frac{(y_B - y_A)}{(20 - 2)} x + \frac{20y_A - 2y_B}{(20 - 2)} \\ y = \frac{(y_D - y_C)}{(x_D - (x_D - 2))} x + \frac{x_D y_C - (x_D - 2)y_D}{(x_D - (x_D - 2))} \end{cases} \quad \begin{cases} x = x_s \\ y = y_s \end{cases}$$

## Chapter 5



# Functional FYRC domain of the *Arabidopsis* JUMONJI14 protein is crucial for root growth restoration in impaired genetic backgrounds

Cattaneo P and Hardtke CS

Unpublished data

## Highlights

- Null-mutation in *JUMONJI 14* partially restores the primary root length of mutants with diminished growth, but not protophloem discontinuity.
- *JMJ14* expression pattern is restricted to the vascular cylinder in the *Arabidopsis* primary root.
- JMJ14 inhibits the expression of target genes by reducing their histone methylation state and thus might indirectly influence root growth.
- The conserved FYRC domain is crucial for JMJ14 to execute its activity.

## My contribution

I designed and performed all experiments included in this chapter.

## ABSTRACT

Eukaryotic genomic DNA is wrapped around histone octamer protein complexes and packed as chromatin in the nucleus. The chromatin condensation states influence the DNA accessibility, thereby contributing to the epigenetic control of gene expression. Among the different covalent modifications, histone methylation was found to govern several developmental programs during the plant life cycle. The reversible state of methylation/demethylation of histone lysine residues is regulated by different methylases and demethylases, respectively. Our study shows that perturbation of the conserved JmjC and FYR domains in the demethylase *JUMONJI 14* (*JMJ14*) can suppress the short root phenotype caused by mutation in the *BREVIS RADIX* (*BRX*) gene. *JMJ14* exhibits a vascular-related expression pattern, however its function in root development has been uncharacterized. Interestingly, the root morphology of *jmj14* displays apparently no differences compared to wild type. We thus investigated the consequences on gene expression induced by the altered H3K4 methylation state in *jmj14*. We identified a set of genes whose expression is perturbed and thus might influence root growth in sensitized genetic backgrounds exclusively. *JMJ14* belongs to a small subgroup of the Jmj protein family, whose members exhibit two FYR domains at the C-terminus. Only *jmj14* was found to suppress impaired root growth. Further analysis would compare the expression domain of the different *JMJ* homologs and elucidate whether they overlap in the root. Moreover, we will test the potential interchangeability between the FYR domains and their biological relevance during root development.

## INTRODUCTION

The nuclear DNA of eukaryotes is packaged as chromatin. The constitutive unit of the chromatin is the nucleosome, 146 base pairs of DNA wrapped around the core histone octamer (Kouzarides, 2007). The flexible N-terminal tails of histone 3 (H3) and 4 (H4) proteins protrude from the nucleosome, allowing covalent modifications that include acetylation, methylation, phosphorylation and ubiquitination. All of these modifications are reversible and they can differentially influence chromatin condensation, which affects gene expression (Kouzarides, 2007). In plants, histone methylation governs different processes, such as cell fate determination and developmental programs during the entire plant life cycle (Ko et al., 2010).

Histone methylation state is the balance between methylation and demethylation, which is controlled by histone methylases and demethylases, respectively. Proteins containing a SET domain catalyse the mono-, di- and tri- methylation of lysines (K) at the N-terminus of histones. Both the distinct methylation states and the position of the amino acids determine a unique biological state (Mosammamarast et al., 2010). For example, demethylation of H3K9 and tri-methylation of H3K27 inhibit gene expression, whereas di- and tri-methylation of H3K4 and H3K26 are associated with gene transcriptional activation (Saze et al., 2008). Until the discovery of the *LYSINE-SPECIFIC DEMETHYLASES 1 (KDM1)* gene family in mammals, histone methylation has been considered an irreversible modification. KDM1s are however unable to remove the methyl groups from tri-methylated lysine, suggesting the presence of other histone demethylases (Shi et al., 2004). JmjC domain-containing proteins, which possess a conserved 2-oxoglutarate-Fe(II)-binding site, have been proposed as potential histone demethylases, reducing any of the three histone lysine methylation states (Saze et al., 2008). In *Arabidopsis* the 21 JmjC domain-containing proteins are divided into distinct groups based on sequence similarities (Lu et al., 2008). The relevance of JmjC proteins during different developmental phases has been shown by the characterization of several loss-of-function mutants in *Arabidopsis*. *early flowering 6 (elf6)* and *relative of early flowering 6 (ref6)* mutants exhibit a compromised timing of flowering transition, while *maternal effect embryo arrest 27 (mee27/JMJ15)* is

involved in female gametophyte development (Gan et al., 2014; Lu et al., 2011; Pagnussat et al., 2015). *JUMONJI 14* (*JMJ14*) influences expression of floral integrators, leading to an early flowering phenotype in *jmj14* loss-of-function mutants (Lu et al., 2010).

In *Arabidopsis*, the JARID1/KDM5 group has six members, *JMJ14*, *JMJ15*, *JMJ16*, *JMJ17*, *JMJ18* and *JMJ19*. Interestingly, they exhibit two phenylalanine/tyrosine-rich domains, FYRN and FYRC, which are normally found in THRITORAX methyltransferases (Lu et al., 2008). These two domains likely mediate the interaction with other factors harbouring JmjC proteins to target chromatin regions (Ning et al., 2015). Ning et al. in 2015 showed that *JMJ14* interacts with NO APICAL MERISTEM - ARABIDOPSIS TRANSCRIPTION ACTIVATION FACTOR - CUP-SHAPED COTYLEDON 50 (*NAC50*) and *NAC52* transcription factors through its FYRC domain, however the molecular mechanism is only characterized partially.

*JMJ14* inhibits gene expression by reducing the H3K4 methylation states that are associated with gene activation (Ning et al., 2015). *jmj14* loss-of-function mutants show a hyper-methylated state of floral integrators, leading to an early flowering transition. However, whether *JMJ14* acts only in the above-ground plant tissues as a floral repressor remains unclear. In our study, we found a new *jmj14* allele that encodes a protein with a truncated FYRC domain. The resulting loss-of-function mutant can partially restore the root growth in genetic backgrounds with reduced meristematic cell proliferation. *JMJ14* expression overlaps with vasculature tissues, but analysis of *jmj14* mutants revealed no morphological differences in root development compared to wild type situation. The root gene expression analysis however pointed towards a remarkable diversity between wild type and *jmj14*. Therefore, *JMJ14* affecting the methylation states of specific target genes might influence developmental programs such as root growth.

## RESULTS AND DISCUSSION

### **Perturbation of the FYRC protein domain in *JMJ14* suppresses the *brx* short root phenotype**

The protophloem conducts and delivers photoassimilates and signalling molecules into the developing root meristem. Among the genetic factors that govern protophloem differentiation, the *Arabidopsis BREVIS RADIX (BRX)* gene is a key player (Depuydt et al., 2013; Rodriguez-Villalon et al., 2014, 2015). Morphological characterization of *brx* loss-of-function mutants revealed undifferentiated cells that interrupt the developing protophloem cell file (Scacchi et al., 2010). The consequently impaired delivery capacity of the protophloem in the growing primary root meristem has dramatic systemic consequences, such as reduced auxin concentration in the young meristem and a more branched lateral root system. *brx* in addition shows a reduction in meristematic cell division and cell elongation, which cause the macroscopic short root phenotype (Gujas et al., 2012).

To dissect the *BRX* network a forward genetic screen has been conducted to isolate second-site mutations that fully or partially suppress the reduced root growth (Cattaneo et al., 2017; Depuydt et al., 2013; Kang et al., 2016; Rodriguez-Villalon et al., 2015). Whole genome sequencing analysis of one *brx* suppressor pointed to a mutation in the *JUMONJI 14 (JMJ14, At4g201400)* gene (Figure 1A). Because the causative second-site mutation was found in the non-coding region, we investigated the impact on *JMJ14* transcripts (Figure 1B). We extracted RNA from wild type and *jmj14* mutant seedlings, amplified a cDNA region of approximately 1 kb that includes the causative residue and sequenced it. The amplification reaction resulted in two different fragments. In the wild type, the two fragments likely correspond to the pre-processed and the mature transcripts, respectively. By contrast, the sequencing analysis in *jmj14* revealed a rearrangement during the splicing process, which led to an early stop codon and a truncated FYRC domain (Figure 1C, S 1A).

To confirm *jmj14* as a genuine *brx* suppressor, we crossed a loss-of-function (*jmj14-1*) allele which carries a T-DNA insertion in the conserved JmjC domain (Lu et al.,

2010), to *brx*. *brx jmj14-1* double mutants partially restore the primary root length (Figures 1D and 1E). Moreover, a *JMJ14::JMJ14* transgene was introduced in *brx jmj14* and *brx jmj14-1*. Root measurements of independent segregating T2 lines revealed the restoration of the *brx* short root phenotype (Figure 1F). Our results confirmed *jmj14* as a genuine suppressor of the *brx* impaired root growth and revealed the biological relevance of the FYRC protein domain for JMJ14 activity.

### ***brx jmj14* fails to restore protophloem continuity**

Given that the macroscopic *brx* phenotype derives from impaired protophloem differentiation (Figure 2A), we investigated whether *jmj14-1* restores the protophloem continuity. Contrary to second-site null-mutation in the *BARELY ANY MERISTEM 3* (*BAM3*) gene, which fully restores both root length and protophloem gaps, *jmj14-1* cannot do so (Figure 2B) (Depuydt et al., 2013). Double mutant and *jmj14-1* are both CLE45-sensitive (Figure 2C). Our observations thus suggest that suppression of the *brx* short root phenotype by *jmj14* is independent of the CLE45-BAM3 network.

Moreover, we tested the phloem-mediated translocation efficiency of carbofluorescein diacetate (CFDA). Application of the probe on cotyledons revealed a slower transport along the phloem (Figure 2D and 2E). Monitoring the inverse auxin marker DII::VENUS in *brx jmj14* root meristem we found a low accumulation of the hormone (Figure 2F). Finally, we quantified lateral root density, which was similar to *brx* (Figure 2G). *jmj14* thus fails to restore protophloem continuity and the linked systemic effects of *brx*. Therefore, we conclude that *jmj14* suppresses the *brx* short root phenotype in a protophloem-independent manner.

## JMJ14 influences meristematic cell proliferation in sensitized backgrounds

In a previous publication we showed that *big brother* (*bb*) loss-of-function partially restores the *brx* short root phenotype. *bb* displays no macroscopic phenotype in root length, however it appears that its enhanced meristematic cell number partially compensates the slow *brx* root growth.

The apparent normal root length of *jmj14* mutants is similar to that of *bb* and Col-0 (Figure 1D and 1E). To investigate analogies in the mechanism by which *jmj14* and *bb* suppress the *brx* root phenotype, we analysed the meristematic activity. *brx jmj14-1* double mutant restores the *brx* reduced cell proliferation partially, but *jmj14-1* interestingly shows no perturbation (Figure 3A). To test whether *jmj14-1* affects cell expansion, we measured mature cortex cell length, which is slightly restored in *brx jmj14-1* (Figure 3B). *jmj14* does not affect cell expansion, although in impaired genetic backgrounds overall cell length is enhanced.

*bb* moreover influences the extent of formative divisions, whose enhancement was hypothesized to slow down the overall root growth (Cattaneo et al., 2017). Analysis of *jmj14-1* cross-sections showed no difference, neither in cell file numbers nor in tissue organization. Also, *brx jmj14-1* fails to compensate the reduced formative divisions within the stele of the *brx* root (Figure 3C and 3D).

The data thus suggest that *jmj14-1* might merely influence meristematic cell division in *brx* background, thereby speeding up longitudinal root growth. To corroborate our hypothesis, we crossed *jmj14-1* to *ops*, another positive regulator of protophloem formation which displays the same root phenotype as *brx* (Truernit et al., 2012). *ops jmj14-1* displayed restored root length similar to *brx jmj14-1* (Figure 3E and 3F). The rescue is again the consequence of the enhanced meristematic activity (Figure 3G). Moreover, similar to *brx jmj14-1* double mutants, the protophloem discontinuity (Figure 3H) and the systemic effects are conserved in *ops jmj14-1* double mutants (Figure 3I). In summary, our findings suggest that *JMJ14* acts independent of *BRX* and *OPS*, and its function in root development becomes evident exclusively in sensitized backgrounds.

## ***JMJ14* shows a vascular-related expression pattern**

As the *JMJ14* expression pattern in the root is unknown we created and analysed transcriptional reporter lines of *JMJ14*. The 1.5 kb region upstream of the ATG indicated that *JMJ14* is expressed in the root vasculature cylinder. The expression started early in the meristem, where the protophloem elongation begins, and continued further up in the root (Figure 4A). *JMJ14* was limited to procambial cells, but it was absent in the xylem and phloem poles.

Interestingly, the observation of JMJ14-CIT under the control of the same promoter revealed a broader expression in the root meristem. JMJ14-CIT was observed in the endodermis, cortex tissues and in the precursors of the vasculature. The expression further up was also slightly broader compared to transcriptional reporter lines (Figure 4B). Our findings were supported by the evidently overlapping vascular pattern that we observed in cotyledons (Figure 4C). Moreover, JMJ14-CIT shows a nuclear localization at the subcellular level, consistent with its histone demethylase activity.

Overall, *JMJ14* is expressed in the root vascular cylinder except in phloem and xylem poles. The broader expression domain of JMJ14-CIT in the meristem suggests potential post-translational modifications, which might influence a potential non cell-autonomous action. Further analysis will reveal whether enlargement of JMJ14 reporters by additional copies of reporter proteins might perturb JMJ14 localization within the meristem.

## **Downstream effects of *JMJ14* in the *Arabidopsis* root**

*JMJ14* belongs to the *Arabidopsis* JmjC domain-containing gene family, which reduces H3K4 methylation states (Lu et al., 2008). Here we investigated the consequences of *JMJ14* overexpression during root development. To this end, a constitutively expressed *UBQ10::JMJ14* transgene was introduced into *brx jmj14* and Col-0 backgrounds. Quantification of the root length of independent segregating T2 lines revealed the restoration of the *brx* phenotype, validating the transgene functionality (Figure 5A). Interestingly, analysis of *UBQ10::JMJ14* in Col-0 revealed no

differences in root length (Figure 5B). Consistently, the root meristem appeared as in wild type (Figure 5C). Our data thus suggest no perturbation of the root meristem organization by JMJ14 gain-of-function. The absence of any phenotype might be explained by the work of Ning and co-workers reported in 2015. JMJ14 interacts with two transcription factors, NAC50 and 52, through its FYR domains and is recruited thereafter on the target chromatin regions. Supposing that the stoichiometry of the protein complex is one to one, the exclusive enhancement of JMJ14 might mask any consequence. *NAC50* overexpression however significantly amplified JMJ14 flowering repression activity (Ning et al., 2015). To date it is unclear what causes the ineffectiveness of *JMJ14* overexpression in the root. Cell quantification in the meristem and characterization of cell differentiation processes further up in the root could elucidate this aspect.

In plants, H3K4 methylation is normally associated with gene activation. Given that JMJ14 is a demethylase, we monitored the transcriptome of *jmj14-1* 7-day-old roots by mRNA sequencing. The analysis identified in total 2330 genes that were differentially expressed compared to Col-0. While 738 were upregulated, 1592 genes were downregulated (Figure 6A). We analysed the genes with the highest fold-change in expression for the two categories. Interestingly, in the upregulated data set we found *SHRUBBY* (*SHBY*, At5g24740) (Figure S 1B). *SHBY* encodes a protein that partially overlaps with *SHORT ROOT*, *SCARECROW*, *PHLETORA1* and *PHLETORA2* that all control root growth (Koizumi et al., 2013).

In addition, we intersected our gene expression data sets with the JMJ14-dependent differentially methylated genes found by Ning and co-workers in 2015. Between the up regulated genes, 188 were overlapping, while 80 genes were shared between the down regulated data sets (Figure 6B). Several uncharacterized RING/U-box, F-box and NAC genes were found. Because we extracted mRNA from roots, whereas Ning et al., 2015 used whole seedlings, we did expect perfect overlap however.

In summary, the RNA sequencing showed a significant difference in the root gene expression profiles between *jmj14-1* and wild type. Among the differential expressed genes, we found *SHRUBBY* which might correlate with the rescue of the root growth.

Future experiments could confirm SHBY as a target of JMJ14 and the mechanism by which JMJ14 controls root development.

### **JMJ14 homologs fail to suppress *brx* phenotype**

In *Arabidopsis* the six members (*JMJ14*, *JMJ15*, *JMJ16*, *JMJ17*, *JMJ18* and *JMJ19*) of the JARID1/KDM5 group share a unique conserved region at the C-terminus. They exhibit two phenylalanine/tyrosine-rich domains known as FYRN and FYRC (Lu et al., 2008; Ning et al., 2015). They likely mediate the interaction with other factors, which recruit JMJ protein on DNA target regions (Ning et al., 2015). Amino acid differences in FYR domains therefore might influence the JMJ recruitment process. Here we investigated whether *jmj16* and *jmj18* loss-of-function show any macroscopic root phenotype. Root length quantification revealed no significant differences between JMJ14 homologs compared to Col-0 (Figure 7A and 7B). Furthermore, we investigated whether *jmj16* and *jmj18* mutants can suppress the *brx* short root phenotype, similar to *jmj14-1*. We crossed two *jmj16* and *jmj18* T-DNA alleles to *brx* and we analysed the primary root length in the double mutants. Both *brx jmj16* and *brx jmj18* double mutants failed to rescue the *brx* phenotype (Figure 7C and 7D). Similar to JMJ14, JMJ16 represses flowering transition, whereas JMJ18 promotes the transition (Lu et al., 2010; Lu et al., 2011; Yang et al., 2012). Except their role in regulating the flowering time, their expression pattern and activity in the root is unclear. Further analysis could elucidate in detail whether their expression domains overlap throughout the root.

## CONCLUSION

In our study, we uncovered a novel *brx* suppressor of the impaired root phenotype, which acts in a protophloem-independent manner. *JMJ14* expression is associated with plant vasculature. *JMJ14* accomplishes its function through the JmjC domain, which confers demethylase properties. Moreover, we demonstrated the biological relevance that intact FYR domains have for *JMJ14* activity. Perturbed *JMJ14* function interferes with the H3K4 methylation state and thus with the relative expression of target genes. A shift in gene transcription programs may possibly explain the restoration of root growth in sensitized backgrounds. Among the differential expressed genes, we found *SHRUBBY*, a regulator of root growth (Koizumi et al., 2013). Follow up studies could elucidate the mechanism by which *JMJ14* can control root development, address the relevance of *JMJ14* homologs within the root, as well as the role of the FYR protein domains.

## Materials and methods

### Plant materials, growth conditions, and physiological assays

Plant tissue culture, plant transformation, and common molecular biology procedures such as genomic DNA isolation, plant transformation, genotyping, (whole genome) sequencing, and peptide treatments, phloem unloading measurement, and probe translocation assay were performed according to standard procedures as previously described (Cattaneo et al., 2017; Kang et al., 2016, Kang et al.; 2017). For plant tissue culture, seeds were surface-sterilized, germinated and grown vertically on half strength MS agar media with or without 0.3% sucrose under continuous light of ~120 uE intensity at 22°C. All mutants were in the *Arabidopsis* Columbia-0 (Col-0) wild type background, i.e. the described *brx-2*, *ops-2*, *jmj14-1*, *jmj16*, *jmj18* alleles (Gujas et al., 2012; Lu et al., 2010; Lu et al., 2011; Truernit et al., 2012, Yang et al., 2012), as well as the newly isolated *jmj14* allele.

### Reporter constructs

To produce *JMJ14::NLS-3XVENUS* plants, the *JMJ14* promoter (At4g20400) was amplified using oligonucleotides 5'- TCC TCT AGAG AAG ATT GTG GTG GCT GGT G -3' and 5'- CAG CCT GCA GGT TAC AGT GAG ATT AAG TTC ACA AAG -3'. After XbaI-SbfI restriction enzyme digest, the fragment was cloned into the pCAMBIA1005.1 NLS-3XVENUS vector.

To produce *JMJ14::JMj14-CIT* plants, the *JMJ14* promoter (At4g20400) was amplified using oligonucleotides 5'- ATT CCC GGG TTA CAG TGA GAT TAA GTT CAC AAA G -3' and 5'- ATT GGT ACC GAA GAT TGT GGT GGC TGG TG -3'. After KpnI-XmaI restriction enzyme digest, the fragment was cloned into a modified P4-P1r vector to generate the Gateway pENTRY-pJMj14 plasmid. The pENTRY JMj14 was cloned by amplifying the JMj14 CDS without stop codon from cDNA using oligonucleotides 5'- GGG GAC AAG TTT GTA CAA AAA AGC AGG CTT CAT GGA TCA GCT TGC ATC TCT AGC -3' and 5'- GGG GAC CAC TTT GTA CAA GAA AGC

TGG GTT AGG ACT TAT CTC CAT CTT ATC AAC C -3' (note: including the attB1 and attB2 sites, respectively for Gateway cloning). pENTRY-pJMJ14, pENTRY-JMJ14 and pENTRY-CIT vectors were recombined into pH7m34GW plasmid. To create *UBQ10::JMJ14*, the *JMJ14* CDS with stop codon was amplified using oligonucleotides 5'- GGG GAC AAG TTT GTA CAA AAA AGC AGG CTT CAT GGA TCA GCT TGC ATC TCT AGC -3' and 5'- GGG GAC CAC TTT GTA CAA GAA AGC TGG GTT TTA AGG ACT TAT CTC CAT CTT ATC -3' (note: including the attB1 and attB2 sites, respectively for Gateway cloning) and recombined with pENTRY-UBQ10 promoter clone into the pH7m24GW vector.

*Arabidopsis* plants were transformed with the constructs and lines with single insertions were selected in the T2 generation. All quantitative data shown are from single, representative replicate experiments, with genotypes assayed in parallel.

### **Evaluation of the *jmj14* point mutation effects**

7-day-old roots of Col-0 and *jmj14* genotypes grown in parallel on vertical plates were harvested and frozen in liquid nitrogen before total RNA extraction was performed using a Quiagen RNeasy Plant kit. cDNA synthesis was performed as described previously (Depuydt et al., 2013). The ~ 1 kb region which includes the mutation site was amplified using oligonucleotides 5'- CGA AGA AAG TGG ATG GTT GTT TAG - 3' and 5'- CAC AGA AGT CCA TGC ATC ATT AC -3'. The fragments were separated by gel electrophoresis, extracted from gels and sequenced.

### **RNA-sequencing**

For mRNA sequencing, 7-day-old roots of the different genotypes grown in parallel on vertical plates were harvested and frozen in liquid nitrogen before total RNA extraction was performed using a Quiagen RNeasy Plant kit. cDNA synthesis, amplification, size selection, high-throughput sequencing was performed as described previously (Bray et al., 2016).

## References

- Bray BL, Pimentel H, Melsted P, Pachter L (2016) **Near-optimal probabilistic RNA-seq quantification.** *Nature Biotechnology* 34: 525–527.
- Cattaneo P, Hardtke CS (2017) **BIG BROTHER Uncouples Cell Proliferation from Elongation in the Arabidopsis Primary Root.** *Plant Cell Physiol.* 58: 1519-1527.
- Depuydt S, Rodriguez-Villalon A, Santuari L, Wyser-Rmili C, Ragni L, Hardtke CS (2013) **Suppression of Arabidopsis protophloem differentiation and root meristem growth by CLE45 requires the receptor-like kinase BAM3.** *Proc Natl Acad Sci U S A* 110: 7074-9.
- Gan ES, Xu Y, Wong JY, Goh JG, Sun B, Wee WY, Huang J, Ito T (2014) **Jumonji demethylases moderate precocious flowering at elevated temperature via regulation of FLC in Arabidopsis.** *Nature Communications* 5: 5098.
- Gujas B, Alonso-Blanco C, Hardtke CS (2012) **Natural Arabidopsis brx loss-of-function alleles confer root adaptation to acidic soil.** *Curr Biol.* 22: 1962-8.
- Kang YH, Hardtke CS (2016) **Arabidopsis MAKR5 is a positive effector of BAM3-dependent CLE45 signaling.** *EMBO Rep.* 17: 1145-54.
- Kang YH, Breda A, Hardtke CS (2017) **Brassinosteroid signaling directs formative cell divisions and protophloem differentiation in Arabidopsis root meristems.** *Development* 144: 272-280.
- Ko JH, Mitina I, Tamada Y, Hyun Y, Choi Y, Amasino RM, Noh B, Noh YS (2010) **Growth habit determination by the balance of histone methylation activities in Arabidopsis.** *EMBO J.* 29: 3208-15.
- Koizumi K, Gallagher KL (2013) **Identification of SHRUBBY, a SHORT-ROOT and SCARECROW interacting protein that controls root growth and radial patterning.** *Development* 140: 1292-300.
- Kouzarides T (2007) **Chromatin modifications and their function.** *Cell* 128: 693-705.
- Lu F, Li G, Cui X, Liu C, Wang XJ, Cao X (2008) **Comparative analysis of JmjC domain-containing proteins reveals the potential histone demethylases in Arabidopsis and rice.** *J Integr Plant Biol.* 50: 886-96.
- Lu F, Cui X, Zhang S, Liu C, Cao X (2010) **JMJ14 is an H3K4 demethylase regulating flowering time in Arabidopsis.** *Cell Res.* 20: 387–390.
- Lu F, Cui X, Zhang S, Jenuwein T, Cao X (2011) **Arabidopsis REF6 is a histone H3 lysine 27 demethylase.** *Nat Genet.* 2011 43:715-9.
- Mosammaparast N, Shi Y (2010) **Reversal of histone methylation: biochemical and molecular mechanisms of histone demethylases.** *Annu Rev Biochem.* 79 :155-79.
- Ning YQ, Ma ZY, Huang HW, Mo H, Zhao TT, Li L, Cai T, Chen S, Ma L, He X (2015) **Two novel NAC transcription factors regulate gene expression and flowering time by associating with the histone demethylase JMJ14.** *Nucleic Acids Res.* 43: 1469-84.

Pagnussat GC, Yu HJ, Ngo QA, Rajani S, Mayalagu S, Johnson CS, Capron A, Xie LF, Ye D, Sundaresan V (2005) **Genetic and molecular identification of genes required for female gametophyte development and function in Arabidopsis.** *Development* 132: 603–614.

Rodriguez-Villalon A, Gujas B, Kang YH, Breda AS, Cattaneo P, Depuydt S, Hardtke CH (2014) **Molecular genetic framework for protophloem formation.** *Proc Natl Acad Sci U S A* 111: 11551-6.

Rodriguez-Villalon A, Gujas B, van Wijk R, Munnik T, Hardtke CS (2015) **Primary root protophloem differentiation requires balanced phosphatidylinositol-4,5-biphosphate levels and systemically affects root branching.** *Development* 142: 1437-46.

Saleh A, Alvarez-Venegas R, Yilmaz M, Oahn-Le, Hou G, Sadler M, Al-Abdallat A, Xia Y, Lu G, Ladunga I, Avramovaa Z (2008) **The Highly Similar Arabidopsis Homologs of Trithorax ATX1 and ATX2 Encode Proteins with Divergent Biochemical Functions.** *Plant Cell* 20: 568–579.

Saze H, Shiraishi A, Miura A, Kakutani T (2008) **Control of genic DNA methylation by a jmjC domain-containing protein in Arabidopsis thaliana.** *Science* 319: 462–465.

Scacchi E, Salinas P, Gujas B, Santuari L, Krogan N, Ragni L, Berleth T, Hardtke CS (2010) **Spatio-temporal sequence of cross-regulatory events in root meristem growth.** *Proc Natl Acad Sci U S A* 107: 22734-9.

Shi Y, Lan F, Matson C, Mulligan P, Whetstone JR, Cole PA, Casero RA, Shi Y (2004) **Histone demethylation mediated by the nuclear amine oxidase homolog LSD1.** *Cell* 119: 941-53.

Truernit E, Bauby H, Belcram K, Barthélémy J, Palauqui JC (2012) **OCTOPUS, a polarly localised membrane-associated protein, regulates phloem differentiation entry in Arabidopsis thaliana.** *Development* 139: 1306-15.

Yang H, Han Z, Cao Y, Fan D, Li H, Mo H (2012) **A Companion Cell–Dominant and Developmentally Regulated H3K4 Demethylase Controls Flowering Time in Arabidopsis via the Repression of FLC Expression.** *PLoS Genet.* 8: e1002664.

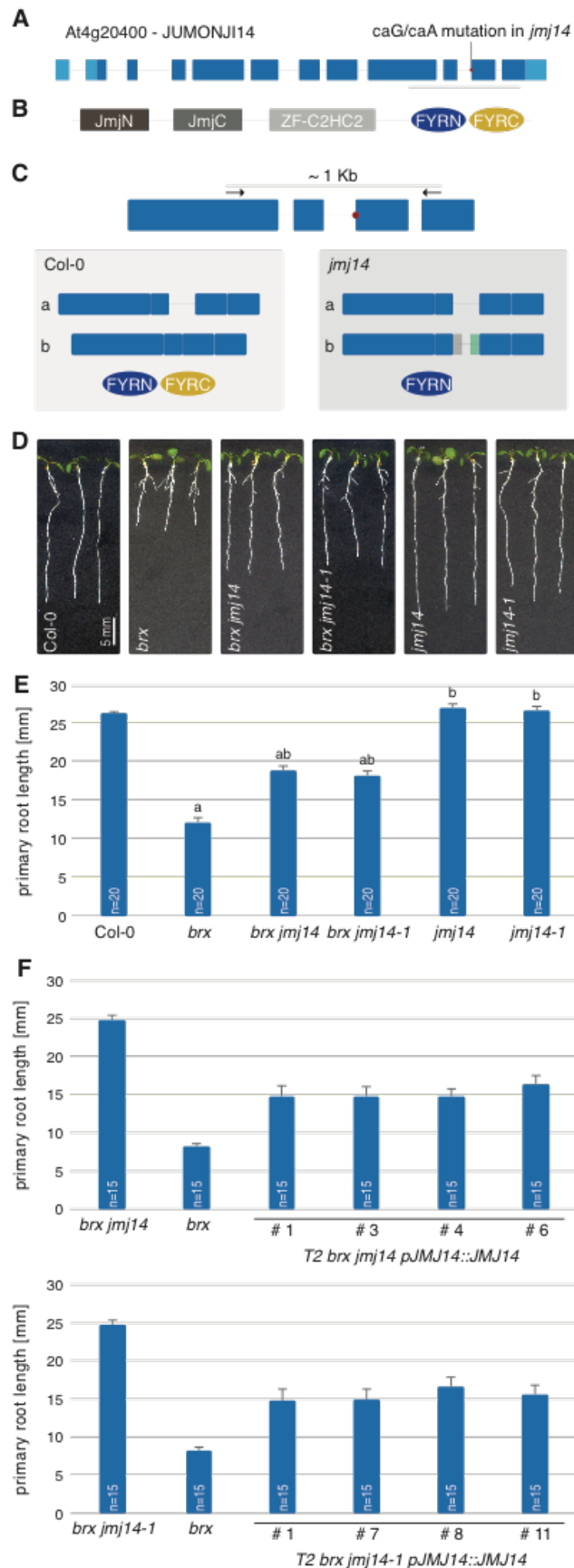


**Figure 1 | Second-site mutation in *JMJ14* partially suppresses the *brx* short root phenotype.**

**A** | Schematic presentation of the *JMJ14* gene with the relative position of the mutation (rectangles: exons; continued lines: introns). **B** | Schematic presentation of the conserved JMJ14 protein domains. **C** | The 1 kb region used to evaluate the biological relevance of the point mutation on the splicing activity. For both Col-0 and *jmj14* mutant a representation of the two amplified fragments based on the sequencing results is given (a and b); schematic representation of the FYR protein domains shows the effects of the splicing in Col-0 and *jmj14*. The grey and the green rectangles represent the portion of transcript that are lost and gained, respectively, during the rearrangement of the splicing process. **D** | Representative seedlings of the indicated genotypes at 6 days after germination (dag). **E** | Average primary root length of the indicated genotypes at 6 dag. **F** | Average primary root length of the indicated genotypes at 7 dag. Differences as compared with the Col-0 wild type background (a) or *brx* mutant background (b) are statistically significant as indicated (Student's t-test;  $P < 0.01$ ; mean  $\pm$  SEM).

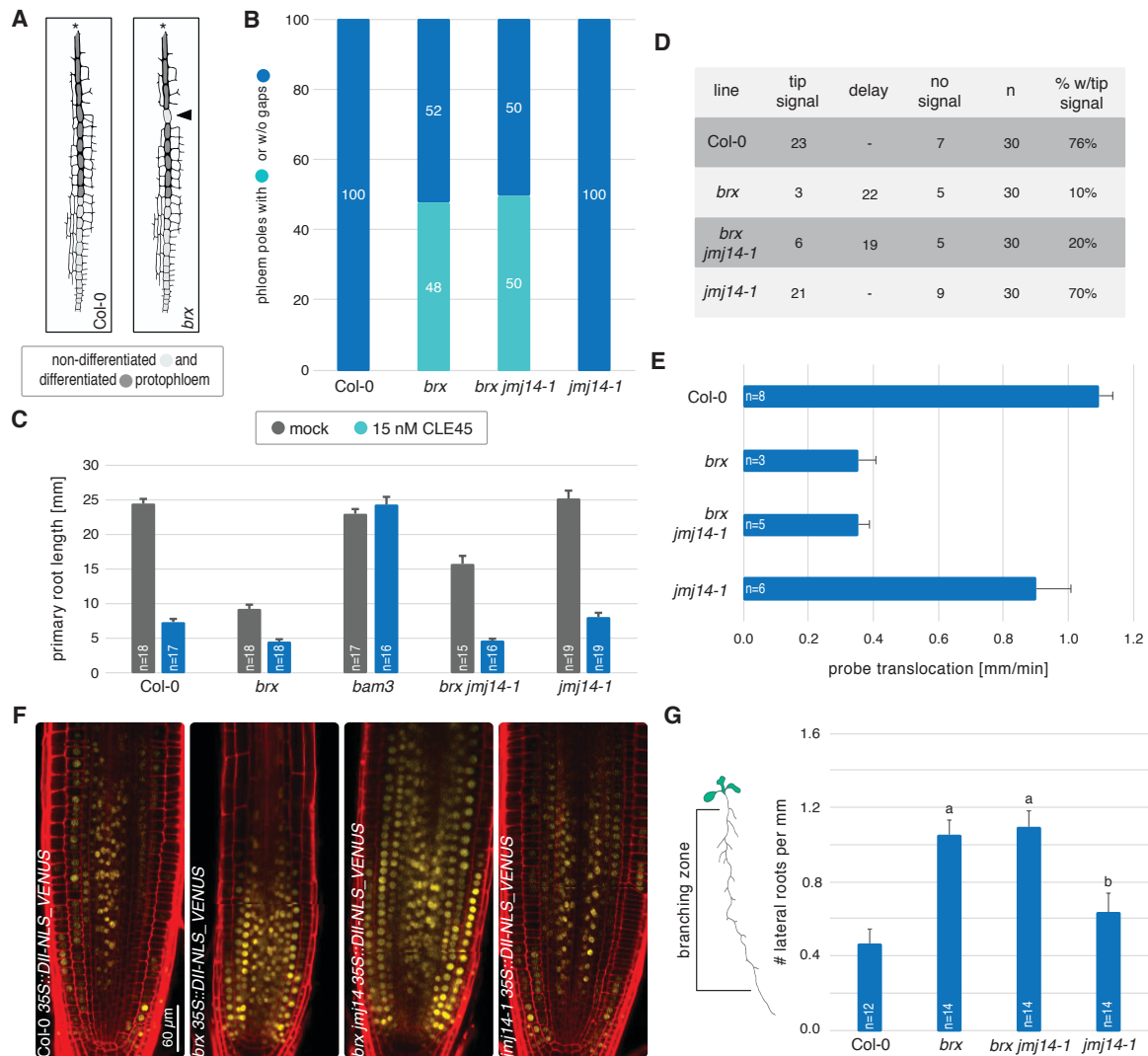


## Figure 2 | Consequences of protophloem discontinuity in *brx jmj14* double mutant.

A | Schematic pattern of the developing protophloem sieve element strands in Col-0 and *brx* mutant; undifferentiated “gap” cells are highlighted (arrowhead) in *brx*. B | Quantification of the gap frequency for the indicated genotypes. Differences between Col-0 and *jmj14* vs. *brx* and *brx jmj14* were statistically significant ( $P < 0.001$ , Fisher’s exact test), but not within those pairs. C | Average primary root length of the indicated genotypes responding to CLE45 peptide in the medium at 7 dag. All treatments were statistically significant as compared with mock treatment ( $P < 0.001$ , Student’s *t*-test), except for *bam3* on CLE45. D | Classification of the CFDA signal at the end of the phloem-translocation assay. E | CFDA translocation velocity *in vivo* measurements, based exclusively on seedlings in which the dye reached the root tip. F | Auxin activity monitored by the DII::VENUS inverse reporter (yellow fluorescence) for the indicated genotypes at 7 dag, composite images (red fluorescence: propidium iodide). G | Lateral root density of the branching zone in the indicated genotypes at 12 dag. Differences as compared with the Col-0 wild type background (a) or *brx* mutant background (b) are statistically significant as indicated (Student’s *t*-test;  $P < 0.01$ ; mean  $\pm$  SEM).

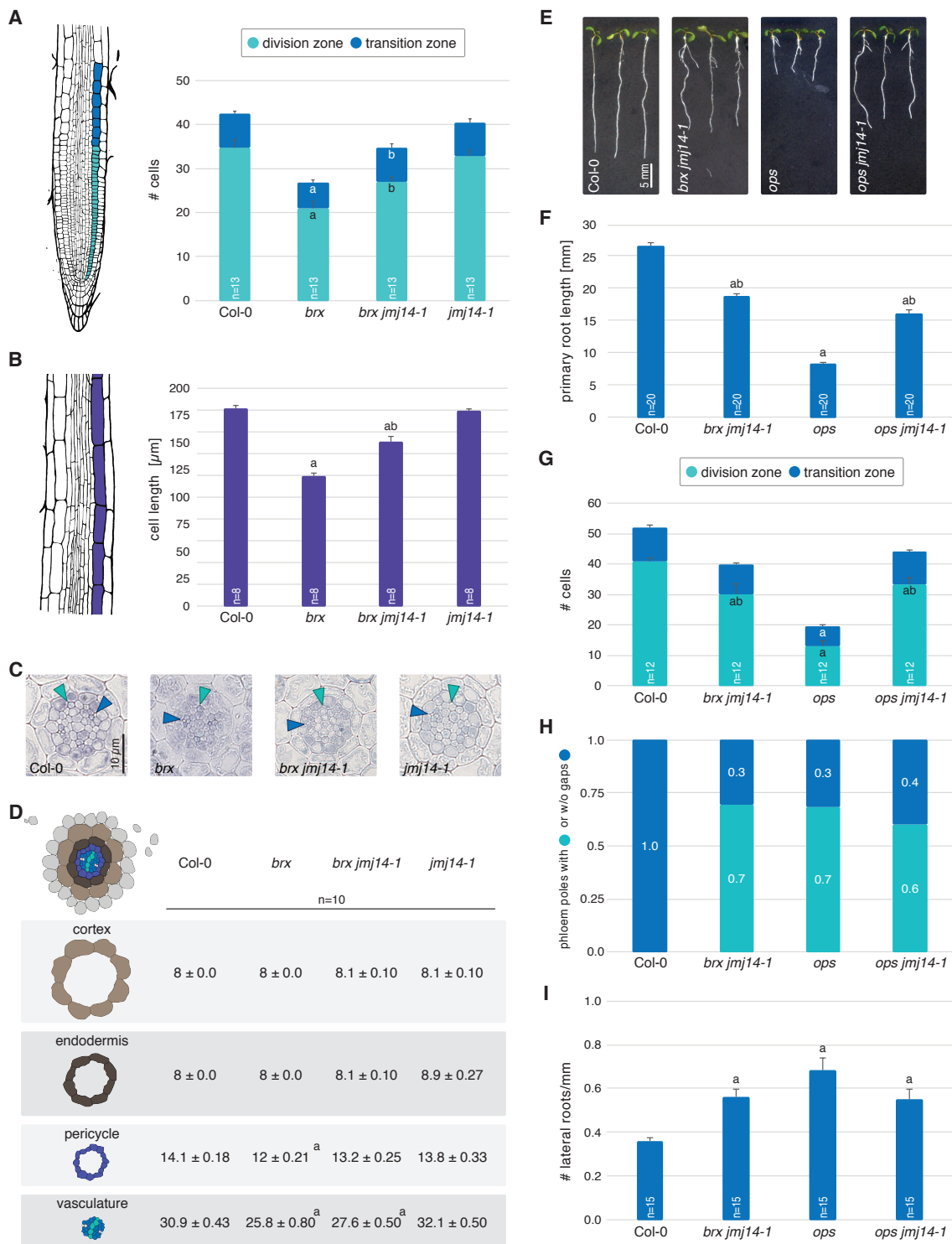


**Figure 3 | Evaluation of *jmj14* root growth and suppression of the *ops* short root phenotype.**

**A** | Quantification of the cortex cell number in the division and transition zone of 7 dag seedlings of the indicated genotypes. **B** | Length of the mature cortex cells in the indicated genotypes at 7 dag. Average of the average for 8 roots, with approximately 10 cells scored per root. **C** | Representative histological cross-sections of 6 dag roots of the indicated

genotypes taken at the position where protoxylem has differentiated (green arrowheads; blue arrowheads: protophloem). D | Quantification of cell file number in roots of the indicated genotypes at 6 dag. Differences as compared with the Col-0 wild type background (a) or *brx* mutant background (b) are statistically significant as indicated (Student's t-test;  $P < 0.01$ ; mean  $\pm$  SEM). E | Representative seedlings of the indicated genotypes at 6 dag. F | Average primary root length of the indicated genotypes at 6 dag. G | Quantification of the cortex cell number in the division and transition zone of 7 dag seedlings of the indicated genotypes. H | Quantification of the gap frequency for the genotype indicated at 5 dag. Differences between Col-0 and all other genotypes were statistically significant ( $P < 0.001$ , Fisher's exact test). I | Lateral root density of the branching zone in the indicated genotypes at 12 dag. Differences as compared with the Col-0 wild type background (a) or *ops* mutant background (b) are statistically significant as indicated (Student's t-test;  $P < 0.01$ ; mean  $\pm$  SEM).

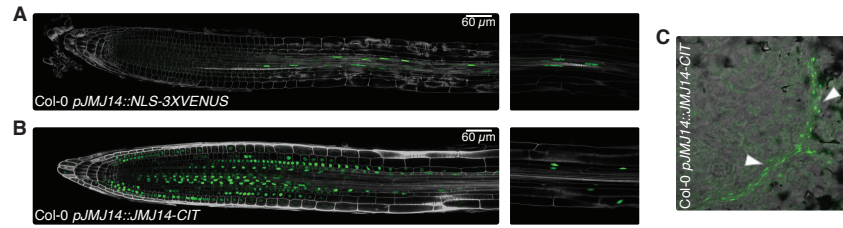


**Figure 4 | JMJ14 root pattern.**

A | NLS-3XVENUS reporter gene expression (green fluorescence) driven by the *JMJ14* promoter in roots of 5 dag Col-0 seedlings, composite images (white fluorescence: calcofluor-white). B | Expression of JMJ14-CIT fusion protein (green fluorescence) under control of *JMJ14* promoter in roots of 5 dag, composite images (white fluorescence: calcofluor-white). C | Corresponding JMJ14-CIT expression in cotyledons of 5 dag Col-0 seedlings (arrowheads: vasculature).

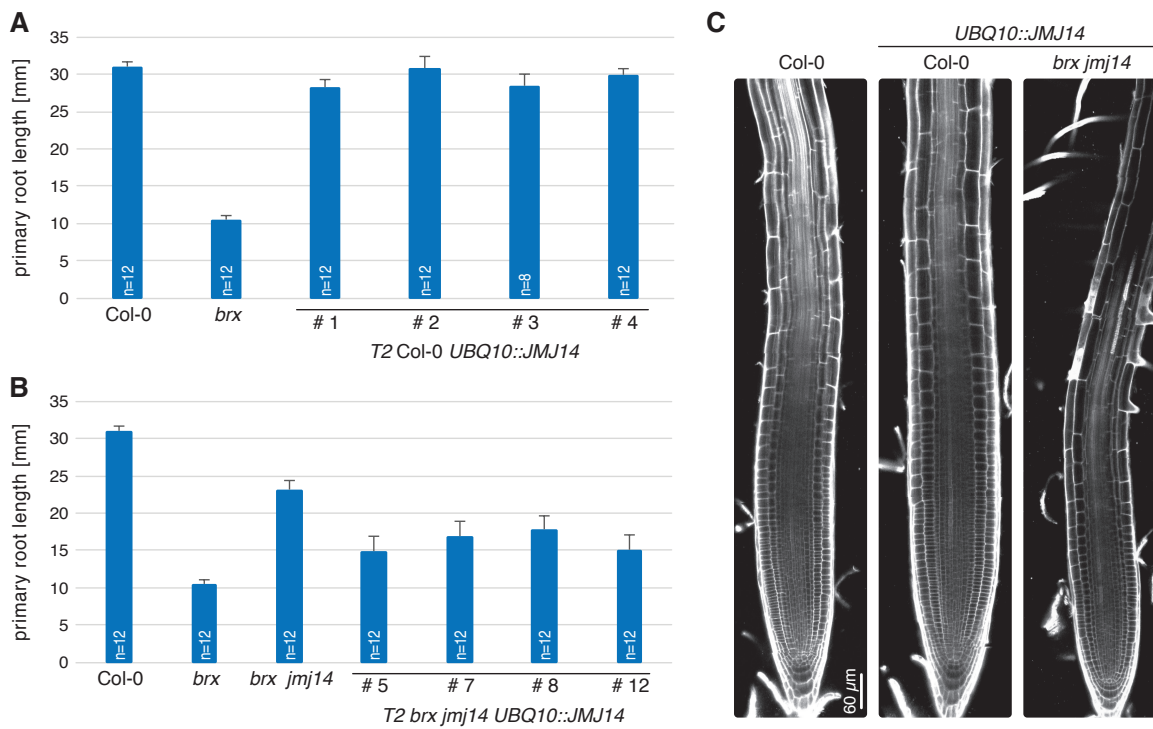


**Figure 5 | JMJ14 overexpression in root.**

A | Average primary root length of the indicated genotypes at 7 dag. B | Average primary root length of the indicated genotypes at 7 dag. C | Confocal images (greyscale) of 7 dag propidium iodide-stained root meristem of the indicated genotypes.

**A**

	Total genes q-value < 0.01	up regulate	down regulate
<i>jmj14-1</i> vs. Col-0	2330	738	1592

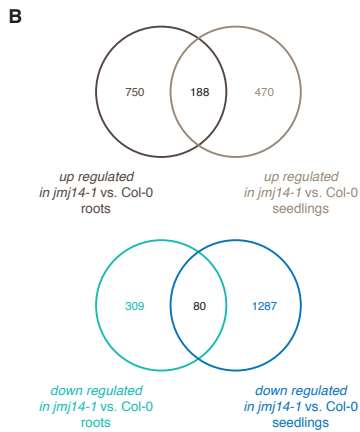


### Figure 6 | *jmj14-1* mRNA sequencing.

A | Differentially expressed genes in *jmj14-1* roots at 7 dag.  
B | Venn diagrams comparing the *jmj14-1* RNAseq with the Ning et al., 2015 dataset.

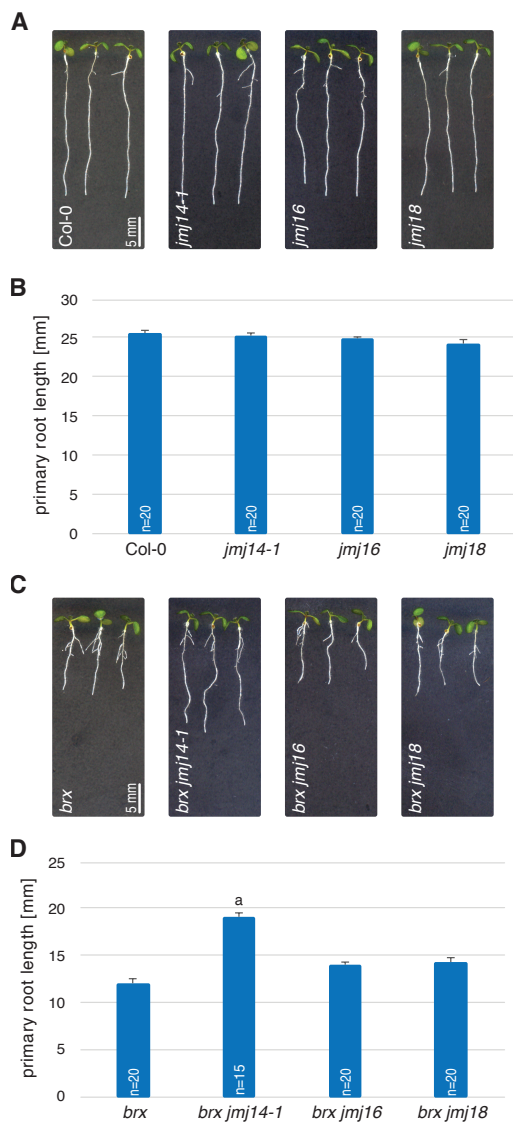


### Figure 7 | *jmj* homologs mutant root phenotype.

A | Representative seedlings of Col-0 and *jmj* homologs loss-of-function mutants at 6 dag.  
B | Average primary root length of the indicated genotypes at 6 dag.  
C | Representative seedlings of *brx* mutant and *brx jmj* homologs double mutants at 6 dag.  
D | Average primary root length of the indicated genotypes at 6 dag. Differences as compared with the *brx* mutant background (a) are statistically significant as indicated (Student's t-test;  $P < 0.01$ ; mean  $\pm$  SEM).

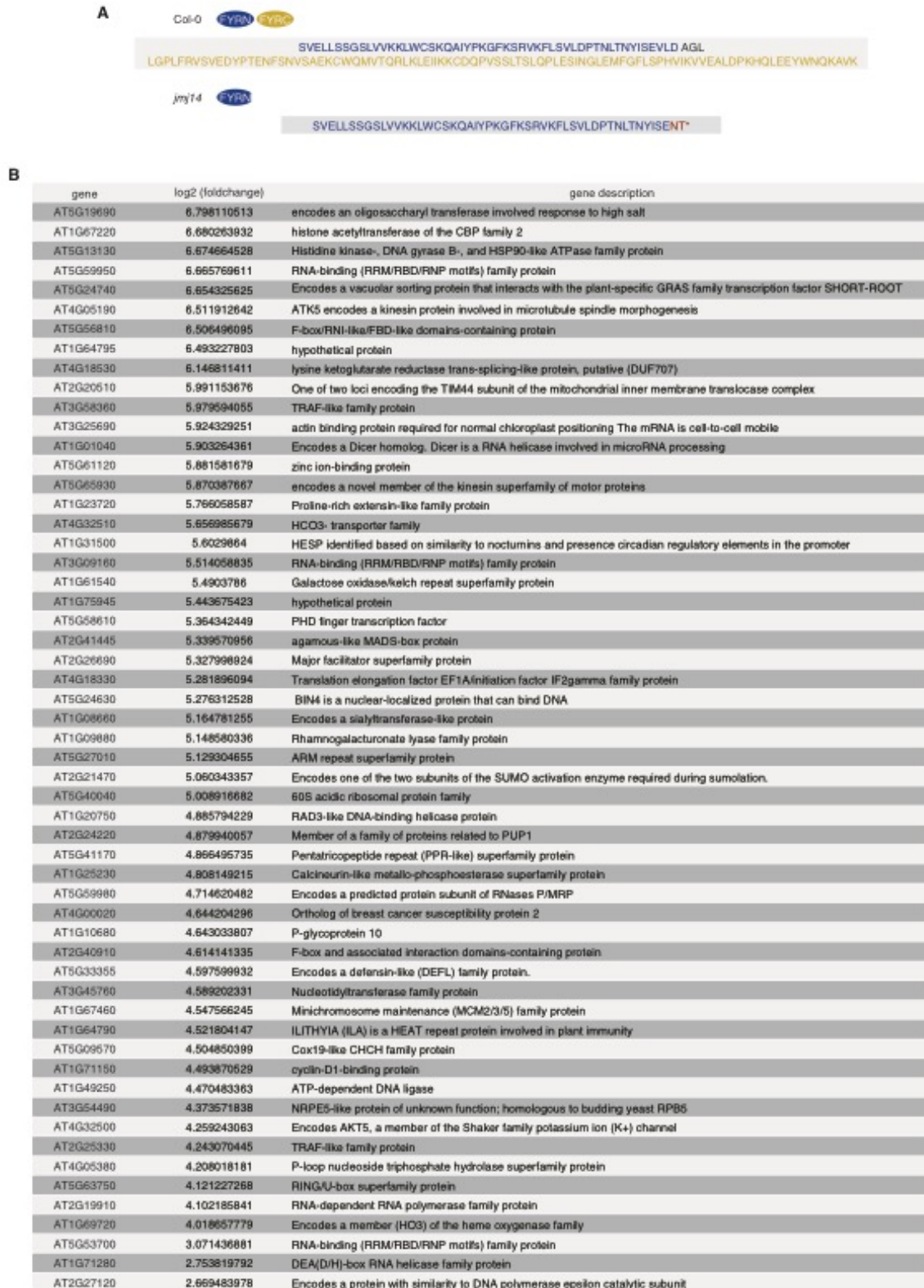


**Figure S1 | Supplementary figure.**

A | Effects of the *jmj14* second site mutation on FYRN and FYRC protein domains. B | Most significant up regulated genes in *jmj14-1*.

## CONCLUSION AND OUTLOOK

The plant vascular network functions distributing water, photoassimilates and signalling molecules through the whole plant body (Helariutta, 2007). The xylem transports water and ions from the root to the leaves, while the phloem transports the so called sap, containing sugars and signalling molecules from the above-ground source organs to sink organs, such as the root (Lucas et al., 2013). In proximity of the root meristem, the protophloem functions as a bridge between the differentiated metaphloem and the actively developing and growing tissues (Rodriguez-Villalon et al., 2015). Several studies have partially elucidated the molecular mechanisms controlling the differentiation of the protophloem. Notably, the achievement of a fully differentiated protophloem pole requires the spatio-temporal regulation of *BRX* and *CLE45/BAM3* activity (Depuydt et al., 2013; Rodriguez-Villalon et al., 2014). The main objective of my research was to improve the understanding of the *BRX* pathway, with particular emphasis on the identification of new regulators of the protophloem sieve element development.

In the first two chapters I discussed the application of the antagonistic peptide technology (Song et al., 2013). To overcome the lack of *CLE45* loss-of-function mutants I evaluated the consequences of *CLE45::CLE45G6T* expression in Col-0 background. Contrary to my expectations, the antagonistic *CLE45G6T* peptide turned to be a mild variant of the wild type *CLE45*. My observations demonstrated that the technology cannot be applied to all peptide indistinctly, but requires a deep understanding on the interaction between the ligand and the receptor. Likewise, the application of the technology has to consider the amino acid context and also the differential sensitivity to conformational changes. Although I showed that it is not the ultimately strategy to overcome the lack of loss-of-function mutants for *CLE* peptides, it is a useful tool to study some peptides function (i.e. *CLE3*, *CLE26* and *CLE40*). Interestingly the *CLE45G6T* plants failed to develop continuous protophloem, similar

to *brx* mutants. My observations corroborate also the notion that the local hyperactivity of the module CLE45/BAM3 locks protophloem cells in the undifferentiated stage.

To identify new genetic players of the *BRX* network I invested part of my research screening for *brx* suppressors. Contrary to the approach that was previously followed (Depuydt et al., 2013), I adopted a new multi-faceted strategy. In particular, I considered the protophloem “gaps” rescue to uncover new suppressors involved in protophloem development.

As reported in chapter three, I identified several unknown *bam3* alleles. The isolation of different *bam3* alleles loci improved the understanding of the importance of both cytoplasmic and extra-cellular residues necessary for ligand perception and activation of the downstream signalling cascade.

A possible explanation for the high number of *bam3* alleles isolated could be the large gene size (2840 kb), which makes it an easy target for the EMS mutagenesis. Additionally, the inability to uncover other members of the *CLE45/BAM3* pathway such as co-receptors and players of the downstream signalling cascade, might be masked by genetic redundancy.

Until now it is unknown whether the CLE45/BAM3 signal propagates into parallel pathways downstream. Mutation in a single gene might not be sufficient to fully restore the protophloem continuity, therefore the high stringency strategy could overlook partial suppressors.

Notably, we screened approximately 2,500 M1 plants. Based on the frequency by which we identified *bam3* alleles I concluded the screen was saturated.

For these reasons, the uncovering of new candidates involved in sieve element differentiation based on the rescue of the *brx-2* gap phenotype could be precluded.

Designing a new genetic screen, which will take into account the genes protophloem-related identified (i.e. *MAKR5*, *OPS*), could therefore lead to uncover new molecular players controlling protophloem sieve element differentiation.

Among the *brx* suppressors, a second site null mutation in the gene *BIG BROTHER* (*BB*) was found to partially suppress the reduced root growth vigour. During my research I addressed the genetic link between *BRX* and *BB*, I described the framework which explains the rescue of the *brx* short root and I elucidated the role of *BB* during the primary root development.

My observations demonstrated initially that *BIG BROTHER* is not linked to the *BRX* network. The suppression of the *brx* short root occurs in a protophloem-independent manner. Therefore, my study turned to a comprehensive characterization of *BB* during primary root development. Previous studies documented that *BB* restricts the cell proliferation phase promoting the transition to cell differentiation and cell expansion (Dish et al., 2006; Vanhaeren et al., 2016). The characterization of *BB* however has been limited to the above-ground organs such as leaves and flowers. Interestingly, I discovered a similar role for *BB* in controlling root growth. The dissection of *bb* root meristems highlighted the increased cell number, but no differences in the mature cell length. Despite the larger meristem, *bb* has no notable effect on root length. The simultaneous enhancement of formative divisions in the radial dimension has been suggested thus to counteract the longitudinal growth. Nevertheless, in adverse conditions such as in *brx* background, *bb* partially restores the root length.

In summary I demonstrated that *bb* loss of function prolongs cell proliferation but not cell elongation in the Arabidopsis root meristem. Because of the high demand of plant derived products in the modern society, perspective studies might investigate the relevance of *BB* homologs in other plant species and evaluate whether such mutations might be exploited in crop improvement.

In the last chapter, I uncovered and confirmed another *brx* suppressor, *JUMONJI 14* (*JMJ14*), which partially rescues the root growth phenotype. My observations however, demonstrated that *jmj14*, similar to *bb*, suppresses the *brx* short root in a protophloem-independent manner. I addressed whether *jmj14* controls cell division in the root meristem, but I observed no perturbation of cell proliferation activity neither in the longitudinal nor in radial growth. Because *jmj14* has not a remarkable phenotype

in the root, I investigated the domains of activity in the Arabidopsis primary root. Interestingly *JMJ14* displays a vascular related expression pattern, however the *JMJ14* protein apparently has a broader domain of activity in the root meristem. Follow up studies could therefore elucidate whether extra copies of fluorescent tag might limit the mobility of *JMJ14* and its role in root growth.

Previous studies described that *JMJ14* encodes an active H3K4 demethylase (Ning et al., 2015). The *jmj14* RNAseq analysis revealed a significant change in the root gene expression profile. Interestingly I found the gene *SHRUBBY* (At5g24740) to be highly upregulated. *SHBY* encodes a protein that partially overlaps with *SHORT ROOT*, *SCARECROW*, *PHLETORA1* and *PHLETORA2*, that all control root growth (Koizumi et al., 2013). I hypothesize that *jmj14* may indirectly modulate root growth vigour through *SHBY* signalling pathway, however additional studies are necessary to confirm this notion and they could also elucidate the mechanism by which *JMJ14* influences root development.

During my research I also demonstrated the relevance of the FYRN/C protein domains, which are crucial for *JMJ14* activity. Surprisingly the *JMJ14* closest homologs cannot rescue the *brx* short root, despite amino acid similarities in the FYR region. Perspective analysis could therefore address the importance of *JMJ14* homologs in root development and the specificity of the FYR protein domains.

At the beginning of my study, the main objective was to uncover new molecular players and to provide genetic evidences necessary to decode the *BRX* pathway. This work thus, illustrates the several attempts I conducted to expand our knowledge on protophloem sieve element differentiation. My findings however have not lead to the identification of new regulators. Nevertheless, I contributed to broaden the understating of *BAM3* function and noticeably I discovered and studied genes (i.e. *BIG BROTHER* and *JUMONJI14*), whose molecular function in root development was unknown.

## References

- Depuydt S, Rodriguez-Villalon A, Santuari L, Wyser-Rmili C, Ragni L, Hardtke CS (2013) **Suppression of Arabidopsis protophloem differentiation and root meristem growth by CLE45 requires the receptor-like kinase BAM3**. Proc Natl Acad Sci U S A 110: 7074-9.
- Disch S, Anastasiou E, Sharma VK, Laux T, Fletcher JC, Lenhard M (2006) **The E3 ubiquitin ligase BIG BROTHER controls arabidopsis organ size in a dosage-dependent manner**. Curr Biol.16: 272-9.
- Helariutta Y (2007) **Cell signalling during vascular morphogenesis**. Biochem Soc Trans. 35: 152-5.
- Koizumi K, Gallagher KL (2013) **Identification of SHRUBBY, a SHORT-ROOT and SCARECROW interacting protein that controls root growth and radial patterning**. Development 140: 1292-300.
- Lucas WJ, Groover A, Lichtenberger R, Furuta K, Yadav SR, Helariutta Y, He XQ, Fukuda H, Kang J, Brady SM, Patrick JW, Sperry J, Yoshida A, López-Millán AF, Grusak MA, Kachroo P (2013) **The plant vascular system: evolution, development and functions**. J Integr Plant Biol. 55: 294-388.
- Ning YQ, Ma ZY, Huang HW, Mo H, Zhao TT, Li L, Cai T, Chen S, Ma L, He X (2015) **Two novel NAC transcription factors regulate gene expression and flowering time by associating with the histone demethylase JMJ14**. Nucleic Acids Res. 43: 1469-84.
- Rodriguez-Villalon A, Gujas B, Kang YH, Breda AS, Cattaneo P, Depuydt S, Hardtke CH (2014) **Molecular genetic framework for protophloem formation**. Proc Natl Acad Sci U S A 111:11551-6.
- Rodriguez-Villalon A, Gujas B, van Wijk R, Munnik T, Hardtke CS (2015) **Primary root protophloem differentiation requires balanced phosphatidylinositol-4,5-biphosphate levels and systemically affects root branching**. Development 142: 1437-46.
- Song XF, Guo P, Ren SC, Xu TT, Liu CM (2013) **Antagonistic peptide technology for functional dissection of CLV3/ESR genes in Arabidopsis**. Plant Physiol. 161: 1076-85.
- Vanhaeren H, Inzé D, González N (2016) **Plant Growth Beyond Limits**. Trends Plant Sci. 21: 102-9.

